

Weiß Andreas, BSc

**Exploring the global murine lipidome
A trial study**

MASTER'S THESIS

to achieve the university degree of

Master of Science

Master's degree program: Biochemistry and Molecular Biomedical Science

submitted to

Graz University of Technology

Supervisor

Eichmann, Thomas Mag. Dr.rer.nat
Institute of Molecular Biosciences/University of Graz
Center for Explorative Lipidomics

Graz, June 2018

AFFIDAVIT

I declare that I have authored this thesis independently, that I have not used other than the declared sources/resources, and that I have explicitly indicated all material which has been quoted either literally or by content from the sources used. The text document uploaded to TUGRAZonline is identical to the present master's thesis.

Date

Signature

Danksagung

An dieser Stelle möchte ich mich bei allen bedanken, die mich auf meinen Weg zum Abschluss meines Studiums begleitet und unterstützt haben.

Als Erstes möchte ich mich bei meinen Eltern Sonja und Karl, meinen beiden Brüdern Michael und Karl-Maria, meiner Freundin Claudia sowie all meinen Freunden bedanken, welche während meines Studiums immer eine wichtige Stütze für mich waren.

Ein ebenso großer Dank geht an meinen Betreuer Thomas Eichmann für seine hervorragende und fachlich kompetente Unterstützung meiner Masterarbeit. Mit seiner humorvollen Persönlichkeit, sowie seinem exzellenten fachlichen Wissen, vermittelte er fachbezogene Themen auf verständliche Art und Weise, welches auf meinen Weg zur Masterarbeit einen unschätzbaren Wert darstellte.

Des Weiteren möchte ich mich bei Gerald N. Rechberger für seine Unterstützung mittels seines Fachwissens sowie der Korrektur meiner Masterarbeit bedanken.

Zu guter Letzt möchte ich mich noch bei allen Kolleginnen und Kollegen vom Institut für Molekulare Biowissenschaften bedanken, welche mir eine der besten Zeiten meines Lebens beschert haben. Ein besonderer Dank geht dabei an Rudolf Zechner, Achim Lass, Robert Zimmermann, Gabriele Schoiswohl, Günter Hämmerle, Karina Preiss Landl, Franz Radner, Renate Schreiber, Gernot Grabner, Christoph Heier, Ulrike Taschler, Johannes Repelnig und Magdalena Tschernitz.

Zusammenfassung

Lipide zählen zu den häufigsten und vielfältigsten Biomolekülen in allen Organismen und sind unerlässlich für den Aufbau von Biomembranen, die Weiterleitung von zellulären Signalen und die Bereitstellung von Energiesubstraten. Aufgrund ihrer biologischen Bedeutung etablierte sich in den letzten Jahren das aufstrebende Forschungsgebiet der Lipidomics, dessen Hauptziele die Charakterisierung der Lipidzusammensetzung sowie die detaillierte Beschreibung des Lipidstoffwechsels sind. Aufgrund der Komplexität von Lipidgemischen, hervorgerufen durch die enormen Kombinationsmöglichkeiten unterschiedlicher Lipidrückgrate und Fettsäuren, entwickelte sich die Koppelung aus Flüssigchromatografie und Massenspektrometrie (LC-MS) zur primären Analyseverfahren. Dabei besteht ein lipidomischer Arbeitsablauf grundsätzlich aus Lipidisolierung, Lipidanalyse und Datenverarbeitung.

Ziel dieser Arbeit war es den Arbeitsablauf zur detaillierten Beschreibung von Lipiden am Beispiel unterschiedlicher Mausgewebe zu testen, zu verbessern und auf Schwachstellen zu untersuchen. Dabei konnte durch die Implementierung einer neuen Extraktionsmethode eine schnellere Probenaufarbeitung, ohne toxische Lösungsmittel, erfolgreich umgesetzt werden. Mit dieser Methode wurden anschließend Lipide eines großen, biologischen Sets an Mausgewebeproben isoliert und mittels LC-MS analysiert. Für die Verarbeitung der daraus resultierenden, enormen Datenmenge wurde eine auf Excel basierende Tabellenkalkulation für die semi-automatische Datenverarbeitung erstellt und zur Lipidklassen-spezifischen Datengruppierung, Unterschiedsberechnung und Statistik verwendet. Des Weiteren wurden Hauptkomponentenanalysen und „heatmap“-Darstellungen getestet um signifikante Unterschiede zu visualisieren.

Neben der Vielzahl an Verbesserung des Arbeitsablaufes, welche in dieser Arbeit umgesetzt wurden, konnten auch Schwachstellen (z.B. interne Standardisierung) identifiziert werden. Die Verbesserung dieser ist das Ziel weiterer Arbeiten.

Abstract

Lipids are one of the most abundant and diverse class of biomolecules in living cells. The cellular importance of lipids for membrane formation, signal transduction, and energy supply is well known. Lipidomics describes a fast growing research area focusing on the large-scale profiling and the systemic quantification of lipids from cells, tissues, or biological fluids. Due to the high complexity of lipids, based on numerous combination possibilities of different lipid backbones and fatty acids, as well as their broad abundance range, liquid chromatography coupled to mass spectrometry (LC-MS) evolved as method-of-choice for lipidomic analysis. Thereby, a common lipidomic workflow can be subdivided into three major working steps, namely lipid isolation, lipid analysis, and data processing.

The major aim of this study focused on the assessment and improvement of the currently used workflow on the example of a big, biological sample set. In course of this work a new lipid extraction method could be established, which allows fast forward sample preparation without the use of toxic, organic solvents. This method was further tested for efficient lipid extraction on a large scale, biological set of murine tissues from wildtype and adipose triglyceride lipase-deficient mice. To handle the vast amount of data, resulting from the LC-MS analysis of these samples, an Excel-based, semi-automated data processing sheet for “big data analysis” was developed and used for lipid class specific data processing and statistics. Additionally, principal component analyses as well as “heatmap” illustrations were applied on the results to assess and optimize the comprehensive visualization of lipid data.

In summary, this study achieved several improvements of the lipidomic workflow and additionally identified several weak points (e.g. internal standardization). Recommended solutions will be tested in future studies.

Table of content

| | |
|---|-----------|
| 1. Introduction | 8 |
| 1.1. Lipids | 8 |
| 1.1.1. Lipid categories | 8 |
| 1.1.2. Lipid functions in mammalian organism | 10 |
| 1.1.3. Lipid storage | 11 |
| 1.1.4. Fatty acid mobilization from lipid depots | 12 |
| 1.2. Chromatographical methods for lipid analysis | 13 |
| 1.3. Mass spectrometry | 14 |
| 1.3.1. Electrospray ionization | 14 |
| 1.3.2. Quadrupole – Mass analyzer | 16 |
| 1.3.3. Time of flight – Mass analyzer | 16 |
| 1.3.4. Quadrupole Time of flight – Hybrid mass analyzer | 17 |
| 1.4. Lipidomics | 18 |
| 1.4.1. Lipidomics workflow | 19 |
| 2. Aims | 22 |
| 3. Materials and methods | 23 |
| 3.1. Chemical and reagents | 23 |
| 3.2. Internal lipid standard solution mix | 23 |
| 3.3. Murine tissue isolation | 23 |
| 3.4. Matyash lipid extraction method (MTBE method) | 24 |
| 3.5. UPLC | 24 |
| 3.6. MS-qTOF | 25 |
| 3.7. Lipid data Analyzer 2 (LDA 2) | 26 |
| 3.8. Principal component analysis (PCA) | 26 |
| 4. Results | 27 |
| 4.1. Sample preparation - full lipid extraction, Folch versus Matyash | 27 |
| 4.2. Data processing I - Lipid identification and peak assignment, picking, and integration | 28 |
| 4.3. Data processing II - Data normalization and statistical analysis | 31 |

| | |
|---|-----------|
| 4.3.1. Development of an Excel based “data processing sheet” | 31 |
| 4.3.1.1. DPS – Sample Information | 32 |
| 4.3.1.2. DPS – LDA 2 data input and automated sorting..... | 33 |
| 4.3.1.3. DPS – Data normalization..... | 34 |
| 4.3.1.4. DPS – Data output..... | 35 |
| 4.3.2. Data visualization | 39 |
| 4.3.2.1. Global data visualization | 39 |
| 4.3.2.2. Top-down data analysis - PCA..... | 42 |
| 4.3.2.3. Visual data analysis - heatmap | 46 |
| 4.4. Workflow evaluation & improvement - Internal standardization | 49 |
| 5. Discussion | 52 |
| 6. References | 57 |
| 7. Table of figures..... | 60 |
| 8. List of abbreviations | 61 |
| 9. Appendix..... | 63 |

1. Introduction

1.1. Lipids

Over years, many definitions tried to describe the complex characteristics of lipids. As comprehensive classification, lipids can be defined as hydrophobic or amphipathic organic biomolecules, highly diverse in structure, function, and solubility [1], [2].

1.1.1. Lipid categories

The consortium of “Lipid Metabolism and Pathway Strategy” (Lipid MAPS) subdivides lipids in eight major categories, namely fatty acyls, glycerolipids (GLs), glycerophospholipids, sphingolipids (SLs), sterol lipids, prenyl lipids, saccharolipids, and polyketides (PKs) (Fig. 1).

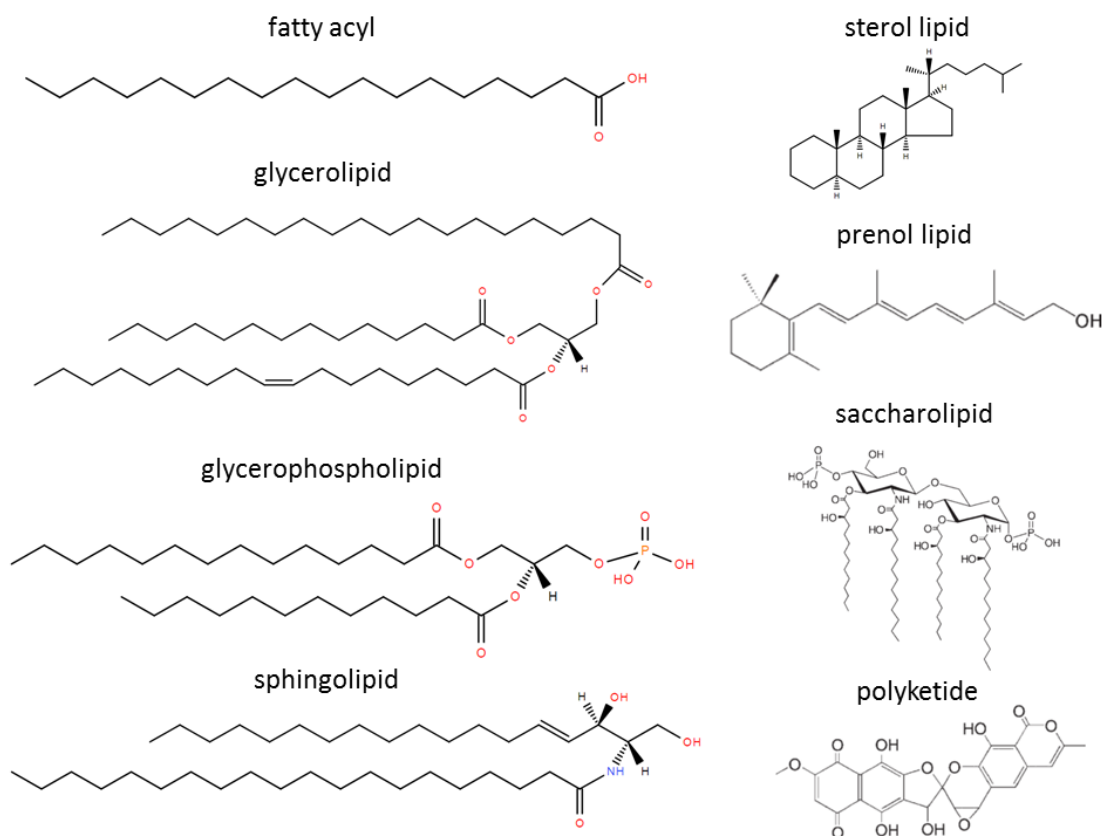


Figure 1: Representative structures for the eight major lipid categories. Source: Ref. 1 (table of figures).

The simplest structure of a lipid class is represented by fatty acids (FAs), which are the basis for building up more complex lipid classes. FAs are carboxylic acids, which can vary in their level of saturation as well as their chain length and occur both unbound as well as attached to different backbones, like glycerol or sphingosine.

Lipids of the GL class exhibit a glycerol backbone esterified with up to three FAs. Depending on the number of bound FAs, GLs are subdivided into mono- (MAG, one FA), di- (DAG, two FAs) or triacylglycerol (TAG, three FAs). Thereby, TAG depicts the main energy reservoir of living cells and is stored in cellular lipid droplets. Glycosylated GLs are classified as glyceroglycolipids [3].

Glycerophospholipids, short phospholipids (PLs) are another very important lipid class in living organism. Besides the attachment of a FA in *sn*-1 and *sn*-2 position PLs exhibit a hydrophilic headgroup at the *sn*-3 position of the glycerol backbone. This combination of hydrophobic FA residues and hydrophilic headgroups makes PLs very important amphiphilic molecules. For lipid classification in eukaryotes, PLs are subdivided into distinct classes depending on the different headgroups. Most abundant subclasses of PLs in biological systems are phosphatidylcholine (PC), phosphatidylethanolamine (PE), phosphatidylinositol (PI), and phosphatidylserine (PS). Cardiolipin (CL) depicts a complex PL class, in which two phosphatidic acids are attached at the *sn*-1 and *sn*-3 position of a central glycerol molecule. Hence, CL molecules contain four FAs residues [4].

All lipid classes containing sphingosine as basic structure element are clustered together as SLs. Depending on sphingosine modification, several subclasses of SL are described. Thereby, O- and N-linkage of the sphingosine molecule with e.g. different FAs or sugar residues is possible, which drastically increases the diversity of this lipid class. Ceramides (Cers) are characterized by a FA esterified to the amino group of sphingosine. Further linkage of a choline headgroup to the terminal hydroxyl-group of ceramides gives rise to the subclass of sphingomyelins (SMs). Terminal condensation of carbohydrates to Cer results in glycosphingolipids, which are classified depending on their sugar composition. The simplest and most abundant subclass of glycosphingolipids are hexosyl-ceramides (Hex-Cers), in which a ceramide is terminally mono-glycosylated [2], [5].

Steroids and cholesterol lipids are members of the sterol lipid class. All members of this class contain cholesterol as four-ring core structure. Besides the important cellular

functions of free cholesterol in membrane homeostasis, several cholesterol derivatives play pivotal roles in biological systems. Cholesteryl-esters (CEs) of FAs depict the storage form of cholesterol, whereas diverse modifications of cholesterol give rise to a variety of important biological molecules, like bile acids or steroid hormones, e.g. glucocorticoids, estrogens, and androgens [2], [6].

The five-carbon isopentenyl diphosphate and dimethylallyl diphosphate molecules are an important precursor for prenyl lipids. Isoprenoids precursor are commonly produced via the mevalonic acid pathway and are generated by successive addition of C₅ units. Carotenoids are simple isoprenoids and function as antioxidants and as a precursor of vitamin A. Quinones and hydroquinones class contain a isoprenoid residue attached to a quinonoid core of non-isoprenoid origin and are represented by vitamin E, K, as well as ubiquinone [2], [7].

Saccharolipids form membrane bilayer compatible structures and contain a sugar backbone linked to a FA. The acylated glucosamine precursor of lipid A is one example for saccharolipids. Lipid A is a component of lipopolysaccharides in gram-negative bacteria and contains a disaccharide of glucosamine, esterified with up to seven FA chains [2], [8].

PKs are complex secondary metabolites and natural products in animals, plants, bacteria or fungi, synthesized by polymerization of acetyl-CoA and propionyl-CoA subunits. PK synthases are subdivided into three different classes. Type I PK synthases are analog to vertebrate FA synthases and produce macrocyclic lactones in a range from 14 to 40 atoms. Whereas, type II and III PK synthases are similar to bacterial FA synthases and form complex aromatic molecules. Pharmaceutical PKs like geldanamycin, doxycycline, or erythromycin are included in antimicrobial, antiparasitic, and anticancer agents [2], [9].

1.1.2. Lipid functions in mammalian organism

Lipids represent highly abundant and important mammalian biomolecules and are crucial for membrane-biogenesis and integrity, energy-metabolism, and cellular signal events. Most biological membranes are formed by bilayer sheets of amphiphilic PLs, interacting among themselves with their hydrophobic FA residues. The resulting hydrophilic head

groups on both surface sides of biomembranes face the aqueous environment and enable compartmentalization of cells and cell organelles. Depending on chemical and physical properties, membrane PLs can form local subdomains for protein binding, which provides a regulative function to embed integral membrane proteins [10]. Furthermore and in contrast to water-soluble protein messengers, signaling lipid molecules, like e.g. FAs can cross hydrophobic biomembranes and bind to intracellular receptors, acting as signal transduction pathway activating ligands or mediators, as well as substrates of lipid kinases and phosphatases [11]. Regarding cellular energy metabolism, β -oxidation is one of the major mechanisms in eukaryotic cells, stepwise degrading FAs to generate reducing equivalents (FADH₂, NADH) and further substrates to fuel ATP synthesis. Thereby, TAG reflects the major FA storage form and source for intracellular free FAs.

1.1.3. Lipid storage

The storage of energy reserves in vertebrates is achieved by the water-free packaging of neutral lipids into so called lipid droplets (LDs) of adipocytes. The LD is surrounded by a monolayer surface of PLs shielding TAG and CE as major core components. Thereby, adipocyte LDs can achieve a size of over 100 μ m [12]. The neutral lipid synthesis, as well as the formation of LDs by recruitment of certain lipids and proteins, occurs in the endoplasmic reticulum [13]. Besides the important function of stored neutral lipids for energy metabolism, LD harbor necessary components for membrane production and signaling events [14]. It has been shown that several proteins and enzymes, important for neutral lipid metabolism, such as diacylglycerol acyltransferase (DGAT) are located at, or in close proximity to cytosolic LDs. DGAT enzymes catalyze the last step of TAG synthesis by catalyzing the linkage of a fatty acyl CoA with the free hydroxyl group of DAG. In mammalian organisms, two different DGAT enzymes exist (DGAT1, DGAT2). The active site of DGAT1 is located in the lumen of endoplasmic reticulum membrane, whereas DGAT2 additionally localizes to LDs. Additional differences between these enzymes are their acyl donor and acyl acceptor preference. DGAT1 deficient knockout mice revealed a reduced TAG level in tissues like liver or adipose tissues. In contrast, DGAT2 lacking mice show a defect skin barrier and suffer a premature death [15], [16].

1.1.4. Fatty acid mobilization from lipid depots

The mobilization of FAs from LD associated TAG, short lipolysis, depends on the consecutive action of several major enzymes: adipose triglyceride lipase (ATGL) activated by comparative gene identification-58 (CGI-58), hormone-sensitive lipase (HSL), and monoacylglycerol lipase (MGL) (Fig. 2).

In 2004, ATGL was simultaneously identified in three different laboratories as the rate-limiting enzyme of the lipolytic cascade, hydrolyzing specifically TAG [17]–[19]. The lipolytic activity of ATGL can be activated by CGI-58 [20]. The lack of CGI-58 in mice causes various phenotypes, e.g. growth retardation, a lethal skin barrier defect, hepatic steatosis, and an impaired TAG catabolism [21]. In comparison to the phenotypes resulting from the lack of CGI-58, several studies revealed severe differences in the physiological phenotypes of ATGL deficient mice. ATGL deficiency contributes to impaired fat metabolism and reduced lifespan. The absence of ATGL yields a massive TAG accumulation in nearly all tissues and the unimpeded accumulation of TAG in cardiac muscles causes premature death by cardiac dysfunction [14]. However, lethal skin barrier defects are not observed for ATGL deficient organisms.

50 years ago, HSL and the MGL were identified as major enzymes catalyzing the hydrolysis of neutral lipids [22]. HSL activity is regulated by two major mechanism, the protein-kinase A mediated phosphorylation of HSL and resulting LD recruitment and the activation of HSL by perilipin proteins [23], [24]. HSL primarily hydrolyzes FAs in *sn*-1 or *sn*-3 position of DAG generating MAG [25]. Besides that, HSL can hydrolyze TAG and MAG to a minor extend [16]. Knockout studies with HSL deficient mice revealed intracellular accumulation of DAG in various tissues [26]. Subsequently, MGL is responsible for the final lipolytic step by catalyzing the hydrolysis of MAG and the formation of free glycerol [27].

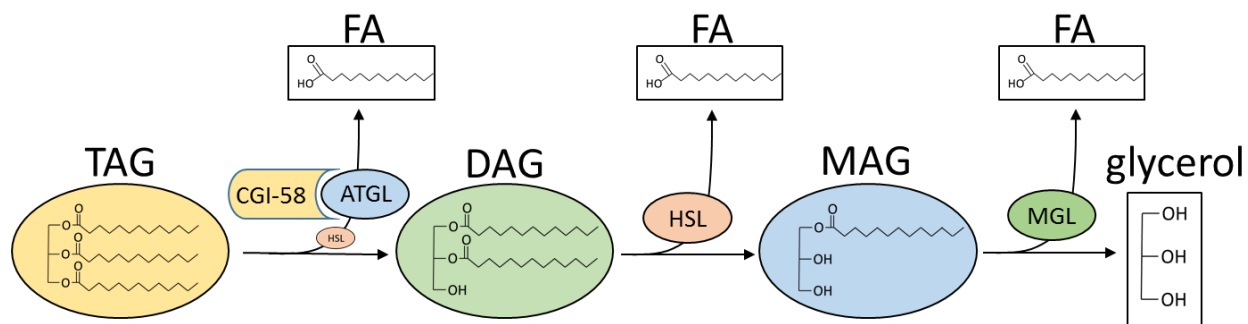


Figure 2: Simplified TAG lipolysis and involved enzymes and intermediates. ATGL, activated by CGI-58, hydrolyzes TAG to generate DAG and free FAs. Further hydrolysis of DAG to MAG is catalyzed by HSL. Additionally, HSL can contribute to TAG hydrolase activity. Finally, MGL cleaves the last FA from MAG. The free glycerol can be released or further utilized in carbohydrate metabolism or lipogenesis.

1.2. Chromatographical methods for lipid analysis

Chromatography is an established analytical technique for the separation of complex substance mixtures, due to different physical properties of the analyte molecules. General chromatographic principles base on the separation of dissolved sample molecules in a gas or liquid mobile phase and their subsequent transport through a liquid or solid stationary phase. The interactions between dissolved substances and functional groups of the stationary phase enable this separation process. Over the years, gas chromatography (GC) and liquid chromatography (LC) emerged as methods of choice for lipid analysis. Thereby, GC often requires prior analysis derivatization of target analyte molecules due to volatility reasons. In contrast, LC is usually performed in the native analyte state and modern LC systems represent the tentative endpoint of a long history of technical progression. In LC, dissolved analyte components are pumped under high pressure through a column packed with a solid phase, mostly silica, which can be modified with diverse functional groups. Depending on column chemistry, different types of LC can be distinguished, like normal phase- (NP), reversed phase- (RP), ion exchange-, or size exclusion chromatography. Regarding lipid analysis, RP-LC is the most frequently used method, which silica-based stationary phase is functionalized with non-polar residues (phenyl, C-8, C-18, etc.). RP-LC provides lipid species separation over a broad polarity range. Hydrophilic interaction chromatography (HILIC), a NP-LC method, represents another frequently used lipid separation technique. In contrast to RP-LC separation, HILIC separates lipid classes according to their polar headgroups. Due to the

broad range of applicability, high-performance liquid chromatography (HPLC) as well as advanced ultra-high-performance liquid chromatography (UHPLC) have become established methods in lipid analysis over the last years. Main differences of UHPLC as compared to HPLC are smaller column particle size ($< 2 \mu\text{m}$) and resulting higher mobile phase backpressure (up to 1,000 bar). Despite the higher costs, UHPLC separation speed and efficiency are unrivaled.

1.3. Mass spectrometry

Mass spectrometry (MS) is an analytical technique based on the sorting and the detection of ionized molecules by their mass to charge (m/z) ratio. A typical mass spectrometer contains three major components, the ion source, the mass analyzer, and the detector. Ionization techniques vary depending on sample phase and can be subdivided in soft or hard ionization. Before the system transmits ions to the detector, the magnetic or electric field of the mass analyzer separates the ionized molecules in a high vacuum according their m/z . In MS-based lipid analysis, the magnetic sector field (MSF) analyzer played an important historical role. Nevertheless, due to drawbacks like high costs, large size, and difficulty of operation, MSF is hardly used for lipid analysis nowadays. Advanced MS instruments like quadrupole-time-of-flight (qTOF), ion trap, and orbitrap instruments are the current state-of-the-art in lipidomics [28].

1.3.1. Electrospray ionization

Following early experiments of generating a beam of macromolecules in vacuum by Malcolm Dole in 1986, John Fenn continued the idea 15 years later [29] and was rewarded 2002 with the Nobel prize in chemistry for the development of the electrospray ionization (ESI) technique [30]. The establishment of the ESI process in LC-MS was a milestone in analytical bioscience and is nowadays indispensable for lipid analysis. The general ESI process can be divided into three major steps. The nebulization of dissolved sample into charged droplets, the release of the charged ion by solvent evaporation, and the ion-transport from atmospheric pressure into the vacuum region of the mass analyzer [31]. The dissolved analyte molecules become charged by oxidation/reduction processes

and pass through a charged capillary. In positive ionization mode, a positive electric potential is applied on the capillary and a negative potential on the entry of mass analyzer. The orifice of the capillary forms the anode and only cations are released. Due to the high voltage (~4kV for lipids) and depending on the applied electric potential, charged droplets form the so called Taylor cone and spray as a fine aerosol into the ESI chamber. Supported by a heated N₂ stream, droplets progressively evaporate until their size reaches the Rayleigh limit which results in Coulomb fission releasing charged single molecules as well as smaller charged droplets (Fig. 3). Two theories describing the ionization process. The charge residue model suggests that charged droplets undergo continuing Coulomb fission until only one single charged molecule is existing in one droplet [32]. The ion evaporation model suggests that droplets evaporate until the field strength at the surface is large enough for ion desorption [33]. Counter ions in form of cations (e.g. H⁺, Na⁺, NH₄⁺, K⁺) or anions (e.g. OH⁻, Cl⁻, HCOO⁻, H₃COO⁻) available in the mobile phase support ionization of charge-neutral polar analytes. The major benefits of ESI in lipid analysis are the soft ionization and mainly single charged lipid molecules [28].

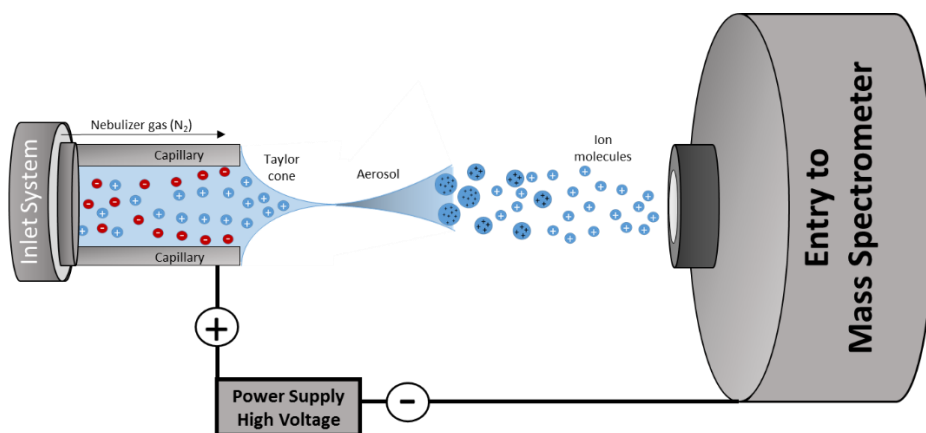


Figure 3: Scheme of ESI source and process in positive ionization mode.

1.3.2. Quadrupole – Mass analyzer

The quadrupole mass analyzer transfer ions in an oscillating radio frequency electrical field, created between four parallel cylindrical rods. The potential change between the rods allows the passage of ions in a wide m/z range. The combination of three quadrupoles represents the small-sized, and widely used triple quadrupole MS (MS-QQQ) system. Beside single ion transmission, the MS-QQQ setting allows fragmentation experiments in an inert gas (e.g. He, N₂, or Ar) filled collision cell, also called as "collision-induced decomposition" (CID), as well as passing and scanning of defined complete or fragment ion molecules. MS-QQQ combined with LC or used for direct infusion of analytes (shotgun) provides high sensitivity and selectivity for lipid analysis through diverse possible MS experiments, such as selected/multiple reaction monitoring, neutral-loss scan (NL), precursor-ion scan (Pre), or product-ion analysis [28].

1.3.3. Time of flight – Mass analyzer

Ion molecules in a TOF mass analyzer are accelerated in a defined electrical field. All ions experience the same kinetic energy and separation is based on the different velocity of ions with unequal m/z ratio in an evacuated, energy-free flight tube. The kinetic energy ($mv^2/2$) of an accelerated analyte ion in the electrical field (V) is equivalent to the potential energy. Consequently, the m/z ratio can be calculated by knowing the electron charge (e), flight tube length (l), and the required flight time (t) of the ion, by following formula:

$$m/z = \frac{2eV * t^2}{l^2}$$

Therefore, heavier ions reach the detector later than lighter ones [28]. Major drawbacks of the linear TOF technique are limitations of resolution and identification issues between metastable ions and their origin precursor ions. Advanced reflector TOF systems reflect the ion beam through a constant electrostatic field (repeller field) to the detector. Besides stretching the ion flight path length, heavier ions can enter deeper into the repeller field and are recorded later than light ions. Thus, ion-molecule separation in reflector TOF

system displays increased resolution and reduced simultaneous detection of different ion m/z (Fig. 4).

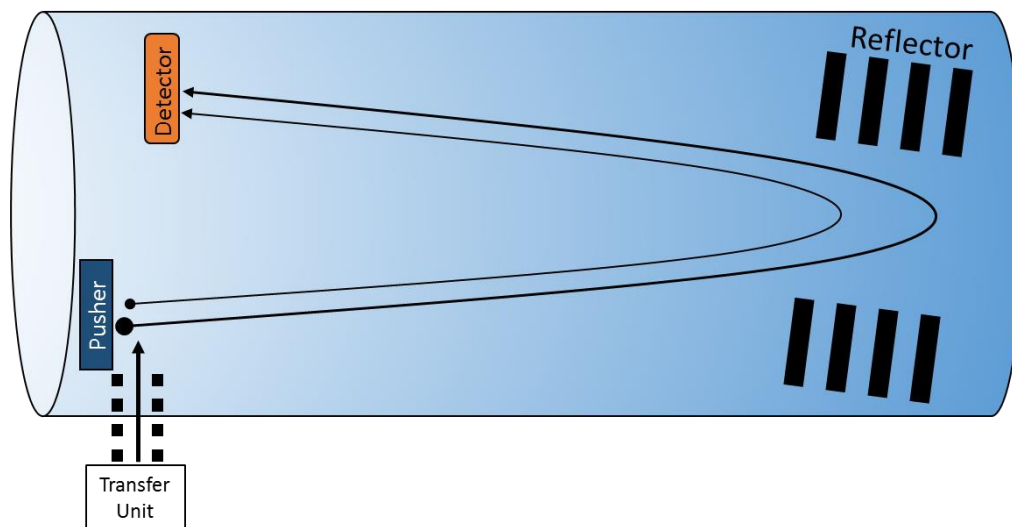


Figure 4: Scheme of a reflector TOF. The pusher accelerates ions with the same kinetic energy in a defined electrical field. The reflector field deflects ions to the detector, thereby heavier ions penetrate deeper into the reflector field and are recorded later than faster, light ions.

1.3.4. Quadrupole Time of flight – Hybrid mass analyzer

The improvement of the MS-TOF technique by front-end coupling with a single quadrupole provides high-resolution, mass accuracy, increased sensitivity and ion transmission efficiency, and emerges to one of the widely used mass analyzer systems for lipid analysis. Thereby, the limitation of performing MS/MS experiments in TOF systems accelerates the development of advanced quadrupole-time-of-flight (qTOF) hybrid mass analyzer. Commonly used MS-qTOF systems are assembled with two quadrupole stages (Q1, Q2) and a reflector TOF. For MS/MS experiments, Q1 can operate as a mass filter to transmit analyte ions of interest, whereas Q2 executes CID to originate fragments of precursor ions [34]. Alternating CID and full scan data acquisition displays currently one of the main qTOF modes (e.g. Agilent: all-Ion, Waters: MSE). Drawbacks of MS-qTOF systems are the incapability of direct NL and Pre analysis.

1.4. Lipidomics

Lipidomics is a young, uprising analytical research field in molecular biology “omics” disciplines and focuses on the large scale study of intact molecular lipid species of the entire lipidome. Thereby, the term lipidome comprises the entire lipid species components in a cell, an organ, or a biological system. Lipidomics aims to identify “all” lipid species of a given sample, including structural information, like fatty acid chain composition, double bond location and isomer distribution. Additionally, the quantification of the identified lipid species reflects a primary topic, since quantitative information on lipid species are of great importance for metabolic pathway analysis, lipid-lipid and lipid-protein interaction studies, as well as for the robust description of the metabolic status of healthy and diseased organisms [28].

For more than half a century researchers studied lipid pathways and interactions [35]. Nevertheless, the terms “lipidome” [36] and “lipidomics” [37] first appeared in literature in the early 21st century, mainly because the improvement and availability of new analytical technologies over the last ~20 years enabled detailed lipid investigations. Since then, lipidomic studies are steadily increasing resulting in 516 lipidomic publications in 2017 (NCBI). To date, lipidomic studies focus on the identification of novel and low abundant lipid classes and species, method development for quantitative analysis, and the full description of lipid levels in biological samples. Resulting data are used for metabolic network and biomarker analysis as well as to describe altered distribution of lipids in different pathological conditions. Besides that, big efforts are made to assure further improvement and automatization of bioinformatical approaches for high-throughput processing and lipidomic database development [38].

HPLC and LC coupled MS as well as nuclear magnetic resonance (NMR) display the main technologies for lipidomic investigations and contributed mainly to the successful development of lipidomics [28].

1.4.1. Lipidomics workflow

The typical MS-based lipidomic workflow for biological samples can be subdivided into three major parts, namely sample preparation, sample analysis, and data processing (Fig. 5). Sample preparation includes sample isolation as well as lipid/analyte extraction. Thereby, lipid extraction is necessary to separate the hydrophobic lipid molecules, embedded in biological matrix, from other interfering compounds. 1957 Folch introduced a method for full lipid extraction, which emerged over the years to one of the most commonly used methods for lipidomic sample work-up [39]. Thereby, the Folch method is a simple and scalable biphasic lipid extraction. However, when using the Folch method for routine laboratory analysis several drawbacks are noticeable. The toxicity and high density of the main solvent chloroform, the incompatibility with most plastic lab ware, as well as the high solvent volume needed for robust extraction turn out to be unfavorable for high-throughput lipid analysis. Extracted lipids reside in the bottom, organic phase mostly covered by an interphase of precipitated proteins, which has to be pierced for analyte isolation. Therefore, possible sample contamination has to be monitored very precisely. Over the last years, various chloroform-free full lipid extraction methods described by Matyash (MTBE) [40] or Löfgren (BUME) [41] emerged alongside the common gold standard methods Folch [39] and Bligh & Dyer [42]. Nevertheless, the reliability and the good extraction capacity favorites the latter mentioned methods for a robust implementation into the lipidomic workflow.

Following extraction, the lipid samples can be analyzed by different analytical methods like NMR or MS. Due to the better sensitivity, MS is currently the technology-of-choice for lipidomic investigations and therefore widely used in this research field. Over the last years two basic MS analysis types evolved side by side. On the one hand, methods, which apply analyte separation prior to MS analysis (e.g. LC-MS, GC-MS) and on the other hand MS analysis without front end separation, short shotgun-MS. Additionally, MS methods can be categorized in targeted and untargeted approaches. Thereby “targeted” and “untargeted” describes the method of data acquisition. In contrast to high-resolution scanning of the full m/z range in an untargeted measurement, targeted measurements isolate previously selected m/z values in low resolution, neglecting other,

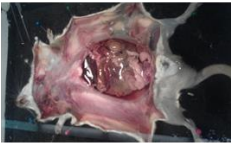
contemporaneously occurring ions. These technical differences lead to higher selectivity and sensitivity of targeted analysis with the drawback of a decreased global sample information. Targeted MS analysis is widely used for the specific profiling of distinct lipid species and requires MS instruments, which can execute several different isolation and fragmentation experiments, e.g. MS-QQQ. Untargeted MS analysis requires high-resolution instruments, like MS-qTOF or Orbitrap instruments and can be used for global lipidomic profiling. Additionally, untargeted MS studies are highly dependent on, (i) robust MS systems, ensuring high mass accuracy and resolution, (ii) highly sophisticated software solutions, which enable global feature analysis and statistics, and (iii) robust lipid databases for species identification, either self-made or open to the public. The steady improvement of MS systems in terms of stability and sensitivity leads to a continuous increase in data complexity. Therefore, pre-separation of the sample for both targeted and untargeted analyses, becomes more and more indispensable. Analytically problematic but biologically given effects, such as the presences of isobaric or isomeric molecules, as well as ionization issues due to a high concentration difference between analytes can be alleviated by front-end chromatographic coupling.

Data processing, bioinformatics work-up, and statistics depict the final steps of the lipidomic workflow. Whereas targeted MS experiments require intensive MS method development in terms of lipid species and ionization parameter identification, manufacturer specific software solutions conduct the post-acquisition data processing highly accurate and automated. In contrast to that, untargeted lipidomic experiments are easy to realize and contain virtually all lipid information of a sample but require time-consuming post-processing methods and accurate databases for analyte identification and data processing. Thereby, correct spectra interpretation and data processing is mandatory to transform raw MS data into meaningful, robust and reproducible results.

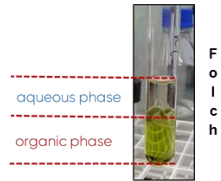
Quality controls, internal standardization, as well as defined experiment parameters are mandatory to achieve accurate results independent of the used MS approach. Hence, the robustness and reliability of the complete lipidomic workflow is of utmost importance to generate statistically significant results [43].

Sample preparation

Sample isolation

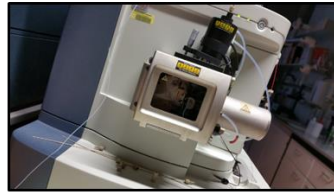


Lipid extraction



MS - Analysis

MS-qTOF

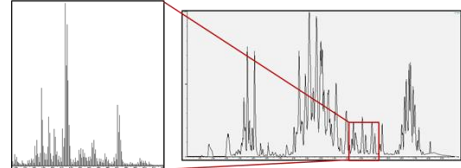


MS-QQQ



Bioinformatics

Lipid identification & peak detection



Data processing & statistics

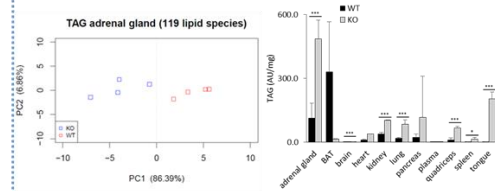


Figure 5: A lipidomics workflow. The lipidomics workflow is subdivided into three major parts: Sample preparation, MS-Analysis, and bioinformatics.

2. Aims

The aim of this study was to improve the current lipidomics workflow of the Core facility Mass Spectrometry/Lipidomics at the IMB-Graz. Thereby, specific steps of the workflow should be assessed and improved:

- 1.) Sample preparation: Assessment of the initial Folch lipid extraction in comparison to optional methods
- 2.) Sample analysis: Execution of the current workflow (including sample collection and analysis) on a big, biological sample set and evaluation of potential weak points.
- 3.) Data processing: Exploring the first steps in big data management, processing, and visualization. Unifying lipid species mass lists and refining raw data processing methods.
- 4.) Workflow evaluation: Reflecting the entire workflow and sum up recommendations for future improvements.

Taken together, this trial study should reveal possible weak points of the current workflow in terms of applicability on big sample set/big data and suggest improvements. Furthermore, it should help to gather first experience in the generation of a comprehensive, abundance-based lipid database.

3. Materials and methods

3.1. Chemical and reagents

2-Propanol, tert-butylmethylether (MTBE), chloroform, phosphoric acid and formic acid were purchased from Roth (Karlsruhe, GER), ammonium acetate from Avantor (Center Valley, PA, USA), water from VWR International (Fontenay-sous-Bois, FRA), aqua bidestilata (ddH₂O) from Fresenius Kabi (Graz, AUT), acetic acid from Merck (Kenilworth, NJ, USA), methanol (MeOH) from Chem-Lab (Zedelgem, BE), butylated hydroxytoluene (BHT) from Alpha Aesar (Karlsruhe, GER). All solvents were at least HPLC grade.

3.2. Internal lipid standard solution mix

For normalization, an internal standard (ISTD) solution mix was prepared, containing 500 nM of different lipid species. Cer (d18:1/17:0), lysophosphatidylcholine (LPC 17:0), PC 24:0 (12:0/12:0), PC 34:0 (17:0/17:0), PE 24:0 (12:0/12:0), PE 34:0 (17:0/17:0), PS 34:0 (17:0/17:0), and TAG 45:0 (15:0/15:0/15:0), TAG 51:0 (17:0/17:0/17:0), TAG 57:0 (19:0/19:0/19:0). Lipid standards were purchased from Avanti Polar Lipids (Alabaster, AL, USA). Lipids were resolved in a total volume of 5 ml MeOH/chloroform/BHT (1/1/0.1%, v/v/v%).

3.3. Murine tissue isolation

The isolation of 21 different tissues of fasted wild-type and ATGL deficient mice was done with the help of Dr. Gabriele Schoiswohl. In short, tissues were harvested from over 8 weeks old female (n=4/genotype) and male (n=5/genotype) mice. Isolated tissues were washed in phosphate buffered saline (PBS: 1 mM KH₂PO₄, 155 mM NaCl, 3 mM, Na₂HPO₄ · 7 H₂O), subsequently weighed, transferred into cryo-vials, and snap frozen in liquid nitrogen. Isolated blood samples were centrifuged for 10 min (3,000 rpm, 4 °C) and the upper, plasma layers were transferred into new vials. All snap frozen samples were stored in -80 °C freezer until lipid extraction.

3.4. Matyash lipid extraction method (MTBE method)

The original method [40] was customized for the implementation into the Core facility lipid workflow as well as for mammalian tissue samples (Fig. 6).



Figure 6: General MTBE lipid extraction workflow.

Weighed samples were transferred into 2 ml “SafeSeal” Eppendorf vials from Sarstedt (Nümbrecht, GER) for further sample work-up. Prior extraction two cleaned 3 mm steel beads were added to each tube. Lipid extraction was started by adding 700 μ l MTBE/MeOH/HAc/BHT (3/1/1%/0.1%, v/v/v%/v%) mixture to each sample. Additionally, each sample contain 4 μ l of the ISTD solution mix. Extraction mixtures were further homogenized for 2x15 s (frequency 30/s) using a Retsch Mixer Mill 400 (Haan, GER). Next, samples were mixed using a HLC-HTM130 thermomixer at full speed on RT for 30 min. To induce phase separation, 140 μ l ddH₂O were added to each sample. Subsequently, samples were briefly vortexed 5 to 10 times and centrifuged at 13,200 rpm for 10 min on RT. 500 μ l of the lipid-containing, upper organic phase were transferred into 1.5 ml eppendorf tubes and evaporated under a gentle stream of nitrogen. Dried lipids were resolved in 2-propanol/MeOH/H₂O (PMW, 70/25/10, v/v/v). Solvent volume was adapted for sample weight. Dissolved lipids were directly used for LC-MS analysis or stored on -20 °C.

3.5. UPLC

Liquid chromatography was performed on an AQUITY-UPLC system (Waters Corporation, Milford, MA, USA), equipped with a Luna Omega C-18 reversed phase column (2.1 x 50 mm, 1.6 μ m; Phenomenex, Torrance, CA, USA). For chromatographic separation, a customized gradient introduced by Johannes Repelnig [44], was used (Table 1). Mobile phase solvent A consisted of water/methanol (1/1, v/v), solvent B of 2-propanol. Both solvents contained 8 μ M phosphoric acid, 10 mM ammonium acetate and 0.1 % formic acid. The column compartment was kept at 50 °C [45].

Table 1: UPLC gradient

| time (min) | A (%) | B (%) | Flowrate (ml/min) |
|-------------------|--------------|--------------|--------------------------|
| 0 | 80 | 20 | 0.1 |
| 1.00 | 80 | 20 | 0.1 |
| 1.05 | 80 | 20 | 0.3 |
| 2.00 | 80 | 20 | 0.3 |
| 4.00 | 55 | 45 | 0.3 |
| 17.00 | 15 | 85 | 0.3 |
| 18.00 | 0 | 100 | 0.3 |
| 19.00 | 0 | 100 | 0.3 |
| 19.05 | 80 | 20 | 0.3 |
| 19.50 | 80 | 20 | 0.3 |
| 19.55 | 80 | 20 | 0.1 |
| 20.00 | 80 | 20 | 0.1 |

3.6. MS-qTOF

Untargeted analysis was performed on a SYNAPT™ G1 q-TOF HD mass spectrometer (Waters Corporation), equipped with an ESI source. The following source parameters were applied: capillary temperature 100 °C, desolvatization temperature: 400 °C with nitrogen as nebulizer gas, capillary voltage was set to 2.6 kV in positive and 2.1 kV in negative ionization mode. In the MS setup, two alternating scan modes were used for MS^E. The first scan mode was a full scan. For fragmentation of all generated ions, a collision energy ramp was applied (25–45 V) in the second scan mode. The same settings were used for both scan modes (mass range: *m/z* 50–1800; scan time: 1 s; data collection: centroid). An external pump (L-6200, Hitachi, Biedermannsdorf, AUT) achieved the lock spray at a flow rate of 0.5 ml/min split in a 1:13 ratio. As reference substance, leucine/enkephaline ([M+H]⁺: *m/z* 556.2771 and [M-H]⁻: *m/z* 554.2615) was used. For a continuous mass correction, the lock mass was measured every 15 s, independent of the other scan modes. The Mass Lynx 4.1 software (Waters Corporation) was used for data acquisition.

3.7. Lipid data Analyzer 2 (LDA 2)

Automatic peak integration for lipid composition analysis were performed with the LDA 2 software [46]. The batch quantitation settings were: retention time tolerance before/after: 0.3 min; retention time shift: 0 min; relative base peak cut off: 0.1 ‰; isotopic quantitation of 2 isotopes where 1 isotopic peak has to match. Final integrated AU values of each sample were exported as excel sheets. Additionally, lipid classes with ISTDs were normalized with LDA 2 and exported as separate excel sheets.

3.8. Principal component analysis (PCA)

PCA was performed in R (version 3.4.3), a software solution for statistical computing and graphics. Two different R scripts for PCA analysis, developed by Jürgen Hartler, were used to examine differences within the lipid composition (either between lipid classes or phenotypes). The PCA analysis transforms intensities of single lipid species (initial coordinates) of a given class to a new coordinate system, i.e. principal components. Principal components are coordinates where species with higher intensity variations contribute to a higher extent [47]. The components are sorted based on the variation content in descending order (PC1 contains the highest deviation information). Plotting PC1 versus PC2 illustrates similarities within biological replicates (should cluster) and provides information whether there are differences between the various tissues (clusters should separate).

4. Results

4.1. Sample preparation - full lipid extraction, Folch versus Matyash

2008, an extraction method which overcomes many of the Folch method drawbacks was published by Matyash et al. [40], by using methyl-tert butyl ether (MTBE) as an organic extraction solvent. In contrast to Folch, the Matyash method uses non-toxic solvents, needs low solvent amounts, is compatible with plastic lab ware, and the low density of MTBE leads to an upper, organic phase.

To improve the current sample preparation workflow, the first experiments aim to assess the capacity and advantages of the MTBE method in comparison with the used Folch extraction. In that course, several extractions were compared using heart and liver tissue from chicken as reference material. Besides whole tissue extraction also the applicability of mill-based tissue homogenization in combination with MTBE extraction was tested.

For the determination of the abundant lipid classes lysophosphatidylcholine (LPC), SM, Cer, PC, PI, and TAG, which were used for the method comparison, all extractions contained a mix of TAG 51:0, PC 34:0 and LPC 17:0 as normalization standards. The method comparison revealed similar extraction efficiencies for Folch and Matyash. Interestingly, PI of both tissues could be recovered to a higher extend by using MTBE method (Fig. 7). In contrast to Folch, the compatibility of MTBE with plastic allowed mill based homogenization. Thereby, Eppendorf Safeseal vials showed highest robustness during 2x15 s homogenization using 3 mm steel beads [48].

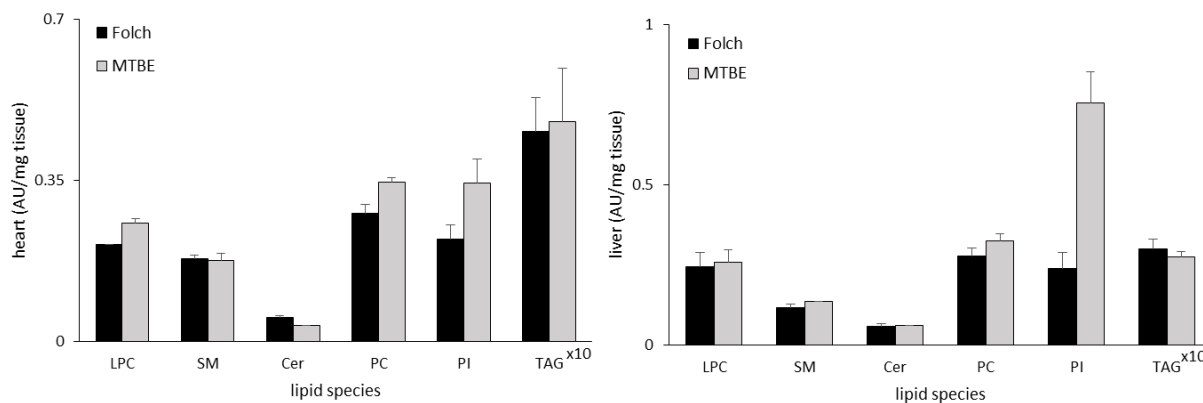


Figure 7: Selected lipid classes of chicken heart and liver extracted using Folch and MTBE method. Lipid content was analyzed by UHPLC-qTOF-MS analysis. Data are presented as means + std. dev. (n=4) normalized to ISTD (TAG 51:0, PC 34:0, LPC 17:0) and tissue weight.

For the assessment of all further steps of the lipidomics workflow, the newly implemented Matyash/MTBE method was applied on 12 different tissues of female wild-type and ATGL deficient mice. Dried lipid extracts were resolved in PMW and the required volume was adapted for each tissue and genotype (Table S1). All samples were analyzed by UPLC-qTOF-MS and stored afterwards at -20 °C for further analysis.

4.2. Data processing I - Lipid identification and peak assignment, picking, and integration

Correct lipid species identification is one of the most important steps in lipid analysis. False positive identification of lipid classes and species will ultimately yield unreproducible, incorrect results. To avoid false positive identification the current approach utilizes the Lipid Data Analyzer 2 software (LDA 2) [46]. The LDA 2 requires manually generated mass lists of several lipid species of different classes for automatic peak picking and integration. Therefore, all available information on retention time and specific ionization of several lipid species was combined into detailed lipid class mass lists. Identification of lipid species was achieved by comparing signals of interest with signals of internal standard (ISTD) and extrapolation of retention time for chain length differences. Furthermore, lipid molecules of different lipid classes were identified using high-resolution mass and their class specific adduct-ion formation (example given fig. 8). For more detailed lipid information MS/MS data were investigated.

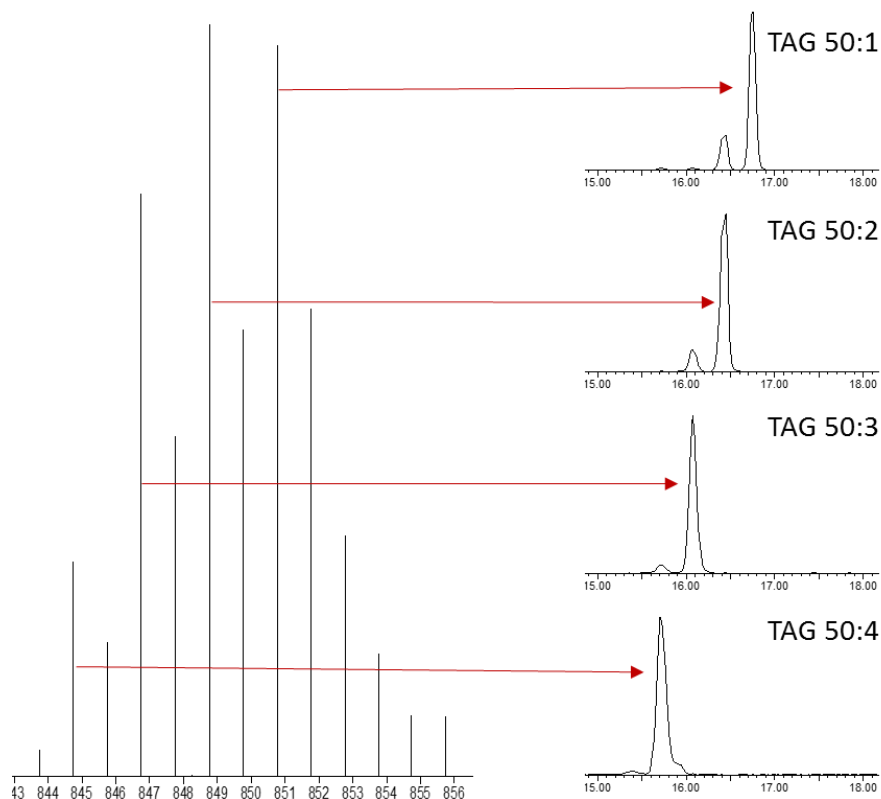


Figure 8: Peak identification of TAG species as ammonium adduct. Illustration of the peak identification process with Mass Lynx software. The exact masses of adduct ion were picked from centroid mass spectral and retention time was used for mass list generation.

Finally, the mass list sheets contained all necessary information for any identified lipid species. Those information included retention time of the analytes separated by the described chromatography method, sum formulas, lipid species information (number of carbon chain length and double bonds), molecular weight, as well as the high-resolution mass of the most abundant adduct-ion for each lipid species (example given fig. 9). All in all, 12 different lipid classes and over 450 lipid species with even and odd FA chains could be assigned. For data processing, mass lists of all lipid classes were merged into two different excel sheets, depending on the charge state of their most abundant adduct ion. The final mass lists for further data processing contained manually assigned species of the lipid classes TAG, PC, PE, PS, PI, LPC, Cer, hydroxy Cer (Cer-OH), Hex-Cer, hydroxy Hex-Cer (Hex-Cer-OH), SM and ubiquinone for positive ESI data and PE, PS, and PI for negative ESI data (Table S2).

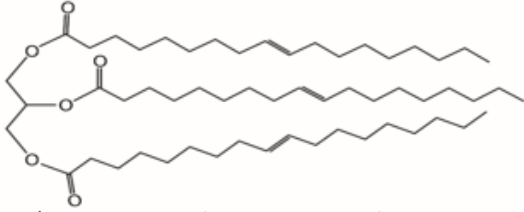
| tri-acylglycerol (TAG) | | | | | | | | | |  | | |
|------------------------|-----|----|-----|---|---|---|---|---------------|--------------------------------|--|---------------|-----------------|
| Backbone | | | | | | | | | | C | 12 | |
| | | | | | | | | | | H | 1.007825 | |
| | | | | | | | | | | O | 15.99491 | |
| | | | | | | | | | | P | 30.973761 | |
| | | | | | | | | | | N | 14.00307 | |
| | | | | | | | | | | e | 0.0005486 | |
| | | | | | | | | | | H+ | 1.0072764 | |
| | | | | | | | | | | D | 2.014102 | |
| | | | | | | | | | | Na | 22.989769 | |
| | | | | | | | | | | positive | | |
| | | | | | | | | | | ammonium adduct | Sodium adduct | Hydrogen adduct |
| Seitenkette | dbs | C | H | O | P | N | D | high res mass | mass(form[NH4+]) name[NH4+] | | | tR (min) |
| 42 : | 0 | 45 | 86 | 6 | 0 | 0 | 0 | 722.6424 | 740.6768 | 745.6322 | 723.6502 | 15.02 |
| 42 : | 1 | 45 | 84 | 6 | 0 | 0 | 0 | 720.6268 | 738.6611 | 743.6165 | 721.6346 | 14.95 |
| 42 : | 2 | 45 | 82 | 6 | 0 | 0 | 0 | 718.6111 | 736.6455 | 741.6009 | 719.6189 | 14.17 |
| 42 : | 3 | 45 | 80 | 6 | 0 | 0 | 0 | 716.5955 | 734.6298 | 739.5852 | 717.6033 | 13.67 |
| 42 : | 4 | 45 | 78 | 6 | 0 | 0 | 0 | 714.5798 | 732.6142 | 737.5696 | 715.5876 | 13.30 |
| 42 : | 5 | 45 | 76 | 6 | 0 | 0 | 0 | 712.5642 | 730.5985 | 735.5539 | 713.5720 | 12.77 |
| 42 : | 6 | 45 | 74 | 6 | 0 | 0 | 0 | 710.5485 | 728.5829 | 733.5383 | 711.5563 | 12.45 |
| 44 : | 0 | 47 | 90 | 6 | 0 | 0 | 0 | 750.6737 | 768.7081 | 773.6635 | 751.6815 | 15.59 |
| 44 : | 1 | 47 | 88 | 6 | 0 | 0 | 0 | 748.6581 | 766.6924 | 771.6478 | 749.6659 | 15.18 |
| 44 : | 2 | 47 | 86 | 6 | 0 | 0 | 0 | 746.6424 | 764.6768 | 769.6322 | 747.6502 | 14.76 |
| 44 : | 3 | 47 | 84 | 6 | 0 | 0 | 0 | 744.6268 | 762.6611 | 767.6165 | 745.6346 | 14.35 |
| 44 : | 4 | 47 | 82 | 6 | 0 | 0 | 0 | 742.6111 | 760.6455 | 765.6009 | 743.6189 | 13.93 |
| 44 : | 5 | 47 | 80 | 6 | 0 | 0 | 0 | 740.5955 | 758.6298 | 763.5852 | 741.6033 | 13.65 |
| 44 : | 6 | 47 | 78 | 6 | 0 | 0 | 0 | 738.5798 | 756.6142 | 761.5696 | 739.5876 | 13.40 |
| 46 : | 0 | 49 | 94 | 6 | 0 | 0 | 0 | 778.7050 | 796.7394 | 801.6948 | 779.7128 | 16.14 |
| 46 : | 1 | 49 | 92 | 6 | 0 | 0 | 0 | 776.6894 | 794.7237 | 799.6791 | 777.6972 | 15.75 |
| 46 : | 2 | 49 | 90 | 6 | 0 | 0 | 0 | 774.6737 | 792.7081 | 797.6635 | 775.6815 | 15.36 |
| 46 : | 3 | 49 | 88 | 6 | 0 | 0 | 0 | 772.6581 | 790.6924 | 795.6478 | 773.6659 | 14.96 |
| 46 : | 4 | 49 | 86 | 6 | 0 | 0 | 0 | 770.6424 | 788.6768 | 793.6322 | 771.6502 | 14.65 |
| 46 : | 5 | 49 | 84 | 6 | 0 | 0 | 0 | 768.6268 | 786.6611 | 791.6165 | 769.6346 | 14.21 |
| 46 : | 6 | 49 | 82 | 6 | 0 | 0 | 0 | 766.6111 | 784.6455 | 789.6009 | 767.6189 | 13.91 |
| 48 : | 0 | 51 | 98 | 6 | 0 | 0 | 0 | 806.7363 | 824.7707 | 829.7261 | 807.7441 | 16.64 |
| 48 : | 1 | 51 | 96 | 6 | 0 | 0 | 0 | 804.7207 | 822.7550 | 827.7104 | 805.7285 | 16.29 |
| 48 : | 2 | 51 | 94 | 6 | 0 | 0 | 0 | 802.7050 | 820.7394 | 825.6948 | 803.7128 | 15.90 |
| 48 : | 3 | 51 | 92 | 6 | 0 | 0 | 0 | 800.6894 | 818.7237 | 823.6791 | 801.6972 | 15.53 |
| 48 : | 4 | 51 | 90 | 6 | 0 | 0 | 0 | 798.6737 | 816.7081 | 821.6635 | 799.6815 | 15.16 |
| 48 : | 5 | 51 | 88 | 6 | 0 | 0 | 0 | 796.6581 | 814.6924 | 819.6478 | 797.6659 | 14.87 |
| 48 : | 6 | 51 | 86 | 6 | 0 | 0 | 0 | 794.6424 | 812.6768 | 817.6322 | 795.6502 | 14.50 |
| 48 : | 7 | 51 | 84 | 6 | 0 | 0 | 0 | 792.6268 | 810.6611 | 815.6165 | 793.6346 | 14.21 |
| 50 : | 0 | 53 | 102 | 6 | 0 | 0 | 0 | 834.7676 | 852.8020 | 857.7574 | 835.7754 | 17.06 |
| 50 : | 1 | 53 | 100 | 6 | 0 | 0 | 0 | 832.7520 | 850.7863 | 855.7417 | 833.7598 | 16.75 |
| 50 : | 2 | 53 | 98 | 6 | 0 | 0 | 0 | 830.7363 | 848.7707 | 853.7261 | 831.7441 | 16.45 |
| 50 : | 3 | 53 | 96 | 6 | 0 | 0 | 0 | 828.7207 | 846.7550 | 851.7104 | 829.7285 | 16.07 |
| 50 : | 4 | 53 | 94 | 6 | 0 | 0 | 0 | 826.7050 | 844.7394 | 849.6948 | 827.7128 | 15.68 |

Figure 9: LDA 2 mass-list example. Mass list of TAG containing all assigned information of identified lipid species in mammalian tissues e.g. the number of carbon atoms and double bonds, high-resolution mass of the molecule ions, possible adduct-ions and retention time, according to the format rules for LDA 2 application.

Next, all MS raw data were analyzed using LDA 2 version 2.6.1 [46], which utilized mass list entries for automatic peak detection and integration. For all further data processing evaluations, LDA 2 data for all lipid species were exported as raw peak areas in .xls file format.

Altogether, MS raw data of the 192 measurements (12 tissues, 2 genotypes, 4 mice per genotype, and 2 charge states) were analyzed and yield approximately 42,000 data points (Fig. 10).

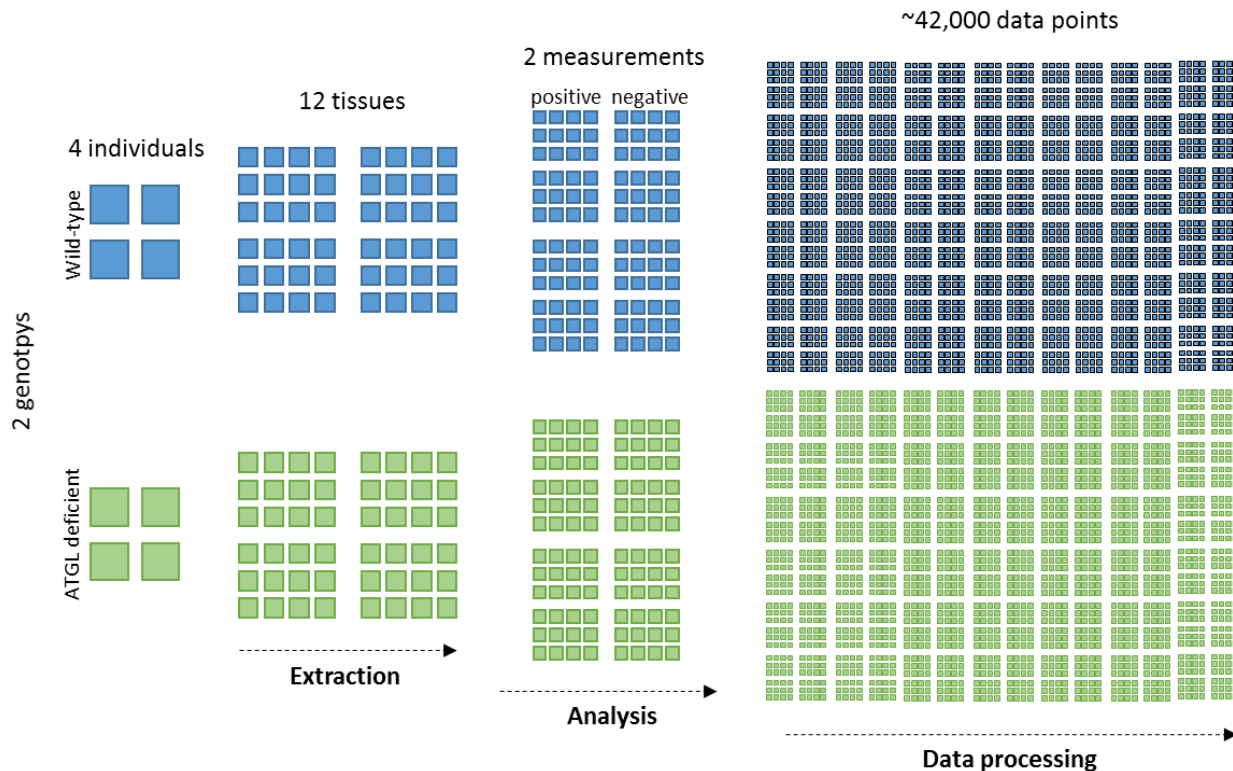


Figure 10: Visualization of data increase in course of the lipidomics workflow on a big, biological sample set.

4.3. Data processing II - Data normalization and statistical analysis

Raw data normalization and subsequent statistical analysis is the most important but also the most time consuming and error-prone part in data processing. The level of complexity correlates with increasing amount of data. One solution to reduce the required time and possible bias of manual data processing are software based data processing pipelines. Thereby Microsoft Excel represents one option for big data processing by the use of recursive formula. Although Excel is not a specialized big-data processing software, it is widely available and can be used to make MS data processing accessible for “non-bioinformatic” MS user.

4.3.1. Development of an Excel based “data processing sheet”

Therefore, the next aim of this work was the development of a semi-automated, Excel-based data processing sheet (DPS) for LDA 2 raw data processing. Thereby, the DPS

should be based on a formula system, which allows automated execution of several calculation steps after an initial data input and should be adaptable to sample set size (Fig. 11). To achieve this aims several spreadsheets containing various sample information and calculation steps were implemented into the DPS file.

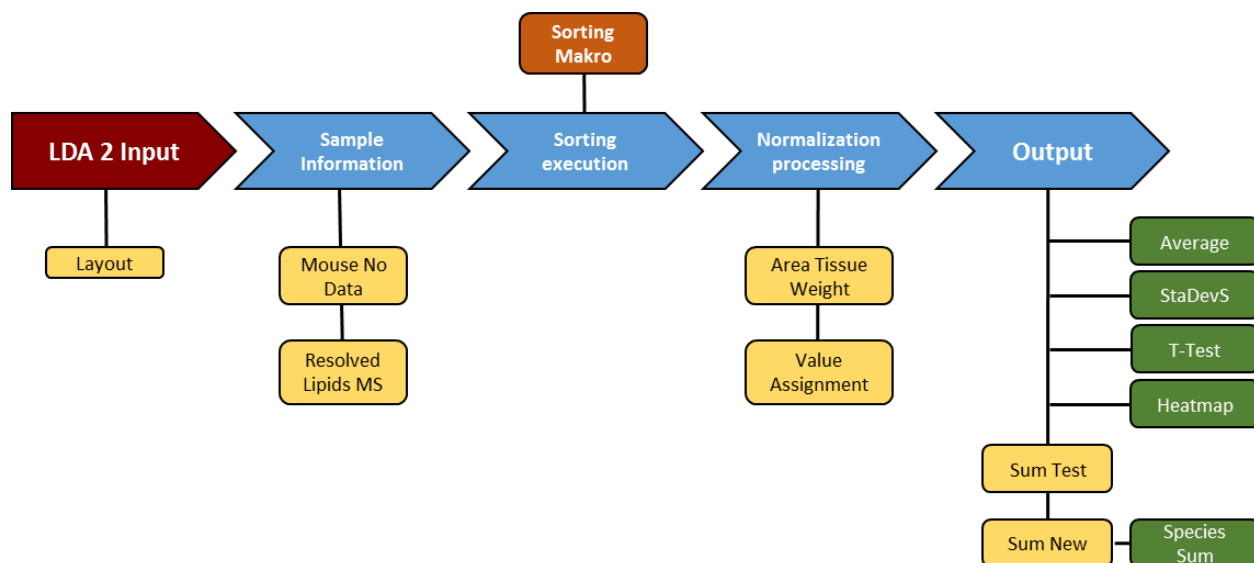


Figure 11: Flowchart for data processing of LDA 2 output data with DPS.

4.3.1.1. DPS – Sample Information

Since the information of the LDA 2 output is depending on parameters like raw data and mass list file name as well as on the annotation of lipid species, it was necessary to define a uniform nomenclature prior to the MS analysis. To define all necessary pre-analysis information, sample names were given according to an intra-laboratory code consisting of “date_project name_chromatography_tissue_mouse ID”. For automated data processing, several additional sample information, like mouse number, genotype, tissue name, and tissue weight were inserted into the “Mouse No Data” spreadsheets (Fig. 12). Upon entry, “Short Tags” were generated by a formula picking up the first three letters of each tissue. This 3-letter code was necessary for further data sorting steps. The genotype column contained additionally a continuous number for further processing steps. “Resolved Lipids MS” is a second spreadsheet for manual data import, containing all essential information of lipid extract treatment like used solvent volume, final sample dilution, as well as UPLC injection volume. The dilution and injected volume entry

becomes important in the further course of the process when data are normalized without ISTD, which formula is linked to a separate sheet. The LDA 2 software supports normalization by defined ISTD species. Nevertheless, the software takes the median of all ISTD values from all measurements and set them this the base value. This base value can be inserted into the LDA ISTD balance factor field of the DPS to reset all normalized values.

| Short Tags: | | bra | duo | jej | ile | col | sto | Adr | liv | Ton | hea | lun | spl | pan | kid | BAT | iWAT | gWAT | qua | gas | sol | pla |
|-------------|----------|---------|-----------|---------|-------|-------|---------|---------------|-------|--------|-------|------|--------|----------|--------|------|------|------|------------|----------------|--------|--------|
| Mouse No | Genotype | Tissues | | | | | | | | | | | | | | | | | | | | |
| | | brain | duode num | jejunum | ileum | colon | stomach | Adrenal Gland | liver | Tongue | heart | lung | spleen | pancreas | kidney | BAT | iWAT | gWAT | quadriceps | gastrocne mius | soleus | plasma |
| 95982 | KO 1 | 456 | 234 | 261 | 148 | 137 | 109 | 3 | 231 | 42 | 133 | 131 | 36 | 67 | 240 | 488 | 329 | 278 | 210 | 210 | 14 | 89 |
| 95987 | KO 2 | 421 | 65 | 50 | 136 | 83 | 97 | 5.5 | 140 | 75 | 146 | 116 | 41 | 33 | 241 | 445 | 472 | 302 | 217 | 208 | 13 | 100 |
| 95988 | KO 3 | 403 | 64 | 135 | 107 | 132 | 49 | 4 | 117 | 47 | 131 | 120 | 39 | 87 | 214 | 403 | 299 | 243 | 222 | 197 | 12 | 97 |
| 95990 | KO 4 | 434 | 41 | 166 | 88 | 85 | 45 | 5 | 172 | 46 | 120 | 95 | 30 | 58 | 180 | 345 | 344 | 254 | 176 | 172 | 11 | 102 |
| 95970 | WT 1 | 414 | 228.6 | 287 | 195 | 132 | 120 | 3.8 | 262 | 57.6 | 72.2 | 97.7 | 39 | 103 | 207.7 | 30.9 | 69.4 | 52.8 | 210.8 | 185 | 11.7 | 100 |
| 95995 | WT 2 | 423 | 61 | 155 | 87 | 115 | 61 | 5 | 219 | 47 | 117 | 105 | 37 | 69 | 181 | 16 | 66 | 39 | 203 | 171 | 12 | 94 |
| 95996 | WT 3 | 426 | 50 | 187 | 103 | 116 | 66 | 6 | 230 | 51 | 93 | 120 | 53 | 88 | 222 | 38 | 50 | 40 | 215 | 193 | 12 | 101 |
| 96034 | WT 4 | 436 | 89 | 178 | 122 | 117 | 63 | 5 | 226 | 42 | 93 | 127 | 44 | 93 | 208 | 36 | 75 | 82 | 177 | 210 | 12 | 106 |
| 95934 | WT 4 | 436 | 89 | 178 | 122 | 117 | 63 | 5 | 226 | 42 | 93 | 127 | 44 | 93 | 208 | 36 | 75 | 82 | 177 | 210 | 12 | 106 |

| Injected Volume Q-TOF (µL) | | Resolved Volume of lipids with Dilution for MS (µL) | | | | | | | | | | LDA ISTD balance factor | | | | | | | | | | | |
|----------------------------|----------|---|-----------|---------|-------|-------|---------|---------------|-------|--------|-------|-------------------------|--------|----------|--------|-----|------|------|------------|----------------|--------|--------|--|
| Mouse No | Genotype | Dilution | | 1:5 | | | | | | | | | | 1:5 | | | | | | | | | |
| | | brain | duode num | jejunum | ileum | colon | stomach | Adrenal Gland | liver | Tongue | heart | lung | spleen | pancreas | kidney | BAT | iWAT | gWAT | quadriceps | gastrocne mius | soleus | plasma | |
| 95982 | KO 1 | 500 | | | | | | | 250 | 5000 | 250 | 1500 | 500 | 250 | 250 | 250 | 7500 | | | 250 | | 200 | |
| 95987 | KO 2 | 500 | | | | | | | 250 | 5000 | 250 | 1500 | 500 | 250 | 250 | 250 | 7500 | | | 250 | | 200 | |
| 95988 | KO 3 | 500 | | | | | | | 250 | 16667 | 250 | 1500 | 500 | 250 | 250 | 250 | 7500 | | | 250 | | 200 | |
| 95990 | KO 4 | 500 | | | | | | | 250 | 5000 | 250 | 1500 | 500 | 250 | 250 | 250 | 7500 | | | 250 | | 200 | |
| 95970 | WT 1 | 500 | | | | | | | 250 | 5000 | 250 | 1500 | 500 | 250 | 250 | 250 | 2500 | | | 250 | | 200 | |
| 95995 | WT 2 | 500 | | | | | | | 250 | 5000 | 250 | 1500 | 500 | 250 | 250 | 250 | 2500 | | | 250 | | 200 | |
| 95996 | WT 3 | 500 | | | | | | | 250 | 5000 | 250 | 1500 | 500 | 250 | 250 | 250 | 2500 | | | 250 | | 200 | |
| 96034 | WT 4 | 500 | | | | | | | 250 | 5000 | 250 | 1500 | 500 | 250 | 250 | 250 | 2500 | | | 250 | | 200 | |
| 95934 | WT 4 | 500 | | | | | | | 250 | 5000 | 250 | 1500 | 500 | 250 | 250 | 250 | 2500 | | | 250 | | 200 | |

Figure 12: Snapshot of DPS annotation spreadsheets “Mouse No Data” and “Resolved Lipids MS”. These spreadsheets contained all necessary sample information for further calculation steps. “Mouse No Data” contained information on mouse ID, genotype, tissue name and tissue weight (mg). A “Short Tags” formula automatically picked up the first three letters of each tissue. “Resolved Lipids MS” contained information about lipid extract treatment, like injected volume and dilution (µL). ISTD balance factor can be inserted for a LDA 2 normalization reset (right red box).

4.3.1.2. DPS – LDA 2 data input and automated sorting

Upon import of LDA 2-generated data into the “Layout sheet” (yellow box, Fig. 13) the processing procedure was initiated. Several following actions, like column assignment and insertion of tissue information were automatically executed. Thereby, the “Name Search function” column contained the full tissue name and mouse number from the “RAW LDA 2 Input” column. The “Mouse No” column was filled with mouse number information out of “Name Search function” column based on defaults from “Mouse No Search”. Subsequently, the columns “Row” and “Column” assigned the according information on tissue weight, located in “Mouse No Data” spreadsheet. The sorting button

over the “Tag + Genotype” column allowed alphabetical sorting. The defined number of used replicas in the red box “Number of Replicas” was changeable and was considered in all formula calculations. Only an identical number of replicates between genotypes was allowed (Fig. 13).

| Mouse No | Row | Column | Sort Tag + Genotype | Tissue weight | Name Search function | RAW LDA 2 Input | Number of Replicas: 4 | | | | Mouse No Search: 9 | | | | | |
|----------|-----|--------|------------------------|---------------|----------------------|---------------------------------|-----------------------|-------|------|-------|--------------------|-------|-------|-------|-------|-------|
| | | | | | | | 42:0 | 42:1 | 42:2 | 42:3 | 42:4 | 44:0 | 44:1 | 44:2 | 44:3 | 44:4 |
| 95982 | 5 | 10 | Adr KO 1 | 3 | Adrenal_Gland_95982 | 0913_LDB_HP_Adrenal_Gland_95982 | Value | 604.1 | 0 | 517.2 | 294.96 | 109.1 | 1102 | 2088 | 1467 | 374.3 |
| 95987 | 6 | 10 | Adr KO 2 | 5.5 | Adrenal_Gland_95987 | 0913_LDB_HP_Adrenal_Gland_95987 | Value | 1339 | 0 | 1818 | 965.83 | 279.2 | 2810 | 5514 | 4090 | 1300 |
| 95988 | 7 | 10 | Adr KO 3 | 4 | Adrenal_Gland_95988 | 0913_LDB_HP_Adrenal_Gland_95988 | Value | 368.6 | 0 | 564 | 281.28 | 0 | 977.1 | 1944 | 1200 | 237.9 |
| 95990 | 8 | 10 | Adr KO 4 | 5 | Adrenal_Gland_95990 | 0913_LDB_HP_Adrenal_Gland_95990 | Value | 786.2 | 0 | 1355 | 589.75 | 178.9 | 1117 | 4223 | 2837 | 776.6 |
| 95970 | 9 | 10 | Adr WT 1 | 3.8 | Adrenal_Gland_95970 | 0913_LDB_HP_Adrenal_Gland_95970 | Value | 0 | 0 | 0 | 0 | 0 | 75.65 | 0 | 113.7 | 0 |
| 95995 | 10 | 10 | Adr WT 2 | 5 | Adrenal_Gland_95995 | 0913_LDB_HP_Adrenal_Gland_95995 | Value | 144.5 | 0 | 469.5 | 179.02 | 0 | 623.7 | 1150 | 843.5 | 0 |
| 95996 | 11 | 10 | Adr WT 3 | 6 | Adrenal_Gland_95996 | 0913_LDB_HP_Adrenal_Gland_95996 | Value | 0 | 0 | 71.28 | 0 | 0 | 119.7 | 0 | 129.6 | 0 |
| 95934 | 13 | 10 | Adr WT 4 | 5 | Adrenal_Gland_95934 | 0913_LDB_HP_Adrenal_Gland_95934 | Value | 0 | 0 | 245.7 | 76.37 | 0 | 271.6 | 561.6 | 417.6 | 127.4 |
| 95982 | 5 | 18 | BAT KO 1 | 488 | BAT_95982 | 1106_LDB_HP_BAT_95982 | Value | 15064 | 0 | 12172 | 5358.3 | 2081 | 23088 | 44243 | 36132 | 6507 |
| 95987 | 6 | 18 | BAT KO 2 | 445 | BAT_95987 | 1106_LDB_HP_BAT_95987 | Value | 18493 | 0 | 13590 | 7964.8 | 2891 | 26055 | 55249 | 39952 | 8493 |
| 95988 | 7 | 18 | BAT KO 3 | 403 | BAT_95988 | 1106_LDB_HP_BAT_95988 | Value | 0 | 0 | 0 | 0 | 0 | 0 | 0 | 0 | 0 |
| 95990 | 8 | 18 | BAT KO 4 | 345 | BAT_95990 | 1106_LDB_HP_BAT_95990 | Value | 0 | 0 | 0 | 0 | 0 | 0 | 0 | 0 | 0 |
| 95970 | 9 | 18 | BAT WT 1 | 30.9 | BAT_95970 | 1106_LDB_HP_BAT_95970 | Value | 0 | 0 | 0 | 0 | 0 | 0 | 0 | 0 | 0 |
| 95995 | 10 | 18 | BAT WT 2 | 16 | BAT_95995 | 1106_LDB_HP_BAT_95995 | Value | 1245 | 2635 | 5552 | 3407.3 | 651.8 | 4035 | 8246 | 9301 | 5017 |
| 95996 | 11 | 18 | BAT WT 3 | 38 | BAT_95996 | 1106_LDB_HP_BAT_95996 | Value | 0 | 0 | 0 | 0 | 0 | 0 | 0 | 0 | 0 |
| 96034 | 12 | 18 | BAT WT 4 | 36 | BAT_96034 | 1106_LDB_HP_BAT_96034 | Value | 1241 | 0 | 8125 | 6446.6 | 2112 | 2774 | 6847 | 10382 | 7438 |
| 95982 | 5 | 4 | bra KO 1 | 456 | brain_95982 | 1024_LDB_HP_brain_95982 | Value | 689.2 | 0 | 0 | 0 | 0 | 1545 | 1525 | 788.9 | 0 |
| 95987 | 6 | 4 | bra KO 2 | 421 | brain_95987 | 1024_LDB_HP_brain_95987 | Value | 0 | 0 | 0 | 1365.6 | 0 | 1220 | 1044 | 452.4 | 0 |
| 95988 | 7 | 4 | bra KO 3 | 403 | brain_95988 | 1024_LDB_HP_brain_95988 | Value | 332.8 | 0 | 0 | 1006.7 | 0 | 980.9 | 788.4 | 416.6 | 0 |
| 95990 | 8 | 4 | bra KO 4 | 434 | brain_95990 | 1024_LDB_HP_brain_95990 | Value | 0 | 0 | 0 | 0 | 0 | 1202 | 1130 | 205.3 | 0 |
| 95970 | 9 | 4 | bra WT 1 | 414.3 | brain_95970 | 1024_LDB_HP_brain_95970 | Value | 0 | 0 | 0 | 530.77 | 0 | 0 | 0 | 1776 | 0 |
| 95995 | 10 | 4 | bra WT 2 | 423 | brain_95995 | 1024_LDB_HP_brain_95995 | Value | 0 | 0 | 0 | 0 | 0 | 0 | 0 | 0 | 0 |
| 95996 | 11 | 4 | bra WT 3 | 426 | brain_95996 | 1024_LDB_HP_brain_95996 | Value | 0 | 0 | 0 | 1094.9 | 0 | 0 | 0 | 0 | 0 |
| 96034 | 12 | 4 | bra WT 4 | 436 | brain_96034 | 1024_LDB_HP_brain_96034 | Value | 0 | 0 | 0 | 0 | 0 | 0 | 0 | 2121 | 0 |
| 95982 | 5 | 13 | hea KO 1 | 133 | heart_95982 | 0926_LDB_HP_heart_95982 | Value | 0 | 0 | 0 | 0 | 0 | 0 | 0 | 0 | 0 |
| 95987 | 6 | 13 | hea KO 2 | 146 | heart_95987 | 0926_LDB_HP_heart_95987 | Value | 0 | 0 | 0 | 0 | 0 | 0 | 0 | 0 | 0 |
| 95988 | 7 | 13 | hea KO 3 | 131 | heart_95988 | 0926_LDB_HP_heart_95988 | Value | 0 | 0 | 0 | 0 | 0 | 0 | 0 | 0 | 0 |
| 95990 | 8 | 13 | hea KO 4 | 120 | heart_95990 | 0926_LDB_HP_heart_95990 | Value | 195.9 | 0 | 0 | 0 | 0 | 877.8 | 1135 | 995.8 | 0 |
| 95970 | 9 | 13 | hea WT 1 | 72.2 | heart_95970 | 0926_LDB_HP_heart_95970 | Value | 0 | 0 | 0 | 0 | 0 | 0 | 0 | 0 | 0 |
| 95995 | 10 | 13 | hea WT 2 | 117 | heart_95995 | 0926_LDB_HP_heart_95995 | Value | 0 | 0 | 0 | 0 | 0 | 0 | 0 | 0 | 0 |
| 95996 | 11 | 13 | hea WT 3 | 93 | heart_95996 | 0926_LDB_HP_heart_95996 | Value | 0 | 0 | 0 | 0 | 0 | 0 | 0 | 0 | 0 |
| 95934 | 13 | 13 | hea WT 4 | 93 | heart_95934 | 0926_LDB_HP_heart_95934 | Value | 0 | 0 | 0 | 0 | 0 | 557.4 | 520.2 | 397 | 0 |
| 95982 | 5 | 17 | kid KO 1 | 240 | kidney_95982 | 1024_LDB_HP_kidney_95982 | Value | 0 | 0 | 0 | 0 | 0 | 0 | 0 | 0 | 0 |
| 95987 | 6 | 17 | kid KO 2 | 241 | kidney_95987 | 1024_LDB_HP_kidney_95987 | Value | 11533 | 4482 | 4017 | 0 | 0 | 22123 | 38199 | 30865 | 4483 |

Figure 13: Snapshot of DPS “Layout” spreadsheet for LDA 2 data input. Master spreadsheet for the import of LDA 2 data (e.g. TAG species). By using information from the “Mouse No Data” spreadsheet, several parameters e.g. mouse ID, tissue information, as well as tissue weight, were automatically inserted. Several parameters like “Number of replicas” as well as “Mouse No Search” were changeable.

4.3.1.3. DPS – Data normalization

Next, the normalization process was executed in the “Area Tissue Weight” spreadsheet (Fig. 14, top). First, the formula verified whether the area values were unequal 0, otherwise, the output was “Zero”. Following, the area values were divided by the ISTD balance factor as well as by the tissue weight. For normalization without ISTD, a different formula considered the dilution from the “Resolved Lipids MS” spreadsheet for data normalization.

The “Value assignment” (Fig. 14, bottom) spreadsheet supported additional alignment processes of various sheets. In this intermediate step, all Zero values were assigned “1”, values unequal 0 were assigned "0". This step was mandatory for further data alignment steps.

| | 42.0 | 42.1 | 42.2 | 42.3 | 42.4 | 44.0 | 44.1 | 44.2 | 44.3 | 44.4 | 46.0 | 46.1 | 46.2 | 46.3 | 46.4 | 48.0 | 48.1 | 48.2 | 48.3 | 48.4 | 48.5 | 48.6 | 50.0 | 50.1 | 50.2 | 50.3 | 50.4 | 50.5 |
|---------------------------------|-------|------|------|------|------|------|------|------|------|------|------|------|------|------|------|------|------|------|------|------|------|------|------|------|------|------|------|------|
| 0913_LDB_HP_Adrenal_Gland_95982 | Value | 0.1 | Zero | 0.1 | 0.1 | 0.0 | 0.3 | 0.5 | 0.4 | 0.1 | Zero | 0.7 | 1.2 | 1.5 | 0.5 | 0.1 | Zero | Zero | 4.2 | 2.7 | 0.8 | 0.1 | 0.0 | 1.3 | 21.7 | 95.1 | 10.1 | 4.6 |
| 0913_LDB_HP_Adrenal_Gland_95987 | Value | 0.2 | Zero | 0.2 | 0.1 | 0.0 | 0.4 | 0.7 | 0.5 | 0.2 | Zero | 0.8 | 2.0 | Zero | 0.8 | 0.1 | 2.4 | 6.6 | 5.8 | 4.0 | 1.3 | 0.2 | Zero | 2.2 | 24.7 | 46.0 | 26.4 | 5.8 |
| 0913_LDB_HP_Adrenal_Gland_95988 | Value | 0.1 | Zero | 0.1 | 0.1 | Zero | 0.2 | 0.4 | 0.2 | 0.0 | Zero | 0.5 | 1.1 | 1.1 | 0.3 | 0.0 | 1.7 | Zero | 3.7 | 2.4 | 0.6 | 0.1 | Zero | 1.4 | 20.1 | 26.9 | 7.9 | 3.7 |
| 0913_LDB_HP_Adrenal_Gland_95990 | Value | 0.1 | Zero | 0.2 | 0.1 | 0.0 | 0.2 | 0.6 | 0.4 | 0.1 | Zero | 0.8 | Zero | 1.7 | 0.5 | 0.1 | 2.3 | 5.7 | 5.1 | 2.4 | 0.8 | 0.1 | Zero | 1.9 | 26.4 | 38.8 | 12.8 | 3.9 |
| 0913_LDB_HP_Adrenal_Gland_95970 | Value | 0 | Zero | Zero | Zero | Zero | 0.0 | Zero | 0.0 | Zero | Zero | 0.1 | 0.1 | 0.1 | 0.0 | Zero | 0.3 | 0.7 | 0.6 | 0.3 | 0.0 | Zero | 0.3 | 2.2 | 2.6 | 1.6 | 0.6 | |
| 0913_LDB_HP_Adrenal_Gland_95995 | Value | 0.0 | Zero | 0.1 | 0.0 | Zero | 0.1 | 0.2 | 0.1 | Zero | Zero | 0.3 | 0.5 | 0.5 | 0.2 | 0.0 | 0.8 | 1.9 | 1.9 | 1.1 | 0.2 | 0.0 | 0.0 | 1.0 | 8.8 | 6.0 | 3.9 | Zero |
| 0913_LDB_HP_Adrenal_Gland_95996 | Value | 0 | Zero | 0.0 | Zero | Zero | 0.0 | Zero | 0.0 | Zero | Zero | 0.1 | 0.1 | 0.1 | 0.0 | Zero | 0.2 | 0.5 | 0.5 | 0.2 | 0.0 | 0.0 | Zero | 0.3 | 1.4 | 1.7 | 1.0 | 0.4 |
| 0913_LDB_HP_Adrenal_Gland_95934 | Value | 0 | Zero | 0.0 | 0.0 | Zero | 0.0 | 0.1 | 0.1 | 0.0 | Zero | 0.2 | 0.3 | 0.3 | 0.1 | 0.0 | 0.4 | 1.2 | 1.2 | 0.7 | 0.2 | 0.0 | 0.0 | 0.6 | Zero | 0.4 | 2.8 | 0.2 |
| 1106_LDB_HP_BAT_95982 | Value | 0.0 | Zero | 0.0 | 0.0 | 0.0 | 0.0 | 0.1 | 0.1 | 0.0 | Zero | 0.0 | Zero | 0.1 | 0.1 | 0.0 | 0.2 | 0.2 | 0.2 | 0.1 | 0.0 | Zero | 0.0 | 0.4 | 0.6 | 0.5 | 0.3 | |
| 1106_LDB_HP_BAT_95987 | Value | 0.0 | Zero | 0.0 | 0.0 | 0.0 | 0.0 | 0.1 | 0.1 | 0.0 | Zero | 0.0 | 0.2 | 0.2 | 0.1 | 0.0 | 0.0 | Zero | 0.3 | 0.3 | 0.1 | 0.0 | Zero | 0.0 | 0.9 | 0.8 | 0.6 | 0.3 |
| 1106_LDB_HP_BAT_95988 | Value | 0 | Zero | Zero | Zero | Zero | Zero | Zero | Zero | Zero | Zero | Zero | Zero | Zero | Zero | Zero | Zero | Zero | Zero | Zero | Zero | Zero | Zero | Zero | Zero | Zero | Zero | Zero |
| 1106_LDB_HP_BAT_95990 | Value | 0 | Zero | Zero | Zero | Zero | Zero | Zero | Zero | Zero | Zero | Zero | Zero | Zero | Zero | Zero | Zero | Zero | Zero | Zero | Zero | Zero | Zero | Zero | Zero | Zero | Zero | Zero |
| 1106_LDB_HP_BAT_95970 | Value | 0 | Zero | Zero | Zero | Zero | Zero | Zero | Zero | Zero | Zero | Zero | Zero | Zero | Zero | Zero | Zero | Zero | Zero | Zero | Zero | Zero | Zero | Zero | Zero | Zero | Zero | Zero |
| 1106_LDB_HP_BAT_95995 | Value | 0.1 | 0.1 | 0.3 | 0.2 | 0.0 | 0.2 | 0.4 | 0.4 | 0.2 | 0.1 | 0.5 | 1.4 | 1.7 | 0.9 | 0.3 | 0.9 | 3.8 | 5.2 | 4.2 | 1.5 | 0.2 | 0.1 | 1.2 | 11.1 | 16.7 | 11.4 | Zero |
| 1106_LDB_HP_BAT_95996 | Value | 0 | Zero | Zero | Zero | Zero | Zero | Zero | Zero | Zero | Zero | Zero | Zero | Zero | Zero | Zero | Zero | Zero | Zero | Zero | Zero | Zero | Zero | Zero | Zero | Zero | Zero | Zero |
| 1106_LDB_HP_BAT_96034 | Value | 0.0 | Zero | 0.2 | 0.1 | 0.0 | 0.1 | 0.1 | 0.2 | 0.2 | 0.0 | 0.1 | 0.4 | 0.6 | 0.4 | 0.2 | 0.3 | 0.9 | 1.5 | 1.4 | 0.7 | 0.2 | 0.0 | 0.3 | 3.3 | 4.7 | 3.6 | 2.2 |
| 1024_LDB_HP_brain_95982 | Value | 0.0 | Zero | Zero | Zero | Zero | 0.0 | 0.0 | 0.0 | Zero | Zero | 0.0 | 0.0 | 0.0 | 0.0 | Zero | 0.0 | 0.0 | 0.0 | 0.0 | 0.0 | Zero | 0.0 | 0.0 | 0.1 | 0.1 | 0.1 | 0.0 |
| 1024_LDB_HP_brain_95987 | Value | 0 | Zero | Zero | 0.0 | Zero | 0.0 | 0.0 | 0.0 | Zero | Zero | 0.0 | 0.0 | 0.0 | 0.0 | 0.0 | 0.1 | 0.0 | 0.0 | 0.0 | Zero | 0.0 | 0.0 | 0.1 | 0.1 | 0.1 | 0.0 | 0.0 |
| 1024_LDB_HP_brain_95988 | Value | 0.0 | Zero | Zero | 0.0 | Zero | 0.0 | 0.0 | 0.0 | Zero | Zero | 0.0 | 0.0 | 0.0 | 0.0 | 0.0 | 0.0 | 0.0 | 0.0 | 0.0 | 0.0 | Zero | 0.0 | 0.0 | 0.1 | 0.1 | 0.1 | 0.0 |
| 1024_LDB_HP_brain_95990 | Value | 0 | Zero | Zero | Zero | Zero | 0.0 | 0.0 | 0.0 | Zero | Zero | 0.0 | 0.0 | 0.0 | 0.0 | 0.0 | 0.1 | 0.0 | 0.0 | 0.0 | Zero | Zero | 0.0 | 0.2 | 0.1 | Zero | 0.0 | 0.0 |
| 1024_LDB_HP_brain_95970 | Value | 0 | Zero | Zero | 0.0 | Zero | Zero | Zero | 0.0 | Zero | Zero | Zero | Zero | Zero | Zero | Zero | 0.0 | 0.0 | 0.0 | Zero | Zero | Zero | 0.0 | 0.0 | 0.0 | 0.0 | 0.0 | Zero |
| 1024_LDB_HP_brain_95995 | Value | 0 | Zero | Zero | Zero | Zero | Zero | Zero | Zero | Zero | Zero | Zero | Zero | Zero | Zero | Zero | Zero | Zero | Zero | Zero | Zero | Zero | Zero | Zero | Zero | Zero | Zero | Zero |
| 1024_LDB_HP_brain_95996 | Value | 0 | Zero | Zero | 0.0 | Zero | Zero | Zero | Zero | Zero | Zero | 0.0 | 0.0 | 0.0 | 0.0 | 0.0 | 0.0 | 0.0 | 0.0 | 0.0 | 0.0 | Zero | 0.0 | 0.0 | 0.0 | 0.0 | 0.0 | 0.0 |

| RAW LDA 2 Input | 42.0 | 42.1 | 42.2 | 42.3 | 42.4 | 44.0 | 44.1 | 44.2 | 44.3 | 44.4 | 46.0 | 46.1 | 46.2 | 46.3 | 46.4 | 48.0 | 48.1 | 48.2 | 48.3 | 48.4 | 48.5 | 48.6 | 50.0 | 50.1 | 50.2 | 50.3 | 50.4 | 50.5 |
|---------------------------------|-------|------|------|------|------|------|------|------|------|------|------|------|------|------|------|------|------|------|------|------|------|------|------|------|------|------|------|------|
| 0913_LDB_HP_Adrenal_Gland_95982 | Value | 0 | 1 | 0 | 0 | 0 | 0 | 0 | 0 | 0 | 1 | 0 | 0 | 0 | 0 | 0 | 1 | 1 | 0 | 0 | 0 | 0 | 0 | 0 | 0 | 0 | 0 | 0 |
| 0913_LDB_HP_Adrenal_Gland_95987 | Value | 0 | 1 | 0 | 0 | 0 | 0 | 0 | 0 | 0 | 1 | 0 | 0 | 1 | 0 | 0 | 0 | 0 | 0 | 0 | 0 | 0 | 1 | 0 | 0 | 0 | 0 | 0 |
| 0913_LDB_HP_Adrenal_Gland_95988 | Value | 0 | 1 | 0 | 0 | 1 | 0 | 0 | 0 | 0 | 1 | 0 | 0 | 0 | 0 | 0 | 0 | 1 | 0 | 0 | 0 | 0 | 1 | 0 | 0 | 0 | 0 | 0 |
| 0913_LDB_HP_Adrenal_Gland_95990 | Value | 0 | 1 | 0 | 0 | 0 | 0 | 0 | 0 | 0 | 1 | 0 | 1 | 0 | 0 | 0 | 0 | 0 | 0 | 0 | 0 | 0 | 0 | 1 | 0 | 0 | 0 | 0 |
| 0913_LDB_HP_Adrenal_Gland_95970 | Value | 0 | 1 | 1 | 1 | 1 | 1 | 1 | 1 | 0 | 1 | 1 | 0 | 0 | 0 | 1 | 0 | 0 | 0 | 0 | 0 | 0 | 1 | 1 | 0 | 0 | 0 | 0 |
| 0913_LDB_HP_Adrenal_Gland_95995 | Value | 0 | 1 | 0 | 0 | 1 | 0 | 0 | 0 | 1 | 1 | 0 | 0 | 0 | 0 | 0 | 0 | 0 | 0 | 0 | 0 | 0 | 0 | 0 | 0 | 0 | 0 | 1 |
| 0913_LDB_HP_Adrenal_Gland_95996 | Value | 0 | 1 | 0 | 0 | 1 | 0 | 0 | 0 | 1 | 1 | 0 | 0 | 0 | 0 | 0 | 0 | 0 | 0 | 0 | 0 | 0 | 0 | 0 | 0 | 0 | 0 | 0 |
| 0913_LDB_HP_Adrenal_Gland_95934 | Value | 0 | 1 | 0 | 0 | 1 | 0 | 0 | 0 | 1 | 1 | 0 | 0 | 0 | 0 | 0 | 0 | 0 | 0 | 0 | 0 | 0 | 0 | 1 | 0 | 0 | 0 | 0 |
| 1106_LDB_HP_BAT_95982 | Value | 0 | 1 | 0 | 0 | 0 | 0 | 0 | 0 | 0 | 1 | 0 | 1 | 0 | 0 | 0 | 0 | 0 | 0 | 0 | 0 | 0 | 0 | 0 | 1 | 0 | 0 | 0 |
| 1106_LDB_HP_BAT_95987 | Value | 0 | 1 | 0 | 0 | 0 | 0 | 0 | 0 | 0 | 1 | 0 | 0 | 0 | 0 | 0 | 0 | 0 | 0 | 0 | 0 | 0 | 0 | 0 | 1 | 0 | 0 | 0 |
| 1106_LDB_HP_BAT_95988 | Value | 0 | 1 | 0 | 0 | 0 | 0 | 0 | 0 | 0 | 1 | 0 | 0 | 0 | 0 | 0 | 0 | 0 | 0 | 0 | 0 | 0 | 0 | 0 | 1 | 0 | 0 | 0 |
| 1106_LDB_HP_BAT_95990 | Value | 0 | 1 | 1 | 1 | 1 | 1 | 1 | 1 | 1 | 1 | 1 | 1 | 1 | 1 | 1 | 1 | 1 | 1 | 1 | 1 | 1 | 1 | 1 | 1 | 1 | 1 | 1 |
| 1106_LDB_HP_BAT_95970 | Value | 0 | 1 | 1 | 1 | 1 | 1 | 1 | 1 | 1 | 1 | 1 | 1 | 1 | 1 | 1 | 1 | 1 | 1 | 1 | 1 | 1 | 1 | 1 | 1 | 1 | 1 | 1 |
| 1106_LDB_HP_BAT_95995 | Value | 0 | 0 | 0 | 0 | 0 | 0 | 0 | 0 | 0 | 0 | 0 | 0 | 0 | 0 | 0 | 0 | 0 | 0 | 0 | 0 | 0 | 0 | 0 | 0 | 0 | 0 | 1 |
| 1106_LDB_HP_BAT_95996 | Value | 0 | 1 | 1 | 1 | 1 | 1 | 1 | 1 | 1 | 1 | 1 | 1 | 1 | 1 | 1 | 1 | 1 | 1 | 1 | 1 | 1 | 1 | 1 | 1 | 1 | 1 | 1 |
| 1106_LDB_HP_BAT_96034 | Value | 0 | 1 | 0 | 0 | 0 | 0 | 0 | 0 | 0 | 0 | 0 | 0 | 0 | 0 | 0 | 0 | 0 | 0 | 0 | 0 | 0 | 0 | 0 | 0 | 0 | 0 | 0 |
| 1024_LDB_HP_brain_95982 | Value | 0 | 1 | 1 | 1 | 1 | 0 | 0 | 0 | 1 | 1 | 0 | 0 | 0 | 0 | 0 | 0 | 0 | 0 | 0 | 0 | 0 | 1 | 0 | 0 | 0 | 0 | 0 |
| 1024_LDB_HP_brain_95987 | Value | 0 | 1 | 1 | 0 | 1 | 0 | 0 | 0 | 1 | 1 | 0 | 0 | 0 | 0 | 0 | 0 | 0 | 0 | 0 | 0 | 0 | 1 | 0 | 0 | 0 | 0 | 0 |
| 1024_LDB_HP_brain_95988 | Value | 0 | 1 | 1 | 0 | 1 | 0 | 0 | 0 | 1 | 1 | 0 | 0 | 0 | 0 | 0 | 0 | 0 | 0 | 0 | 0 | 0 | 1 | 0 | 0 | 0 | 0 | 0 |
| 1024_LDB_HP_brain_95990 | Value | 0 | 1 | 1 | 1 | 1 | 0 | 0 | 0 | 1 | 1 | 0 | 0 | 0 | 0 | 0 | 0 | 0 | 0 | 0 | 0 | 0 | 1 | 0 | 0 | 0 | 0 | 0 |
| 1024_LDB_HP_brain_95970 | Value | 0 | 1 | 1 | 1 | 1 | 1 | 1 | 1 | 1 | 1 | 1 | 1 | 1 | 1 | 1 | 1 | 1 | 1 | 1 | 1 | 1 | 1 | 1 | 1 | 1 | 1 | 1 |
| 1024_LDB_HP_brain_95995 | Value | 0 | 1 | 1 | 1 | 1 | 1 | 1 | 1 | 1 | 1 | 1 | 1 | 1 | 1 | 1 | 1 | 1 | 1 | 1 | 1 | 1 | 1 | 1 | 1 | 1 | 1 | 1 |
| 1024_LDB_HP_brain_95996 | Value | 0 | 1 | 1 | 0 | 1 | 1 | 1 | 1 | 1 | 1 | 0 | 0 | 0 | 0 | 0 | 0 | 0 | 0 | 0 | 0 | 0 | 1 | 0 | 0 | 0 | 0 | 0 |

Figure 14: Snapshot of DPS normalization spreadsheets “Area Tissue Weight” and “Value Assignment”. “Area Tissue Weight” formula normalized LDA 2 values using tissue weight and ISTD balance factor. The output for non-detected area values was “Zero”. The “Value Assignment” formula assigned raw values unequal 0 with “0” and values equal 0 with “1”. This sheet was required for further alignment processes.

4.3.1.4. DPS – Data output

Finally, five different output spreadsheets were generated, which included commonly required calculations. The “Average” (Fig. 15, top) and “StaDevS” (Fig. 15, bottom) spreadsheets calculated the mean and standard deviations for each lipid species of the given tissues and genotypes. For non-detected analytes an additional function was implemented into the mean formula to discard 0 values in a group. The number of allowed drop-outs was changeable. The validation of those lipid species was executed by formulas linked to the “Value Assignment” spreadsheet information and the output for an exceeding number of outliers was “No Value”.

| Average | | Allowed invalid values: 2 | | | | | | | | | | | | | | | | | |
|---------------|---------|---------------------------|----------|----------|----------|----------|----------|----------|----------|----------|----------|----------|----------|----------|----------|----------|----------|----------|----------|
| Tissue | Genotyp | 42:0 | 42:1 | 42:2 | 42:3 | 42:4 | 44:0 | 44:1 | 44:2 | 44:3 | 44:4 | 46:0 | 46:1 | 46:2 | 46:3 | 46:4 | 48:0 | 48:1 | 48:2 |
| Adrenal Gland | KO 1 | 0.1 | No Value | 0.2 | 0.1 | 0.0 | 0.2 | 0.6 | 0.4 | 0.1 | No Value | 0.7 | 1.4 | 1.4 | 0.5 | 0.1 | 2.1 | 6.2 | 4.7 |
| Adrenal Gland | WT 1 | 0.0 | No Value | 0.0 | 0.0 | No Value | 0.0 | 0.1 | 0.1 | No Value | No Value | 0.2 | 0.3 | 0.3 | 0.1 | 0.0 | 0.4 | 1.1 | 1.1 |
| BAT | KO 1 | 0.0 | No Value | 0.0 | 0.0 | 0.0 | 0.0 | 0.1 | 0.1 | 0.0 | No Value | 0.0 | No Value | 0.2 | 0.1 | 0.0 | 0.0 | No Value | 0.3 |
| BAT | WT 1 | 0.0 | No Value | 0.2 | 0.1 | 0.0 | 0.1 | 0.3 | 0.3 | 0.2 | 0.0 | 0.3 | 0.9 | 1.1 | 0.6 | 0.2 | 0.6 | 2.4 | 3.3 |
| brain | KO 1 | 0.0 | No Value | No Value | 0.0 | No Value | 0.0 | 0.0 | 0.0 | No Value | No Value | 0.0 | 0.0 | 0.0 | 0.0 | 0.0 | 0.0 | 0.1 | 0.0 |
| brain | WT 1 | No Value | No Value | No Value | 0.0 | No Value | No Value | 0.0 | No Value | No Value | No Value | 0.0 | 0.0 | 0.0 | No Value | No Value | 0.0 | 0.0 | 0.0 |
| heart | KO 1 | 0.0 | No Value | No Value | No Value | No Value | No Value | No Value | No Value | No Value | No Value | No Value | No Value | No Value | No Value | No Value | No Value | No Value | No Value |
| heart | WT 1 | No Value | No Value | No Value | No Value | No Value | No Value | No Value | No Value | No Value | No Value | 0.0 | 0.0 | 0.0 | 0.0 | 0.0 | 0.0 | 0.1 | 0.1 |
| kidney | KO 1 | 0.0 | 0.0 | 0.0 | No Value | No Value | 0.1 | 0.1 | 0.1 | 0.0 | No Value | 0.1 | 0.3 | 0.3 | 0.2 | 0.0 | 0.2 | No Value | 0.8 |
| kidney | WT 1 | 0.0 | 0.0 | 0.0 | 0.0 | 0.0 | 0.0 | 0.1 | 0.1 | 0.0 | 0.0 | 0.1 | 0.1 | 0.2 | 0.2 | 0.1 | 0.1 | 0.3 | 0.4 |
| liver | KO 1 | No Value | No Value | No Value | No Value | No Value | No Value | No Value | No Value | No Value | No Value | No Value | No Value | No Value | No Value | No Value | No Value | No Value | No Value |
| liver | WT 1 | No Value | No Value | No Value | No Value | No Value | No Value | No Value | No Value | No Value | No Value | No Value | No Value | No Value | No Value | No Value | No Value | No Value | No Value |
| lung | KO 1 | 0.0 | 0.0 | 0.0 | 0.0 | No Value | 0.1 | 0.2 | 0.1 | 0.0 | No Value | 0.2 | 0.6 | 0.4 | 0.1 | 0.0 | 0.2 | 3.6 | 2.7 |
| lung | WT 1 | 0.0 | 0.0 | 0.0 | 0.0 | 0.0 | 0.0 | 0.0 | 0.0 | No Value | No Value | 0.0 | 0.0 | 0.0 | 0.0 | 0.0 | 0.1 | No Value | 0.2 |
| pancreas | KO 1 | 0.2 | 0.2 | 0.2 | 0.1 | 0.0 | 0.2 | 0.5 | 0.4 | 0.1 | 0.0 | 0.2 | 3.0 | 1.0 | 0.3 | 0.1 | 0.2 | 5.3 | 5.0 |
| pancreas | WT 1 | 0.0 | 0.0 | 0.0 | 0.0 | 0.0 | 0.0 | 0.0 | 0.0 | 0.0 | 0.0 | 0.2 | 0.1 | 0.1 | 0.0 | 0.0 | 0.0 | 0.7 | 0.4 |
| plasma | KO 1 | No Value | No Value | No Value | No Value | No Value | No Value | No Value | No Value | No Value | No Value | 0.0 | 0.0 | 0.0 | No Value | No Value | 0.0 | 0.0 | 0.0 |
| plasma | WT 1 | No Value | No Value | No Value | No Value | No Value | No Value | No Value | No Value | No Value | No Value | 0.0 | 0.0 | No Value | No Value | No Value | 0.0 | 0.0 | 0.0 |
| quadriceps | KO 1 | 0.1 | 0.1 | 0.1 | 0.0 | 0.0 | 0.1 | 0.2 | 0.1 | 0.0 | 0.0 | 0.1 | 0.4 | 0.3 | 0.2 | 0.0 | 0.1 | 2.0 | 1.4 |
| quadriceps | WT 1 | 0.0 | 0.0 | 0.0 | 0.0 | 0.0 | 0.0 | 0.0 | 0.0 | 0.0 | 0.0 | 0.0 | 0.0 | 0.0 | 0.0 | 0.0 | 0.0 | 0.1 | 0.1 |
| spleen | KO 1 | 0.0 | 0.0 | 0.0 | 0.0 | No Value | 0.0 | 0.0 | 0.0 | No Value | No Value | 0.0 | 0.1 | 0.1 | 0.0 | No Value | 0.2 | 0.5 | 0.2 |
| spleen | WT 1 | No Value | No Value | No Value | No Value | No Value | 0.0 | 0.0 | 0.0 | No Value | No Value | 0.0 | 0.0 | 0.0 | No Value | No Value | 0.0 | 0.0 | 0.0 |
| Tongue | KO 1 | 0.0 | No Value | 0.0 | No Value | No Value | 0.1 | 0.1 | 0.1 | No Value | No Value | 0.1 | 0.4 | 0.6 | 0.2 | 0.0 | 0.5 | 1.1 | 1.6 |
| Tongue | WT 1 | 0.0 | No Value | No Value | No Value | No Value | 0.0 | No Value | 0.0 | No Value | No Value | 0.0 | 0.0 | 0.0 | No Value | No Value | 0.0 | 0.0 | 0.0 |
| 0 | 0 | 0 | No Value | No Value | No Value | No Value | No Value | No Value | No Value | No Value | No Value | No Value | No Value | No Value | No Value | No Value | No Value | No Value | No Value |

| Standard Deviation | | | | | | | | | | | | | | | | | | | |
|--------------------|---------|----------|----------|----------|----------|----------|----------|----------|----------|----------|----------|----------|----------|----------|----------|----------|----------|----------|----------|
| Tissue | Genotyp | 42:0 | 42:1 | 42:2 | 42:3 | 42:4 | 44:0 | 44:1 | 44:2 | 44:3 | 44:4 | 46:0 | 46:1 | 46:2 | 46:3 | 46:4 | 48:0 | 48:1 | 48:2 |
| Adrenal Gland | KO 1 | 0.0 | No Value | 0.1 | 0.0 | 0.0 | 0.1 | 0.2 | 0.1 | 0.1 | No Value | 0.1 | 0.5 | 0.3 | 0.2 | 0.0 | 0.4 | 0.6 | |
| Adrenal Gland | WT 1 | No Value | No Value | 0.0 | 0.0 | No Value | 0.0 | 0.1 | 0.0 | No Value | No Value | 0.1 | 0.2 | 0.2 | 0.1 | 0.0 | 0.3 | 0.7 | |
| BAT | KO 1 | 0.0 | No Value | 0.0 | 0.0 | 0.0 | 0.0 | 0.0 | 0.0 | 0.0 | No Value | 0.0 | No Value | 0.0 | 0.0 | 0.0 | 0.0 | No Value | |
| BAT | WT 1 | 0.0 | No Value | 0.1 | 0.0 | 0.0 | 0.1 | 0.2 | 0.2 | 0.1 | 0.0 | 0.2 | 0.7 | 0.8 | 0.3 | 0.0 | 0.5 | 2.1 | |
| brain | KO 1 | 0.0 | No Value | No Value | 0.0 | No Value | 0.0 | 0.0 | 0.0 | No Value | No Value | 0.0 | 0.0 | 0.0 | 0.0 | 0.0 | 0.0 | 0.0 | 0.0 |
| brain | WT 1 | No Value | No Value | No Value | 0.0 | No Value | No Value | No Value | No Value | No Value | No Value | No Value | No Value | No Value | No Value | No Value | No Value | No Value | No Value |
| heart | KO 1 | No Value | No Value | No Value | No Value | No Value | No Value | No Value | No Value | No Value | No Value | No Value | No Value | No Value | No Value | No Value | No Value | No Value | No Value |
| heart | WT 1 | No Value | No Value | No Value | No Value | No Value | No Value | No Value | No Value | No Value | No Value | 0.0 | 0.0 | 0.0 | 0.0 | No Value | 0.0 | 0.0 | 0.0 |
| kidney | KO 1 | 0.0 | 0.0 | 0.0 | No Value | No Value | 0.0 | 0.0 | 0.0 | 0.0 | No Value | 0.0 | 0.0 | 0.1 | 0.1 | 0.0 | 0.0 | No Value | |
| kidney | WT 1 | 0.0 | 0.0 | 0.0 | 0.0 | 0.0 | 0.0 | 0.0 | 0.0 | 0.0 | 0.0 | 0.0 | 0.1 | 0.1 | 0.1 | 0.1 | 0.0 | 0.1 | 0.1 |
| liver | KO 1 | No Value | No Value | No Value | No Value | No Value | No Value | No Value | No Value | No Value | No Value | No Value | No Value | No Value | No Value | No Value | No Value | No Value | No Value |
| liver | WT 1 | No Value | No Value | No Value | No Value | No Value | No Value | No Value | No Value | No Value | No Value | No Value | No Value | No Value | No Value | No Value | No Value | No Value | No Value |
| lung | KO 1 | 0.0 | 0.0 | 0.0 | 0.0 | No Value | 0.0 | 0.0 | 0.0 | 0.0 | No Value | 0.0 | 0.1 | 0.1 | 0.0 | 0.0 | 0.1 | 1.3 | |
| lung | WT 1 | 0.0 | 0.0 | 0.0 | 0.0 | 0.0 | 0.0 | 0.0 | 0.0 | No Value | No Value | 0.0 | 0.0 | 0.0 | 0.0 | 0.0 | 0.0 | No Value | |
| pancreas | KO 1 | 0.3 | 0.4 | 0.4 | 0.2 | 0.0 | 0.3 | 0.9 | 0.6 | 0.2 | 0.0 | 0.3 | 3.8 | 1.6 | 0.6 | 0.1 | 0.3 | 9.2 | |
| pancreas | WT 1 | 0.0 | 0.0 | 0.0 | 0.0 | 0.0 | 0.0 | 0.0 | 0.0 | 0.0 | 0.0 | 0.0 | 0.1 | 0.1 | 0.0 | 0.0 | 0.0 | 0.6 | |
| plasma | KO 1 | No Value | No Value | No Value | No Value | No Value | No Value | No Value | No Value | No Value | No Value | 0.0 | 0.0 | 0.0 | No Value | No Value | 0.0 | 0.0 | 0.0 |
| plasma | WT 1 | No Value | No Value | No Value | No Value | No Value | No Value | No Value | No Value | No Value | No Value | 0.0 | 0.0 | No Value | No Value | No Value | 0.0 | 0.0 | 0.0 |
| quadriceps | KO 1 | 0.0 | 0.0 | 0.0 | 0.0 | 0.0 | 0.0 | 0.0 | 0.1 | 0.0 | 0.0 | 0.0 | 0.0 | 0.0 | 0.0 | 0.0 | 0.0 | 0.6 | |
| quadriceps | WT 1 | 0.0 | 0.0 | 0.0 | 0.0 | 0.0 | 0.0 | 0.0 | 0.0 | 0.0 | 0.0 | 0.0 | 0.0 | 0.0 | 0.0 | 0.0 | 0.0 | 0.1 | |
| spleen | KO 1 | 0.0 | 0.0 | 0.0 | 0.0 | No Value | 0.0 | 0.0 | 0.0 | No Value | No Value | 0.0 | 0.1 | 0.1 | 0.0 | No Value | 0.1 | 0.2 | |
| spleen | WT 1 | No Value | No Value | No Value | No Value | No Value | 0.0 | 0.0 | 0.0 | No Value | No Value | 0.0 | 0.0 | 0.0 | No Value | No Value | 0.0 | 0.0 | 0.0 |
| Tongue | KO 1 | 0.0 | No Value | 0.0 | No Value | No Value | 0.0 | 0.0 | 0.0 | No Value | No Value | 0.0 | 0.1 | 0.1 | 0.1 | 0.0 | 0.0 | 0.3 | |
| Tongue | WT 1 | 0.0 | No Value | No Value | No Value | No Value | 0.0 | No Value | 0.0 | No Value | No Value | 0.0 | 0.0 | 0.0 | No Value | No Value | 0.0 | 0.0 | 0.0 |
| 0 | 0 | 0 | No Value | No Value | No Value | No Value | No Value | No Value | No Value | No Value | No Value | No Value | No Value | No Value | No Value | No Value | No Value | No Value | No Value |

Figure 15: Snapshot of the DPS “Average” and “StaDevS” spreadsheets. The Number of allowed invalid values were changeable, to discard calculations with a low amount of detected species in a group. The output by achieved number of invalid values were “No Value”.

Statistical significance between wild-type and ATGL deficient murine tissues was calculated with unpaired two-tailed Student’s t-test in the “T-Test Significance” sheet (Fig. 16). T-test parameters as well as significance conditions were changeable (red boxes, Fig. 16).

| T-Test | Allowed invalid values: 2 | | | | T-Test Parameter: 2 | | Tails: 2 | Typ: 2 | Significance < | | | | | | | | | | | | | | |
|---------------|---------------------------|------|------|------|---------------------|------|----------|--------|----------------|------|------|------|------|------|------|------|------|------|------|------|------|------|-----|
| | 42:0 | 42:1 | 42:2 | 42:3 | 42:4 | 44:0 | 44:1 | 44:2 | 44:3 | 44:4 | 46:0 | 46:1 | 46:2 | 46:3 | 46:4 | 48:0 | 48:1 | 48:2 | 48:3 | 48:4 | 48:5 | 48:6 | |
| Tissue | | | | | | | | | | | | | | | | | | | | | | | |
| Adrenal Gland | | | * | | | ** | * | ** | | | *** | ** | ** | ** | | *** | *** | *** | ** | ** | * | | |
| BAT | | | | | | | | | | | | | | | | | | | | | | | |
| brain | | | | | | | | | | | *** | ** | | | | *** | ** | * | | | | | |
| heart | | | | | | | | | | | | | | | | | | | | | | | |
| kidney | * | | | | | * | | | | | | | | | | | * | * | | | | | |
| liver | | | | | | | | | | | | | | | | | | | | | | | |
| lung | ** | *** | *** | | | *** | *** | *** | | | *** | *** | *** | *** | ** | * | | *** | *** | *** | ** | | |
| pancreas | | | | | | | | | | | | | | | | | | | | | | | |
| plasma | | | | | | | | | | | | | | | | | | | | | | | |
| quadriceps | ** | *** | *** | ** | | *** | *** | | *** | * | *** | *** | *** | *** | * | | ** | ** | ** | ** | ** | ** | * |
| spleen | | | | | | | * | | | | * | * | * | * | * | ** | * | * | ** | ** | * | * | * |
| Tongue | *** | | | | | ** | | | | | *** | *** | *** | | | *** | ** | *** | *** | ** | | | *** |

Figure 16: Snapshot of the DPS “T-Test Significance” spreadsheet. Student’s t-test calculation for statistical analysis between genotypes of each tissue and lipid species. Parameters for t-test calculation, as well as significance conditions and allowed invalid values (red boxes, top) were changeable (*p < 0.05, **p < 0.01, ***p < 0.001).

As preliminary data visualization, the “Heatmap” spreadsheet displayed an optical overview of normalized mean data of each tissue, genotype, and lipid species as well as summarized species values. The heatmap color code is generated by using following options in Excel: customized value formation “;” to hide values and “conditional formatting” for colorized fields. This color code (red-low, green-high) indicated differences by intensity (Fig. 17).



Figure 17: Snapshot of the DPS “heatmap” spreadsheet. Visualization of mean values of each single lipid species as well as summarized lipid species in one class (color code: red-low, green-high).

The “SpeciesSum” spreadsheet calculated the mean and standard deviation of summarized lipid species from a given lipid class for each tissue and genotype under the parameter of allowed invalid values in each species mean group. To execute this process, two additional spreadsheets were required, “SumTest” and “SumNew”. “SumTest” supported value verification and “SumNew” assigned verified values. Additionally, the percentage standard deviation was calculated (Fig. 18).

| Allowed invalid values: | | 2 | | |
|-------------------------|---------|----------|----------|----------|
| Tissue | Genotyp | Average | StaDevS | StaDev % |
| Adrenal Gland | KO1 | 485.9 | 89.1 | 18% |
| Adrenal Gland | WT1 | 113.0 | 71.1 | 63% |
| BAT | KO1 | 14.6 | 2.9 | 20% |
| BAT | WT1 | 331.4 | 235.7 | 71% |
| brain | KO1 | 2.9 | 0.1 | 5% |
| brain | WT1 | 0.7 | 0.3 | 42% |
| heart | KO1 | 39.6 | No Value | No Value |
| heart | WT1 | 10.7 | 4.1 | 38% |
| kidney | KO1 | 102.3 | 2.5 | 2% |
| kidney | WT1 | 38.4 | 8.9 | 23% |
| liver | KO1 | No Value | No Value | No Value |
| liver | WT1 | No Value | No Value | No Value |
| lung | KO1 | 84.9 | 20.7 | 24% |
| lung | WT1 | 18.5 | 3.4 | 19% |
| pancreas | KO1 | 117.3 | 193.9 | 165% |
| pancreas | WT1 | 22.5 | 16.0 | 71% |
| plasma | KO1 | 1.0 | 0.3 | 26% |
| plasma | WT1 | 0.8 | 0.2 | 27% |
| quadriceps | KO1 | 66.3 | 8.9 | 13% |
| quadriceps | WT1 | 10.7 | 10.2 | 95% |
| spleen | KO1 | 15.0 | 8.0 | 53% |
| spleen | WT1 | 1.9 | 1.0 | 54% |
| Tongue | KO1 | 203.6 | 31.8 | 16% |
| Tongue | WT1 | 2.2 | 0.6 | 27% |

Figure 18: Snapshot of the DPS “SpeciesSum” spreadsheet. Mean and standard deviation calculation of summarized lipid species under the condition of allowed invalid values in each species mean group. “SumTest” spreadsheet enabled value verification. “SumNew” spreadsheet assigned verified values.

After preparation and testing of the DPS, all 12 lipid classes were analyzed with LDA 2. Lipid species area values, either normalized to their ISTD or raw were used for semi-automated DPS processing.

4.3.2. Data visualization

Data visualization, especially for highly complex samples and big data analyses displays a crucial link between processed information and result interpretation. To display single, as well as global differences in lipid classes and species of different tissues and genotypes several visualization options were tested and assessed.

4.3.2.1. Global data visualization

To identify differences within the massive amount of processed data, the next steps focused on global data visualization. One approach was the application of a global principal component analysis (PCA) with normalized lipid data of all tissues. PCA is a vector-based multivariate analysis method and can be visualized as a two-dimensional scatter plot. PCA dependent data reduction allows comprehensible data plotting to detect differences in lipid concentration as well as lipid composition in various tissues (Fig. 19A). To further “zoom” into the data of tissue clusters within the PCA scatter plot, tissues with a high PCA distance were removed for subsequent PCA analysis. This manual data reduction allowed the detection of additional, smaller differences within the set (Fig. 19B). A commonly used method to identify significant differences between tissues as well as genotypes are statistically methods like two-tailed student’s t-test. Thereby, the statistical significance is determined by the probability- or p-value (Fig. 19C). PCA of high significant TAG differences between murine wildtype and ATGL deficient adrenal gland tissues showed clustering between zero-coordinate of PC1 in the scatter plot (Fig. 19D). In contrast, not significant differences between tissues, like TAG in the pancreas are randomly distributed in the scatter plot (Fig. 19E).

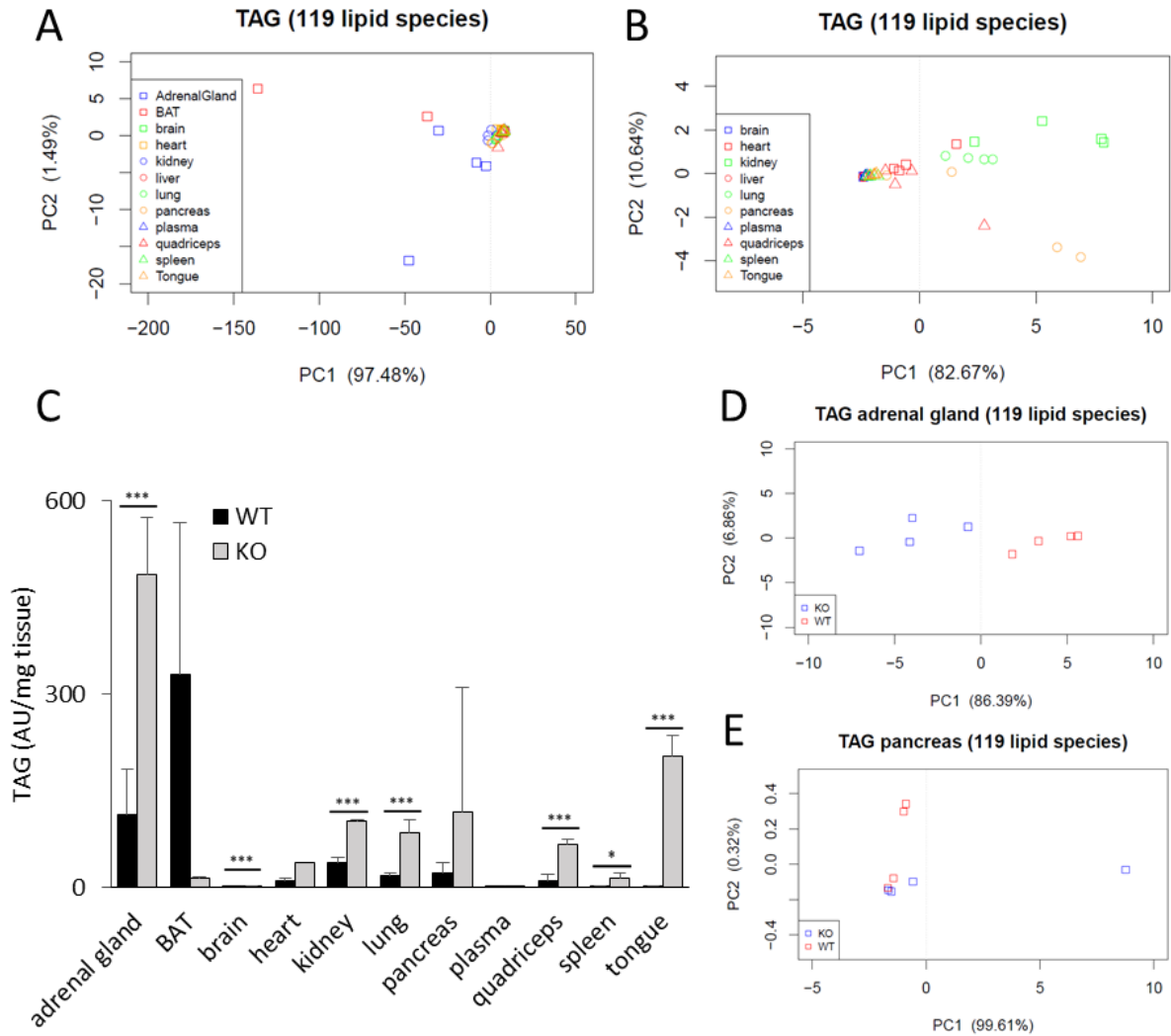


Figure 19: Statistical analysis of TAG in various tissues and genotypes. Data visualization using PCA generated scatter plot of TAG in various wild-type and ATGL deficient mouse tissues (n=4/genotype) normalized to ISTD TAG 45:0. Lipid content was measured with UHPLC-qTOF-MS and processed with LDA 2 and DPS. A) PCA scatter plot of TAG even chain lipid species in wild-type tissues. B) PCA scatter plot of TAG even chain lipid species in wild-type tissues without adrenal gland and BAT. C) TAG content in wild-type and ATGL deficient mouse tissues. D+E) PCA scatter plot for statistically analysis of TAG in wild-type and ATGL deficient adrenal gland and pancreas tissues. Data are presented as means and standard deviations. Determination of statistically significance by unpaired two-tailed Student's t-test (*p < 0.05, **p < 0.01, ***p < 0.001). Wild-type...WT, ATGL deficient...KO.

Heatmaps represent another global visualization method. Thereby, Excel-generated heatmaps allowed an overview of lipid species as well as their differences in the investigated genotypes. In addition, this visualization type could reveal differences in lipid content and chain length between multiple tissues encoded by color. Global heatmap of normalized TAG species revealed differences between FA chain length of several tissues and/or genotypes. Missing lipid species are displayed by white boxes. Red colored boxes

represented low abundant and green boxes high abundant lipid species. DPS generated heatmaps were used to compare TAG species of all tissues and genotypes. TAG ISTDs in liver of both genotypes, as well as in the heart of KO animals were not detectable, hence data of those tissue could not be used for DPS based heatmaps (Fig. 20). However, differences could be observed quickly by investigating the heatmap visualization e.g. compositional shift between wild-type and ATGL deficient TAGs in tongue or quadriceps.

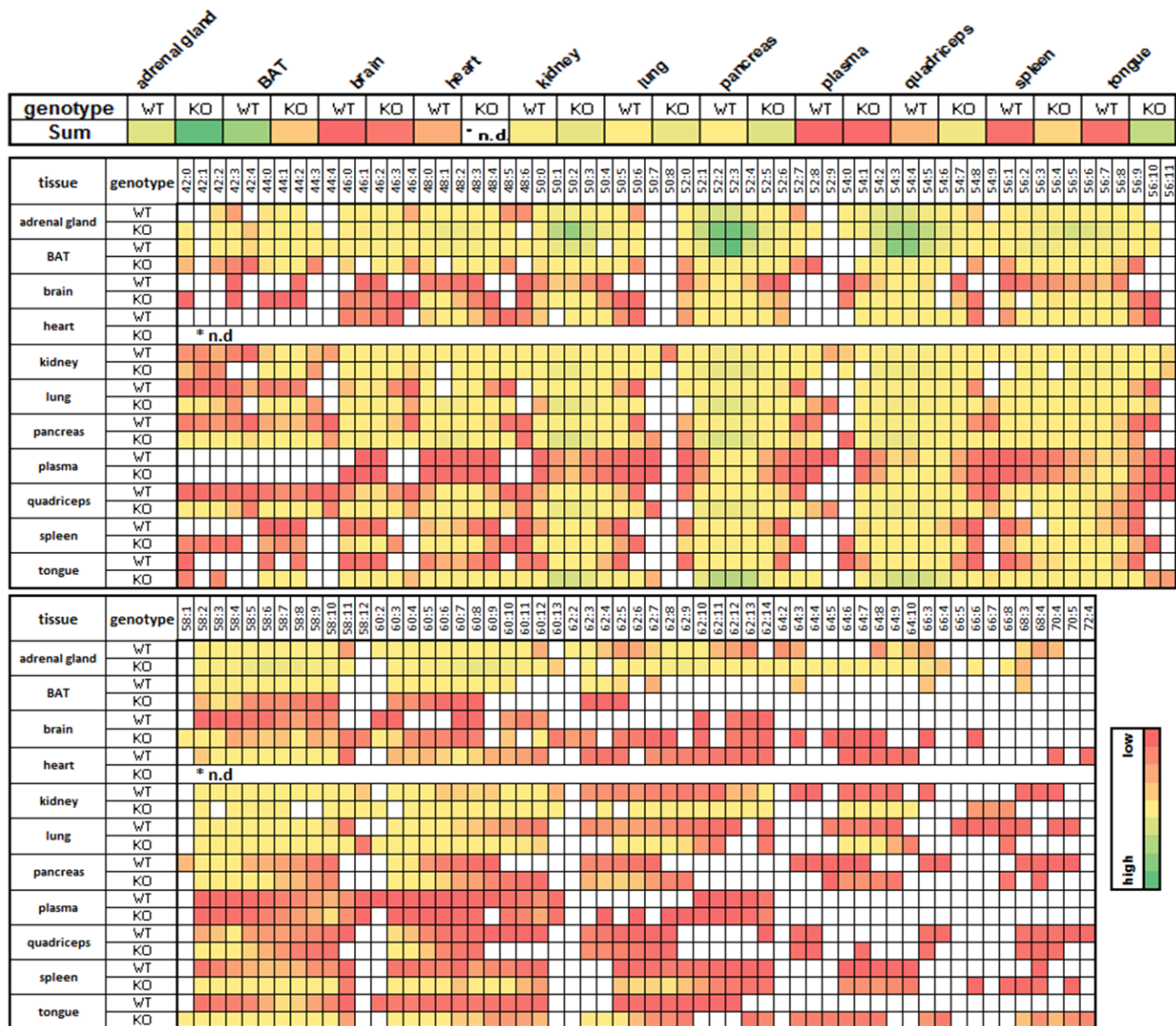


Figure 20: Excel generated heatmap of TAG species in wild-type and ATGL deficient murine tissues. Top) Heatmap represents summarized lipid species of TAG in wild-type and ATGL deficient mouse tissues. Middle + bottom) Heatmaps represent all even chain lipid species of TAG in wild-type and ATGL deficient mouse tissues. Due to size limitations the heatmap was split. Colored boxes represent lipid species content, encoded by the color code on the right side. Lipid species are annotated as carbon atoms: double bonds of the attached FA. Wild-type...WT, ATGL deficient...KO.

4.3.2.2. Top-down data analysis - PCA

To accomplish identification of global lipid differences between tissues in a comprehensive way, a PCA was performed using normalized and raw data of even chain lipid species from all tissues (top-down). Upon that, identified differences were investigated in detail.

First, processed data of PC from all wild-type tissues were used for a “showcase” top-down PCA. The resulting scatter plot of normalized PC data revealed a clear alignment of PC in most tissues except adrenal gland and brown adipose tissue (BAT) (Fig. 21A). Detailed PC species investigation of adrenal gland, BAT, spleen and tongue as control, showed differences in both, PC content and composition. Total PC content was significantly higher in adrenal gland as compared to BAT, tongue, and spleen (Fig. 21B). Further analysis of PC composition additionally revealed distinct lipid composition differences between adrenal glands and BAT (Fig. 21C). To reduce data complexity, saturated as well as unsaturated PC species were summarized according to their chain length. The increased amount of PC in adrenal gland was reflected in PCs of all chain lengths, whereas increased BAT PC was mainly due to an increase in PCs containing 34 and 36 carbon atoms, as compared to tongue and spleen (Fig. 21D). The percental composition plot revealed major composition differences between all four investigated tissues. Spleen contained mostly PC species with a combined FA chain length from 30 to 36 carbon atoms. In contrast, PC species with 34 to 38 carbon atoms were most abundant in adrenal glands. Interestingly, the most abundant PC species in tongue contained combined chain lengths of 34 to 40, whereas BAT species reached their highest composition limit at 36 carbon atoms (Fig. 21E).

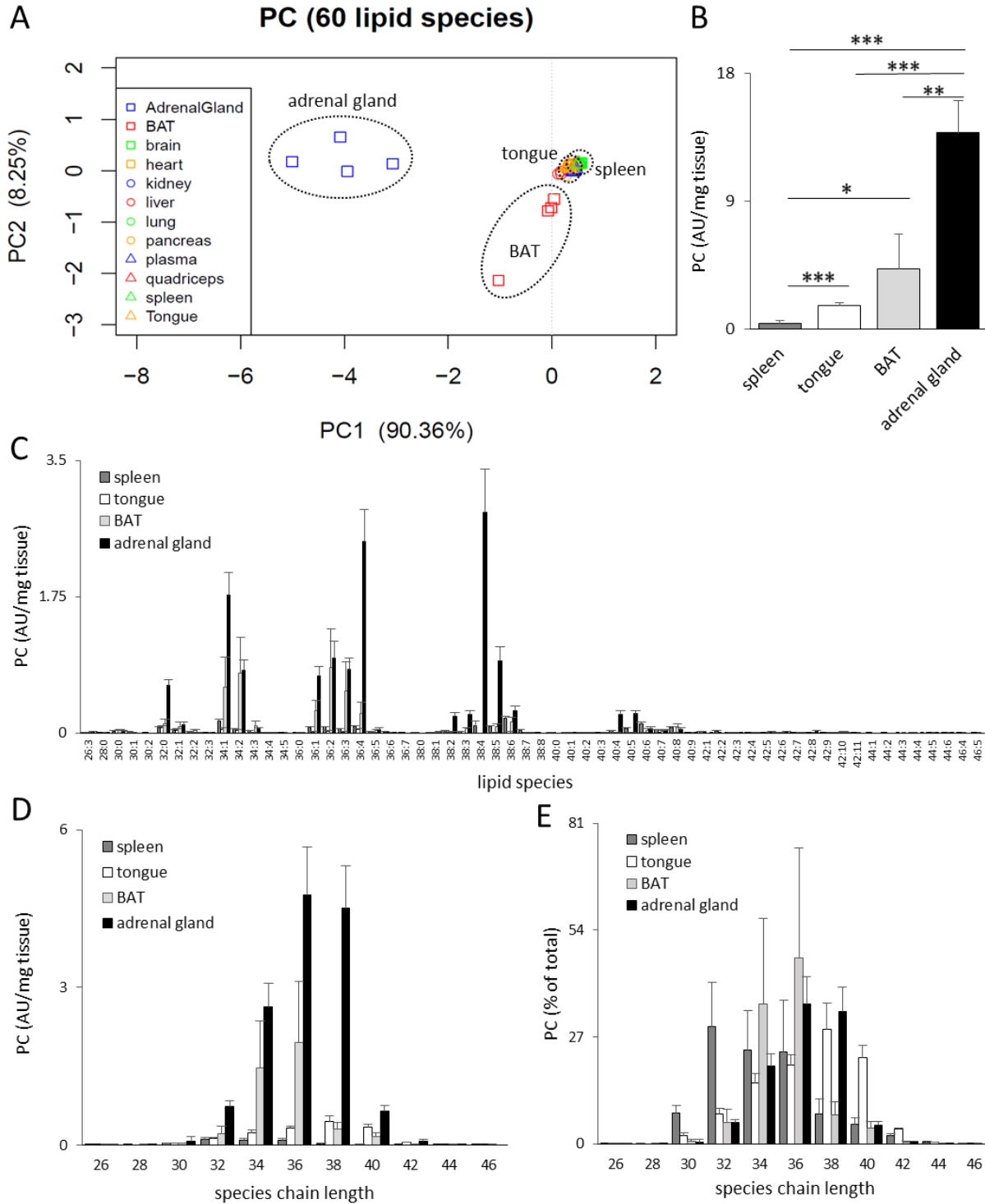


Figure 21: In-depth visualization workflow of PC in different wild-type mouse tissues. Visualization of even chain PC normalized to ISTD PC 34:0 in wild-type murine tissues (n=4). Lipid content was measured with UHPLC-qTOF-MS and processed with LDA 2 and DPS. A) PCA scatter plot of PC lipid species performed with R. Tissues of interest adrenal gland, BAT, spleen and tongue were framed. B) Summarized PC content. C) Quantitative PC species composition. D) Quantitative PC composition of chain-length combined species. E) Percental PC species composition of chain-length combined species. Data are presented as means and standard deviations. Determination of statistically significance by unpaired two-tailed Student's t-test (*p < 0.05, **p < 0.01, ***p < 0.001). Lipid species are annotated as carbon atoms: double bonds of the attached FA.

Since the detailed analysis of PC species revealed differences in tissues, namely tongue and spleen, which clustered in the initial PCA (Fig. 22A, Fig. 21E), we next specifically reduced the underlying data. To eliminate the high impact of BAT and adrenal gland on the PCA, the R-script was modified to ignore data of both tissues (Fig. 22B). Interestingly, PCA showed again major differences and clustering of PCs in the remaining tissues. Two PCA-separated as well as two PCA-clustered tissues, namely liver, plasma, kidney, and brain were used for further detailed analysis. As for the previous analysis, high PC content had the biggest influence on PCA. Both, liver and plasma showed significantly increased PC levels as compared to kidney and brain (Fig. 22C). However, specific differences in PC compositions were less pronounced when compared to initial analysis, which was in line with the initial PCA. Besides the differences in the total PC amount, the overall PC composition was comparable in all four tissues with a trend to partially longer PC species in liver and kidney (Fig. 22D).

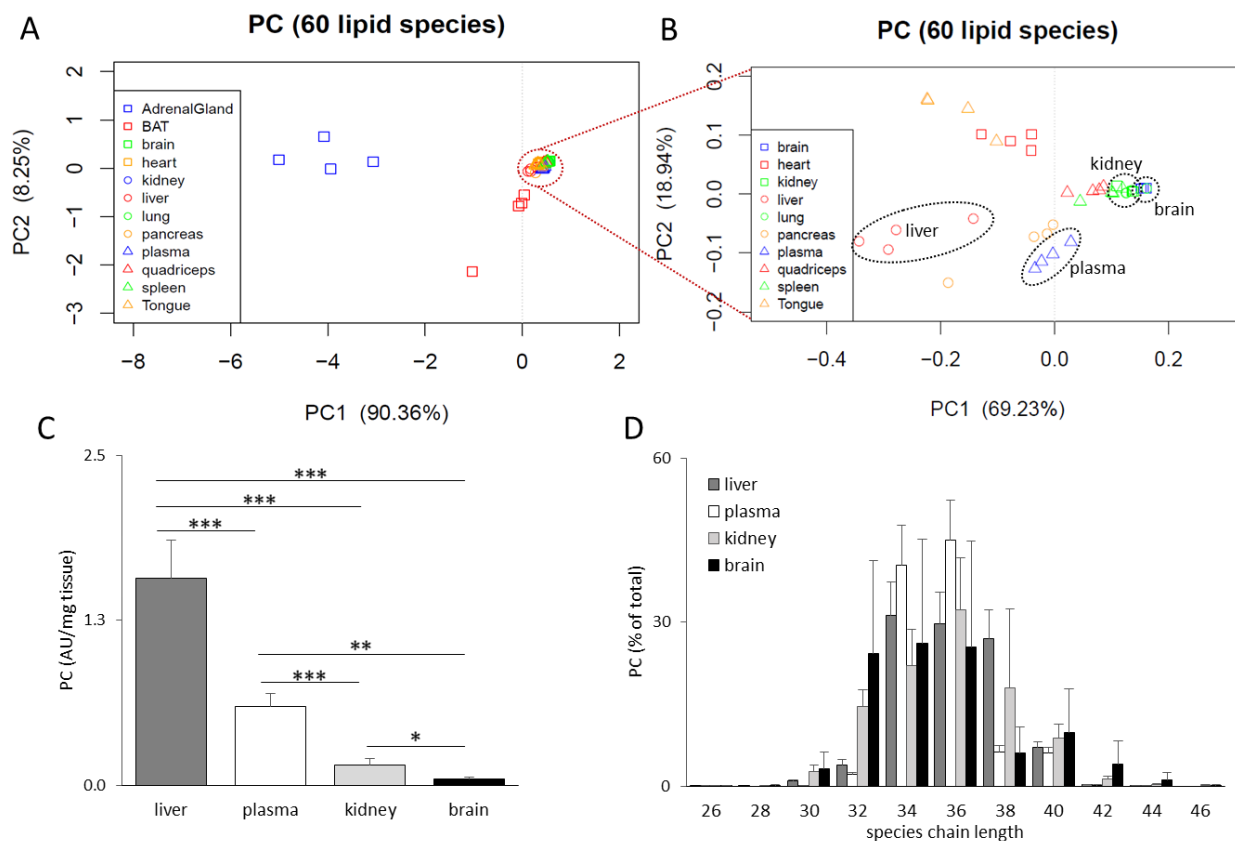


Figure 22: PCA with reduced PC data. Visualization of PC lipid species normalized to ISTD PC 34:0 in various wild-type mouse tissues. Lipid content was measured with UHPLC-qTOF-MS and processed with LDA 2 and DPS. A) PCA scatter plot of normalized PC lipid species in 12 tissues. Red circle shows clustered tissues. B) PCA scatter plot of PC without data for adrenal gland and BAT. C) Summarized PC content. D) Percental PC species composition of chain-length summarized species. Data are presented as means and standard deviations. Determination of statistical significance by unpaired two-tailed Student's t-test (* $p < 0.05$, ** $p < 0.01$, *** $p < 0.001$).

4.3.2.3. Visual data analysis - heatmap

Besides PCA, heatmaps are an additional option to visualize big data. Many online as well as offline tools offer heatmap options. However, many of these tools are associated with drawbacks like black-box data processing, the necessity of confidential data upload, and limited processing options. For this study we next used the specific-formatting option of Excel to generate quasi-heatmaps.

First, Cer data of wild-type tissues were used for heatmap analysis. For the initial study, only tissues with ISTD normalized Cer data were included (detectable signal for ISTD). As expected, heatmap analysis visualized the high diversity of Cer amount and species composition in wild-type tissue (Fig. 23A). Besides global composition differences, pancreas, quadriceps, spleen, and tongue specifically showed Cer species with >24 FAs. Due to the difficulty of a robust concentration estimation based on a color code, a PCA was additionally applied on this data (Fig. 23B). Combined information of PCA and heatmap revealed tongue, spleen, and pancreas as most divergent tissue of this group. These tissues as well as quadriceps as a tissue cluster control were chosen for further analysis. Semi-quantitative analysis of Cer showed significantly increased Cer levels in spleen, tongue, and pancreas as compared to quadriceps (Fig. 23C, insert). Additionally, compositional analysis showed severe differences on Cer species levels. Whereas all tissues contain comparable amounts of Cer species with C22 and C24 FAs, quadriceps showed a high portion of C18-Cer and tongue contains unique very- (>C22 FA) and ultralong (>C28 FA) Cer species (Fig. 23C).

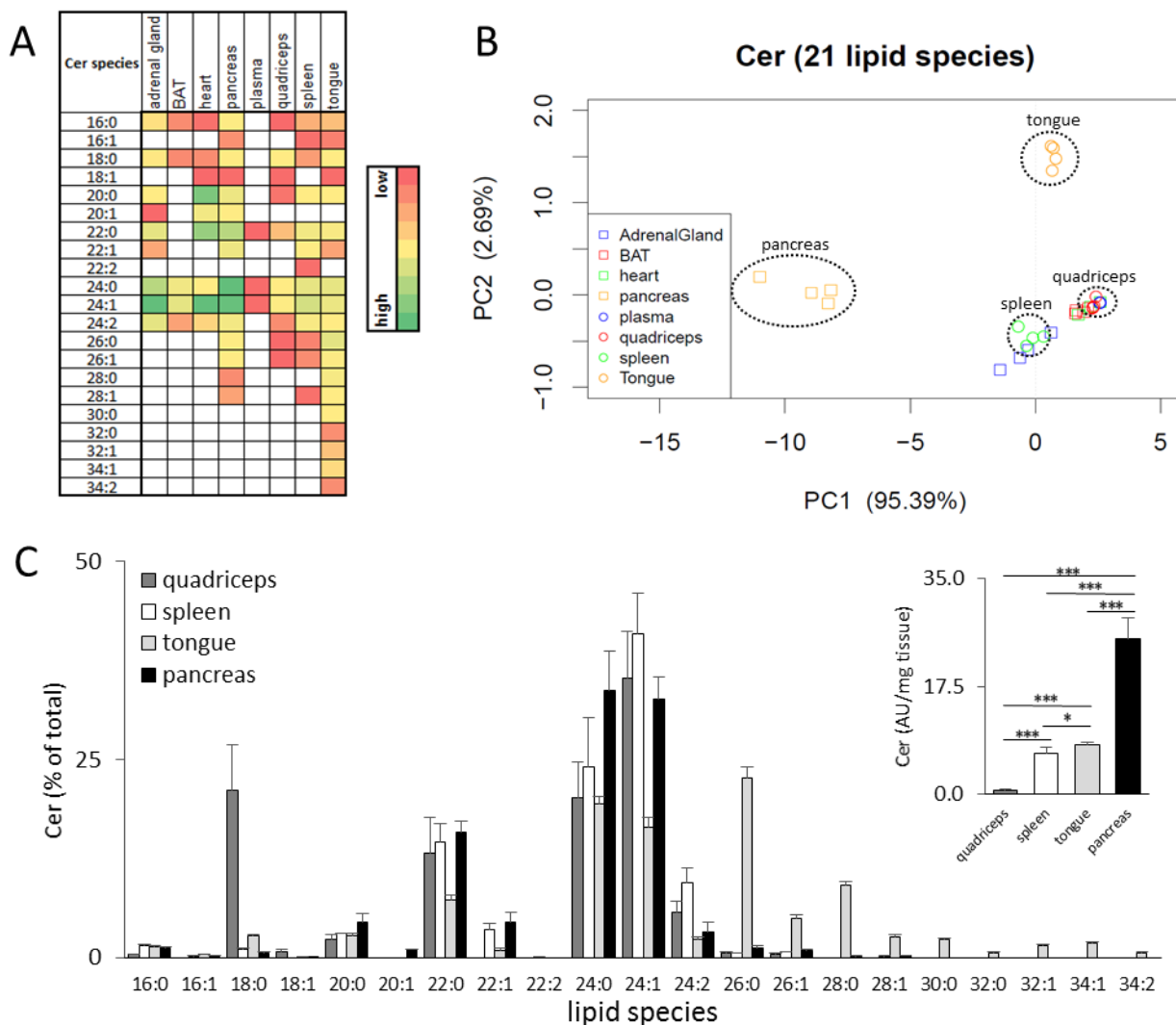


Figure 23: Combined PCA and heatmap analysis of Cer species in wild-type tissues. Analysis of Cer species in tissues with detectable ISTD Cer 17:0. Lipid content was measured with UHPLC-qTOF-MS and processed with LDA 2 and DPS. A) Heatmap of Cer species in various wild-type tissues. Colored boxes represent Cer species content, encoded by the color code on the right side. B) PCA of normalized Cer lipid species. Circles show tissues used for further in-depth analysis. C) Percental Cer species composition and Cer total amount (insert). Data are presented as means and standard deviations. Determination of statistically significance by unpaired two-tailed Student's t-test (* $p < 0.05$, ** $p < 0.01$, *** $p < 0.001$). Lipid species are annotated as carbon atoms: double bonds of the attached FA.

Next, heatmap analysis was applied on the same dataset including a second genotype. Tissues without detectable ISTD Cer 17 were excluded from the analysis. The heatmap revealed differences in Cer-FA composition between genotypes as well as in Cer-FA chain length between several tissues. Furthermore, the heatmap showed high accumulation of very long FA chains in murine tongue tissues (Fig. 24A). Subsequent Cer PCA of wild-type and ATGL deficient murine tongue data significantly separated the different genotypes and clustered biological replicates (Fig. 24B). Additional performed

statistical analysis with two-paired Student's t-test showed significantly reduced Cer levels in KO tongue as compared to WT tissues (Fig. 24C, insert). A further in-depth Cer species analysis of both genotypes confirmed differences and showed that virtually all Cer species are decreased in KO samples. Thereby, especially very long Cer species were decreased drastically (Fig. 24C).

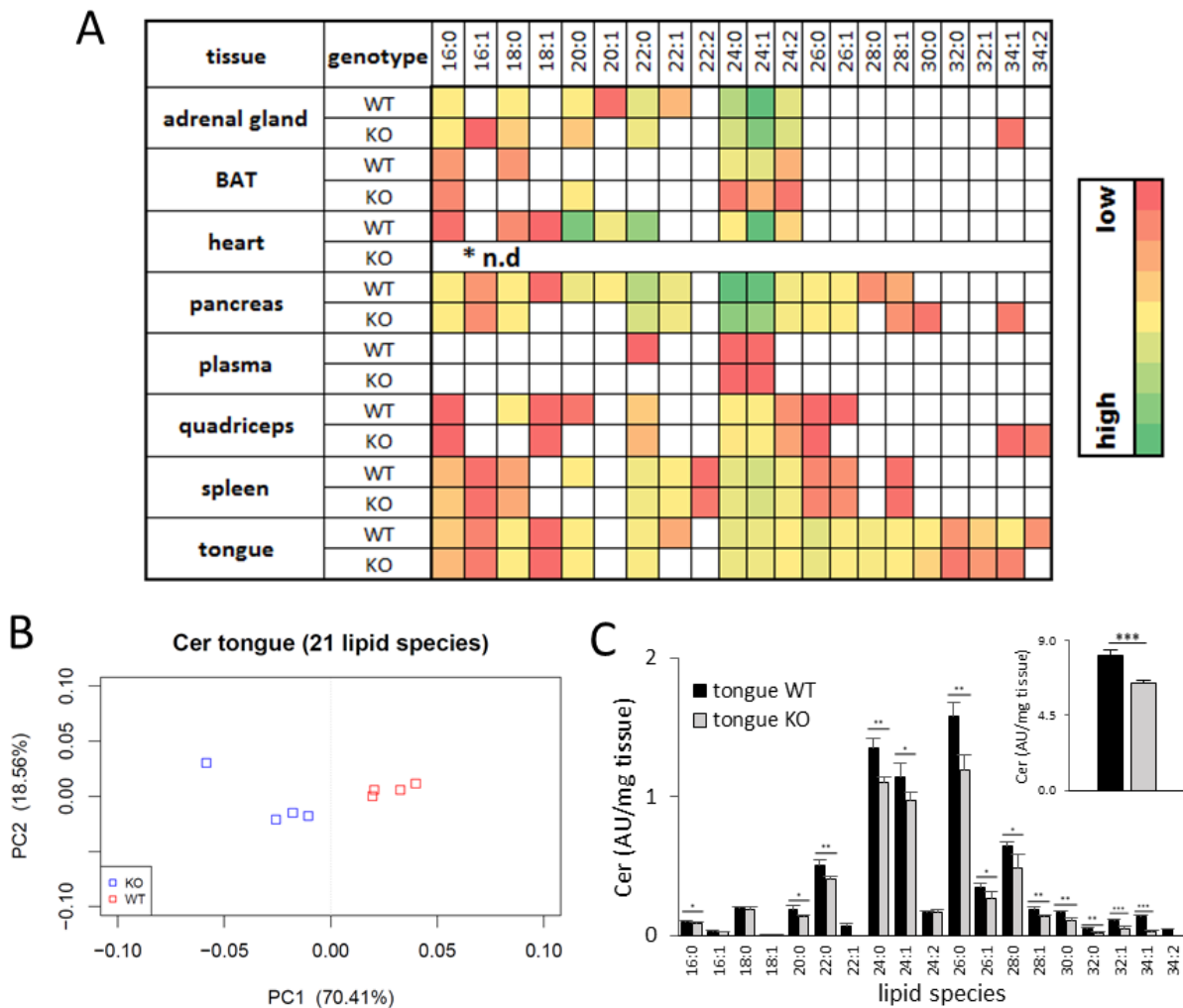


Figure 24: Combined PCA, heatmap and statistical analysis of Cer species in ATGL deficient and wild-type tissues. Analysis of Cer species in tissues with detectable ISTD Cer 17:0. Lipid content was measured with UHPLC-qTOF-MS and processed with LDA 2 and DPS. ISTD was not detectable in ATGL deficient heart tissues as well as in brain, kidney, liver, and lung of both genotypes. A) Heatmap of Cer species in various wild-type and ATGL deficient tissues. Colored boxes represent Cer species content, encoded by the color code on the right side. B) PCA of normalized Cer in wild-type and ATGL deficient murine tongue tissues. C) Cer content (insert) and Cer species composition of wild-type and ATGL deficient murine tongue. Data are presented as means and standard deviations. Determination of statistically significance by unpaired two-tailed Student's t-test (* $p < 0.05$, ** $p < 0.01$, *** $p < 0.001$). Lipid species are annotated as carbon atoms: double bonds of the attached FA. Wild-type...WT, ATGL deficient...KO.

4.4. Workflow evaluation & improvement - Internal standardization

The main focus of this trial study was to reveal weak points of the global lipidomic workflow. Beside limitations with detection of diverse lipid classes (e.g. MAG, DAG, phosphatic acid) on the MS-qTOF system especially the insufficient detection of ISTDs in several tissues was a major drawback for subsequent data processing.

Data of this study revealed that the currently applied internal standardization is not applicable to a multi-tissue, multi-genotype sample set without further adaptations. Several ISTD were below the detection limit in various wild-type tissues (e.g. TAG 45:0 in brain; Cer 17:0 in brain, kidney, liver, and lung). Since, ISTD signals are required for quantification of lipids and for a robust differential lipid analysis, missing ISTD are detrimental for a lipidomic workflow. The loss of ISTD signals is mainly a result of high sample dilution and/or high ion suppression. To avoid this issue in future sample sets, sample amount as well as ISTD concentration had to be specifically adapted for each tissue. Therefore, data of this study were used to calculate optimal ISTD concentrations for all investigated wild-type tissues. First, a lipid class specific response factor (RF) was calculated by dividing peak area of the three most abundant species of each class with the peak area of the class specific ISTD (Table 2).

Table 2: Sample conditions, ISTD concentration and response factor (RF). LOD...Limit of detection

| | AG | BAT | brain | heart | kidney | liver | lung | pancreas | plasma | quadriceps | spleen | tongue |
|--------------------------|-----|------|-------|-------|--------|-------|------|----------|--------|------------|--------|--------|
| Weight (mg, mean) | 5 | 200 | 400 | 100 | 200 | 200 | 100 | 80 | 50 | 200 | 40 | 50 |
| Solvent (µl) | 250 | 2500 | 500 | 1500 | 250 | 5000 | 500 | 250 | 200 | 250 | 250 | 250 |
| ISTD (pmol) | 400 | 400 | 400 | 400 | 400 | 400 | 400 | 400 | 400 | 400 | 400 | 400 |
| <i>RF-TAG</i> | 10 | 500 | 40 | 50 | 500 | <LOD | 200 | 50 | 4 | 100 | 5 | 5 |
| <i>RF-Cer</i> | 2 | 5 | <LOD | 50 | <LOD | <LOD | <LOD | 300 | 0.33 | 20 | 25 | 50 |
| <i>RF-LPC</i> | 2 | 5 | 10 | 10 | 20 | 20 | 10 | 5 | 5 | 10 | 5 | 5 |
| <i>RF-PC</i> | 5 | 10 | 3 | 10 | 3 | 40 | 3 | 5 | 10 | 5 | 2 | 5 |
| <i>RF-PE</i> | 2 | 5 | 50 | 50 | 50 | 20 | 10 | 10 | 0.5 | 10 | 5 | 5 |
| <i>RF-PS</i> | 1 | 1 | 1 | 1 | 1 | 0.25 | 2 | 1 | 0.1 | 1 | 2 | 2 |

Subsequently, theoretical tissue-specific ISTD concentrations were calculated for wild-type tissues considering an adaption of tissue weight and solvent volume. Thereby, the

reduction of the extracted tissue weight will allow lower solvent volumes and higher ISTD signals for similar ISTD concentrations. In case of ISTD signals below the detection limit, a potentially detectable concentration was estimated. The robustness of the new concentrations will be assessed in further studies (Table 3, Figure 25).

Table 3: Theoretical ISTD concentration for various tissues.

| | adrenal gland | BAT | brain | heart | kidney | liver | lung | pancreas | plasma | quadriceps | spleen | tongue |
|------------------------------------|---------------|-------|-------|-------|--------|-------|-------|----------|--------|------------|--------|--------|
| Weight (mean) | 5 | 50 | 100 | 50 | 50 | 50 | 50 | 20 | 50 | 50 | 40 | 25 |
| Solvent (μl) | 250 | 500 | 500 | 750 | 250 | 1000 | 500 | 250 | 200 | 250 | 250 | 250 |
| TAG (pmol) | 4000 | 10000 | 4000 | 5000 | 10000 | 2000 | 10000 | 5000 | 1600 | 10000 | 2000 | 1000 |
| Cer (pmol) | 800 | 100 | 10000 | 5000 | 1000 | 10000 | 5000 | 1000 | 150 | 2000 | 10000 | 10000 |
| LPC (pmol) | 800 | 100 | 1000 | 1000 | 2000 | 200 | 1000 | 500 | 2000 | 1000 | 2000 | 1000 |
| PC (pmol) | 2000 | 200 | 400 | 1000 | 300 | 400 | 300 | 500 | 4000 | 500 | 800 | 1000 |
| PE (pmol) | 800 | 100 | 5000 | 5000 | 5000 | 200 | 1000 | 1000 | 200 | 1000 | 2000 | 1000 |
| PS (pmol) | 400 | 20 | 100 | 100 | 100 | 200 | 200 | 100 | 40 | 100 | 800 | 800 |

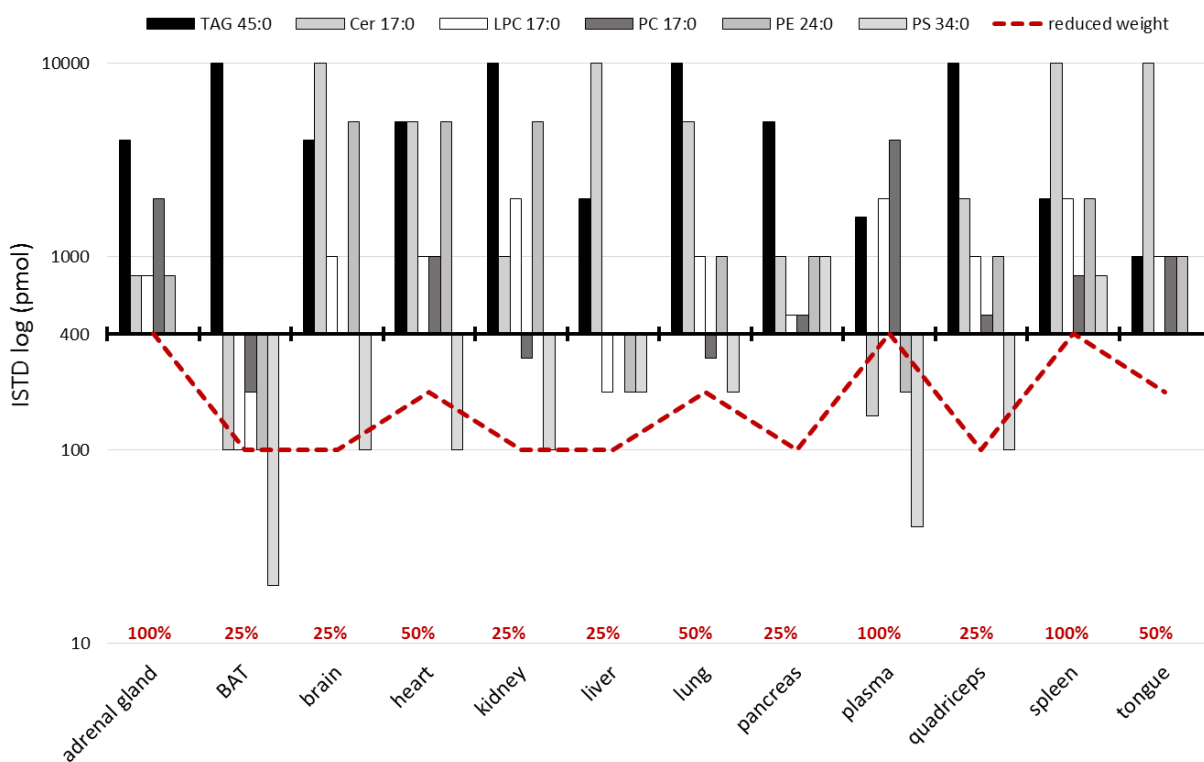


Figure 25: Sample weight, solvent volume and ISTD concentration recommendation for several wild-type tissues. Y-axis shows ISTD concentration in logarithmic scale. The black base line represents the added ISTD concentration (400pmol). Bar charts indicate the calculated new concentration for each lipid class and tissue. Red broken line represents the recommended tissue weight for future lipid analysis in “% of weight used in this study”.

An additional ISTD adaptation for ATGL-deficient tissues couldn't be calculated due to severe response differences of several ISTDs. Depending on the used KO models, a specific ISTD adaption has to be performed in the future.

5. Discussion

The major aim of this study was to test and improve the current workflow for untargeted, global lipid profiling. Thereby, lipid extraction, data processing, and data visualization were tested on a large, biological sample set to identify workflow weak points. This trial study assessment represents the first step for future work on a global, murine lipid database. To ensure a broad variation of sample matrix a total of 378 tissue samples from genetically different mouse models (ATGL wildtype and knock-out) were isolated and used for analysis. The initial experimental part focused on the improvement of the currently used sample preparation and lipid extraction method. The in-house established lipidomic workflow started with a Folch lipid extraction of tissue explants without sample homogenization. However, this method exhibits several drawbacks; i) high volumes of toxic solvents (CHCl_3), ii) CHCl_3 is incompatible with plastic lab ware, iii) lipids reside in the lower phase, which can lead to sample contamination from the protein-rich interphase, and iv) time-consuming extraction steps. Therefore, the Matyash method using MTBE as main extraction solvents was tested and compared with the Folch method. Additionally, a sample homogenization step using a tissue mill was included in the new workflow. Several tests revealed compatibility of MTBE with plastic lab ware as well as the efficiency of the initial homogenization step. Experiments with chicken heart and liver showed similar results in regard to lipid extraction efficacy between both methods. However, extraction of several phospholipid classes was slightly improved by using the Matyash method. Several advantages of the Matyash/MTBE method result in the replacement of the Folch method as standard sample preparation workflow; i) lower solvent consumption, ii) MTBE is compatible with plastic lab ware, iii) MTBE is not toxic, iv) lipids reside in the upper phase, which facilitates fast and clean phase isolation.

Next, the development of mass lists for various lipid classes was required for further LDA 2-based peak picking and data processing steps. Since lipid composition varies greatly in different tissues, raw data of all tissues were manually investigated on their individual lipid species abundance. In course of the manual data investigation several unidentified analytes could be assigned, namely ubiquinones, acyl-carnitines, and glycosylated ceramide classes. However, data on this analytes were not used for further analysis since

no ISTD for these classes was added prior to the extraction. Ultimately, approximately 350 different lipid species with even FA chains of 12 lipid classes were assigned and included into the trial masslists. Additionally, several important information, like the sum formula, the high-resolution mass of all possible adduct ions, as well as the LC method retention time were included. To ensure the integrity of LDA 2 peak picking and peak integration, all resulting data were manually reviewed. The LDA 2 software supports diverse features e.g. sample and group annotation, heatmap and bar chart visualization, internal and external standard, as well as dilution and weight normalization for automated data processing. Nevertheless, our further analysis required raw data information for big data calculation and visualization experiments, hence only the LDA 2 ISTD normalization was applied.

Big data handling represents one of the big challenges of modern lipidomic investigations and displays the connection between measurements and data-to-result processing. Importantly, the handling of massive amounts of raw data requires a robust data pipeline. The generation of a semi-automated Excel worksheet (DPS) for LDA 2 data processing was one major aim of this trial study. Finally, the DPS contained the most important functions necessary for initial data analysis, like mean and standard deviation calculation, total lipid species and class calculation, as well as statistical functions for all samples of the set. Additionally, a first visualization of processed data as heatmap was implemented. The generated DPS contained a user section for sample information entries, which forms the base of automated calculation. Furthermore, all post calculation spreadsheets were based on recursive formulas and user parameters e.g. the number of replica (n/genotype) or the number of "allowed missing values". The final DPS had no sample set size limitation and all spreadsheets were fully expandable.

Another challenge of big data studies is the identification of differences within a sample set. The vast amount of data can make it difficult to find small but statistically robust differences. Hence, global data visualization displays a key feature to prepare data comprehensively. However, common visualization methods like bar graphs or scatter plots fail to picture thousands of data points for multiple sample groups. In course of this study, different PCAs and heatmap visualizations were applied and tested. PCA is commonly used for statistical analysis and data reduction and additionally provides a

scatter plot output option. This PCA scatter plot is based on reduced data of one lipid class from all tissues. Therefore, comprehensive visualization with PCA is limited to one lipid class per analysis. Nevertheless, PCA gives a global overview as well as statistically representative, graphical information on data relationships between different tissues (clustering for high and low abundances). Tissues with different lipid class concentrations and/or species composition are separated in the scatter plot, and vice versa, tissues with similar lipid amounts or composition are clustered. Nonetheless, highly diverse tissues in PCA can distort the result. Hence, to identify differences between clustered groups, it is necessary to remove highly diverging data groups for further analysis. Besides analysis of one lipid class in several tissues also one lipid class in one tissue of several genotypes can be analyzed by PCA. Identified differences between genotypes become valid by genotype separation and clustering of the biological replicates. Based on those two PCA approaches, a further in-depth data analysis on specific differences can be performed to validate PCA results. The additional heatmap approach enables a global visualization of genotypes, tissue, and lipid species of one lipid class. At the one hand, freely available heatmap tools may provide reliable results, but on the other hand, data processing is hardly traceable, doesn't allow post data treatment, and requires upload of confidential data. In contrast, excel offered a quick and simple solution to generate a quasi-heatmap. However the limited color spectra can aggravate heatmap interpretation.

After implementation of the PCA into the data processing workflow it was used for data interpretation. PCA scatter plot of PC lipid class revealed adrenal gland and BAT as most divergent murine wild-type tissues when compared with the whole tissue set. In contrast to clustering tissues, like spleen and tongue, the in-depth analysis of adrenal gland and BAT showed significantly higher PC levels normalized to tissue weight. Subsequently performed comparisons using the percent composition of PC summarized according to their chain lengths revealed further differences. The following PCA performed without adrenal gland and BAT revealed additional differences between tissues, which were clustered in the initial PCA. Thereby, statistical analysis of summarized PC species showed increased abundance in liver, as compared to that of plasma, kidney, and brain. Interestingly, tissues separated in the negative PC1 direction, namely liver and plasma,

showed increased PC content as compared to kidney or brain, both clustering in the positive PC1 direction.

Furthermore, clear differences in Cer concentration and Cer species composition could be identified by combining heatmap and PCA. In-depth PCA and Cer composition analysis of pancreas, tongue, spleen, and quadriceps confirmed the negative PC1 shift of tissues upon high abundance of a given lipid, as observed for PC. Additionally, the PCA plot showed a shift of tongue Cer in the positive PC2 axis, which could be associated with an increased amount of very-long chain Cer species. In combination it can be suggested that tissue lipids are separated by abundance on the PC1 axis and by composition on PC2 axis.

Based on this hypothesis, Cer of tongue from wild-type and ATGL deficient mice were investigated. Thereby, PC1 vector resulted 70.41% of differences in Cer content and PC2 vector resulted 18.56% of differences in Cer composition of those tissues. Further statistical analysis supported this hypothesis. Altogether, data of this study show that both global visualization methods exhibit advantages and disadvantages. A combination of both can greatly help to get first hints on differences between multiple samples. However, stepwise increase of the data “investigation-depth” is necessary to identify significant differences, either on lipid concentration or composition level.

Another major topic of this work became obvious upon sample analysis. The big differences between lipid amount and composition of the investigated tissues identified the uniform internal standardization as major weak point of the currently used lipidomic workflow. To date, internal standardization is a highly discussed topic, since standards for many lipid classes are either not available or very expensive. Nevertheless, class-specific ISTDs are of utmost importance to recognize and consider class-specific alterations, like increased ion suppression or reduced extraction efficiency. Without ISTD information this effects can't be monitored and/or normalized. In our sample set several ISTDs were not detectable in various tissues, either because of high content of the corresponding endogenous lipid class and following ion suppression, or because of high sample dilution. Fat-rich tissues, like brown adipose tissue or liver needed a higher dilution to prevent UHPLC-column overload and MS detector saturation, resulting in a signal drop of ISTDs (e.g. TAG in ATGL-deficient tissues) below the detection limit. In

addition, lipid class abundance differences in several tissues resulted in matrix dependent suppression of ISTD signals, e.g. Cer-ISTD in brain, kidney, and lung tissue in which the endogenous amount of Cer is higher than in other tissues. This examples of erroneous internal standardization were detrimental for the global lipidomic analysis and made it impossible to process all analyzed lipids. However, all data of this study were used to estimate and recommend an optimal internal standardization for each tissue, considering the used sample weight, the lipid extract dilution as well as the lipid class composition. The resulting list of optimal sample amounts, dilutions, and adapted ISTD concentrations couldn't be tested during this master project but display the base of future studies. However, further experiments are indispensable to proof the robustness and validate the new ISTD mixtures.

All in all, this work was able to identify and improve specific weak points of the currently used lipidomic workflow. An improved sample homogenization and lipid extraction as well as a semi-automated data processing tool (DPS) were successfully implemented. Furthermore, this work took first steps in big data visualization and showed, that result visualization is highly complex and requires problem-specific adaption. Data and experience gained in the course of this study will help future projects to facilitate a full description of the global murine lipidome.

6. References

- [1] W. Dowhan, M. Bogdanov, and E. Mileykovskaya, "Functional roles of lipids in membranes," in *Biochemistry of Lipids, Lipoproteins and Membranes*, Fifth Edit., Elsevier B.V., 2008, pp. 1–37.
- [2] E. Fahy *et al.*, "A comprehensive classification system for lipids," *J. Lipid Res.*, vol. 46, no. 5, pp. 839–862, 2005.
- [3] P. Pålsson *et al.*, "Characterization of galactosyl glycerolipids in the HT29 human colon carcinoma cell line," *Arch. Biochem. Biophys.*, vol. 396, no. 2, pp. 187–198, 2001.
- [4] T. H. Haines and N. A. Dencher, "Cardiolipin: A proton trap for oxidative phosphorylation," *FEBS Lett.*, vol. 528, no. 1–3, pp. 35–39, 2002.
- [5] Y.-Y. Liu and Y.-T. Li, "Ceramide Glycosylation Catalyzed by Glucosylceramide Synthase and Cancer Drug Resistance," *NIH Public Access Author*, pp. 1–27, 2014.
- [6] J. H. Wei, X. Yin, and P. V. Welander, "Sterol synthesis in diverse bacteria," *Front. Microbiol.*, vol. 7, no. JUN, pp. 1–19, 2016.
- [7] E. Swiezewska and W. Danikiewicz, "Polyisoprenoids: structure, biosynthesis and function," *Progress. Lipid Res*, vol. 44, no. 4, pp. 235–258, 2005.
- [8] C. R. H. Raetz and C. Whitfield, "Lipopolysaccharide Endotoxins," *NIH Public Access*, vol. 71, pp. 1–57, 2008.
- [9] C. Khosla, R. S. Gokhale, J. R. Jacobsen, and D. E. Cane, "Tolerance and Specificity of Polyketide Synthases," *Annu. Rev. Biochem.*, vol. 68, pp. 219–253, 1999.
- [10] W. Dowhan, E. Mileykovskaya, and M. Bogdanov, "Diversity and versatility of lipid-protein interactions revealed by molecular genetic approaches," *Biochim. Biophys. Acta - Biomembr.*, vol. 1666, no. 1–2, pp. 19–39, 2004.
- [11] K. M. Eyster, "The membrane and lipids as integral participants in signal transduction: lipid signal transduction for the non-lipid biochemist," *AJP Adv. Physiol. Educ.*, vol. 31, no. 1, pp. 5–16, 2007.
- [12] D. L. Brasaemle, G. Dolios, L. Shapiro, and R. Wang, "Proteomic analysis of proteins associated with lipid droplets of basal and lipolytically stimulated 3T3-L1 adipocytes," *J. Biol. Chem.*, vol. 279, no. 45, pp. 46835–46842, 2004.
- [13] D. A. Brown, "Lipid droplets: Proteins floating on a pool of fat," *Curr. Biol.*, vol. 11, no. 11, pp. 446–449, 2001.
- [14] R. Zechner, P. C. Kienesberger, G. Haemmerle, R. Zimmermann, and A. Lass, "Adipose triglyceride lipase and the lipolytic catabolism of cellular fat stores," *J. Lipid Res.*, vol. 50, no. 1, pp. 3–21, 2009.
- [15] C.-L. E. Yen, S. J. Stone, S. Koliwad, C. Harris, and R. V. Farese, "Thematic Review Series: Glycerolipids. DGAT enzymes and triacylglycerol biosynthesis," *J. Lipid Res.*, vol. 49, no. 11, pp. 2283–2301, 2008.
- [16] T. O. Eichmann and A. Lass, "DAG tales: The multiple faces of diacylglycerol - Stereochemistry, metabolism, and signaling," *Cell. Mol. Life Sci.*, vol. 72, no. 20, pp. 3931–3952, 2015.
- [17] C. M. Jenkins, D. J. Mancuso, W. Yan, H. F. Sims, B. Gibson, and R. W. Gross,

- “Identification, cloning, expression, and purification of three novel human calcium-independent phospholipase A2 family members possessing triacylglycerol lipase and acylglycerol transacylase activities,” *J. Biol. Chem.*, vol. 279, no. 47, pp. 48968–48975, 2004.
- [18] R. Zimmermann *et al.*, “Fat mobilization in adipose tissue is promoted by adipose triglyceride lipase,” *Science*, vol. 306, no. November, pp. 1383–1386, 2004.
- [19] J. A. Villena, S. Roy, E. Sarkadi-Nagy, K. H. Kim, and S. S. Hei, “Desnutrin, an adipocyte gene encoding a novel patatin domain-containing protein, is induced by fasting and glucocorticoids: Ectopic expression of desnutrin increases triglyceride hydrolysis,” *J. Biol. Chem.*, vol. 279, no. 45, pp. 47066–47075, 2004.
- [20] A. Lass *et al.*, “Adipose triglyceride lipase-mediated lipolysis of cellular fat stores is activated by CGI-58 and defective in Chanarin-Dorfman Syndrome,” *Cell Metab.*, vol. 3, no. 5, pp. 309–319, 2006.
- [21] F. P. W. Radner *et al.*, “Growth retardation, impaired triacylglycerol catabolism, hepatic steatosis, and lethal skin barrier defect in mice lacking comparative gene identification-58 (CGI-58),” *J. Biol. Chem.*, vol. 285, no. 10, pp. 7300–7311, 2010.
- [22] M. Vaughan, J. Berger, and D. Steinberg, “Hormone-sensitive Lipase and Tissue Hormone-sensitive Lipase and Monoglyceride Activities in Adipose Tissue,” *J. Biol. Chem.*, vol. 239, no. 2, pp. 401–409, 1964.
- [23] P. Strålfors and P. Befrage, “Phosphorylation of hormone-sensitive lipase by cyclic AMP-dependent protein kinase.” *J. Biol. Chem.*, vol. 258, no. 24, pp. 15146–52, 1983.
- [24] H. Miyoshi *et al.*, “Perilipin promotes hormone-sensitive lipase-mediated adipocyte lipolysis via phosphorylation-dependent and -independent mechanisms,” *J. Biol. Chem.*, vol. 281, no. 23, pp. 15837–15844, 2006.
- [25] G. Fredrikson and P. Befrage, “Positional specificity of hormone-sensitive lipase from rat adipose tissue,” *J. Biol. Chem.*, vol. 258, no. 23, pp. 14253–14256, 1983.
- [26] G. Haemmerle *et al.*, “Hormone-sensitive lipase deficiency in mice causes diglyceride accumulation in adipose tissue, muscle, and testis,” *J. Biol. Chem.*, vol. 277, no. 7, pp. 4806–4815, 2002.
- [27] G. Fredrikson, H. Tornqvist, and P. Befrage, “Hormone-sensitive lipase and monoacylglycerol lipase are both required for complete degradation of adipocyte triacylglycerol,” 1986.
- [28] X. Han, *Comprehensive Mass Spectrometry of Lipids*. Hoboken, New Jersey: JohnWiley & Sons, Inc., Hoboken, New Jersey, 2016.
- [29] M. Yamashita and J. B. Fenn, “Electrospray ion source. Another variation on the free-jet theme,” *J. Phys. Chem.*, vol. 88, no. 20, pp. 4451–4459, 1984.
- [30] The Royal Swedish Academy of Sciences, “Mass spectrometry (MS) and nuclear magnetic resonance (NMR) applied to biological macromolecules,” *October*, vol. 1, no. October, pp. 1–13, 2002.
- [31] A. P. Bruins, “Mechanistic aspects of electrospray ionization,” *J. Chromatogr. A*, vol. 794, no. 1–2, pp. 345–357, 1998.
- [32] J. Fernandez De La Mora, “Electrospray ionization of large multiply charged species proceeds via Dole’s charged residue mechanism,” *Anal. Chim. Acta*, vol. 406, no. 1, pp. 93–104, 2000.

- [33] J. V. Iribarne, "On the evaporation of small ions from charged droplets," *J. Chem. Phys.*, vol. 64, no. 6, p. 2287, 1976.
- [34] I. V. Chernushevich, A. V. Loboda, and B. A. Thomson, "An introduction to quadrupole-time-of-flight mass spectrometry," *J. Mass Spectrom.*, vol. 36, no. 8, pp. 849–865, 2001.
- [35] R. Wood and R. D. Harlow, "Structural analyses of rat liver phosphoglycerides," *Arch. Biochem. Biophys.*, vol. 135, no. 1, pp. 272–281, 1969.
- [36] K. Kishimoto, R. Urade, T. Ogawa, and T. Moriyama, "Nondestructive quantification of neutral lipids by thin-layer chromatography and laser-fluorescent scanning: Suitable methods for 'lipidome' analysis," *Biochem. Biophys. Res. Commun.*, vol. 281, no. 3, pp. 657–662, 2001.
- [37] X. Han and R. W. Gross, "Global analyses of cellular lipidomes directly from crude extracts of biological samples by ESI mass spectrometry," *J. Lipid Res.*, vol. 44, no. 6, pp. 1071–1079, 2003.
- [38] X. Han, K. Yang, and R. W. Gross, "Multi-dimensional mass spectrometry-based shotgun lipidomics and novel strategies for lipidomic analyses," *Mass Spec Rev* 31, vol. 47, pp. 134–178, 2012.
- [39] J. Folch, M. Lees, and G. H. S. Stanley, "A simple method for the isolation and purification of total lipids from animal tissues," *J Biol Chem*, vol. 226, no. 1. pp. 497–509, 1957.
- [40] V. Matyash, G. Liebisch, T. V. Kurzchalia, A. Shevchenko, and D. Schwudke, "Lipid extraction by methyl- *tert* -butyl ether for high-throughput lipidomics," *J. Lipid Res.*, vol. 49, no. 5, pp. 1137–1146, 2008.
- [41] L. Löfgren, G.-B. Forsberg, and M. Ståhlman, "The BUME method: a new rapid and simple chloroform-free method for total lipid extraction of animal tissue," *Sci. Rep.*, vol. 6, no. 1, p. 27688, 2016.
- [42] E. G. Bligh and W. J. Dyer, "A rapid method of total lipid extraction and purification," *Natl. Res. Counc. Canada*, vol. 37, no. 8, 1959.
- [43] Y. Y. Zhao, S. P. Wu, S. Liu, Y. Zhang, and R. C. Lin, "Ultra-performance liquid chromatography-mass spectrometry as a sensitive and powerful technology in lipidomic applications," *Chem. Biol. Interact.*, vol. 220, pp. 181–192, 2014.
- [44] J. Repelnig, "Mapping the epidermal lipid landscape by mass spectrometry (master thesis)." University of Graz, pp. 1–72, 2018.
- [45] O. L. Knittelfelder, B. P. Weberhofer, T. O. Eichmann, S. D. Kohlwein, and G. N. Rechberger, "A versatile ultra-high performance LC-MS method for lipid profiling," *J. Chromatogr. B Anal. Technol. Biomed. Life Sci.*, vol. 951–952, no. 1, pp. 119–128, 2014.
- [46] J. Hartler, M. Trötz Müller, C. Chitraju, F. Spener, H. C. Köfeler, and G. G. Thallinger, "Lipid data analyzer: Unattended identification and quantitation of lipids in LC-MS data," *Bioinformatics*, vol. 27, no. 4, pp. 572–577, 2011.
- [47] J. Hartler, H. C. Köfeler, M. Trötz Müller, G. G. Thallinger, and F. Spener, "Assessment of lipidomic species in hepatocyte lipid droplets from stressed mouse models," *Sci. Data*, vol. 1, pp. 1–12, 2014.
- [48] M. Tschernitz, "Assessment of different lipid extraction methods (project protocol)." University of Graz, pp. 1–14, 2017.

7. Table of figures

| | |
|--|----|
| Figure 1: Representative structures for the eight major lipid categories. Ref. 1: http://www.lipidmaps.org/tools/index.html (20.05.2018). | 8 |
| Figure 2: Simplified TAG lipolysis and involved enzymes and intermediates..... | 13 |
| Figure 3: Scheme of ESI source and process in positive ionization mode. | 15 |
| Figure 4: Scheme of a reflector TOF. | 17 |
| Figure 5: A lipidomics workflow..... | 21 |
| Figure 6: General MTBE lipid extraction workflow. | 24 |
| Figure 7: Selected lipid classes of chicken heart and liver extracted using Folch and MTBE method..... | 27 |
| Figure 8: Peak identification of TAG species as ammonium adduct. | 29 |
| Figure 9: LDA 2 mass-list example. | 30 |
| Figure 10: Visualization of data increase in course of the lipidomic workflow on a big, biological sample set..... | 31 |
| Figure 11: Flowchart for data processing of LDA 2 output data with DPS. | 32 |
| Figure 12: Snapshot of DPS annotation spreadsheets “Mouse No Data” and “Resolved Lipids MS”..... | 33 |
| Figure 13: Snapshot of DPS “Layout” spreadsheet for LDA 2 data input. | 34 |
| Figure 14: Snapshot of DPS normalization spreadsheets “Area Tissue Weight” and “Value Assignment”. | 35 |
| Figure 15: Snapshot of the DPS “Average” and “StaDevS” spreadsheets..... | 36 |
| Figure 16: Snapshot of the DPS “T-Test Significance” spreadsheet. | 37 |
| Figure 17: Snapshot of the DPS “heatmap” spreadsheet. | 37 |
| Figure 18: Snapshot of the DPS “SpeciesSum” spreadsheet..... | 38 |
| Figure 19: Statistical analysis of TAG in various tissues and genotypes. | 40 |
| Figure 20: Excel generated heatmap of TAG species in wild-type and ATGL deficient murine tissues.... | 41 |
| Figure 21: In-depth visualization workflow of PC in different wild-type mouse tissues. | 43 |
| Figure 22: PCA with reduced PC data. | 45 |
| Figure 23: Combined PCA and heatmap analysis of Cer species in wild-type tissues. | 47 |
| Figure 24: Combined PCA, heatmap and statistical analysis of Cer species in ATGL deficient and wild-type tissues. | 48 |
| Figure 25: Sample weight, solvent volume and ISTD concentration recommendation for several wild-type tissues. | 50 |

8. List of abbreviations

| | |
|-------------------|--|
| ATGL | Adipose TriGlyceride Lipase |
| BAT | Brown Adipose Tissue |
| CE | Cholesteryl-Erster |
| Cer | Ceramide |
| Cer-OH | Hydroxyl-Ceramide |
| CGI-58 | Comparative Gene Identification-58 |
| CID | Collision Induced Decomposition |
| CL | CardioLipin |
| DAG | DiAcylGlycerol |
| DGAT | DiacylGlycerol AcylTransferase |
| DPS | Data Processing Sheet |
| ESI | ElectroSpray Ionization |
| FA | Fatty Acid |
| GC | Gas Chromatography |
| GL | GlyceroLipid |
| Hex-Cer | Hexosyl-Ceramide |
| Hex-Cer-OH | Hexosyl-Hydroxyl-Ceramide |
| HILIC | Hydrophilic Interaction Chromatography |
| HPLC | High-Performance Liquid Chromatography |
| HSL | Hormone-Sensitive Lipase |
| ISTD | Internal STandarD |
| LC | Liquid Chromatography |
| LD | Lipid Droplet |
| LDA 2 | Lipid Data Analyzer 2 |
| Lipid MAPS | Lipid Metabolism And Pathway Strategy |
| LPC | LysoPhosphatidylCholine |
| m/z | mass to charge |
| MAG | MonoAcylGlycerol |
| MGL | MonoacylGlycerol Lipase |

| | |
|----------------------|--|
| <i>MS</i> | Mass Spectrometry |
| <i>MSF</i> | Magnetic Sector Field |
| <i>MS-QQQ</i> | Triple-Quadrupole Mass Spectrometry |
| <i>MTBE</i> | Methyl-Tert Butyl Ether |
| <i>NL</i> | Neutral-Loss |
| <i>NMR</i> | Nuclear Magnetic Resonance |
| <i>NP</i> | Normal Phase |
| <i>PC</i> | PhosphatidylCholine |
| <i>PCA</i> | Principal Component Analysis |
| <i>PE</i> | PhosphatidylEthanolamine |
| <i>PI</i> | PhosphatidylInositol |
| <i>PK</i> | PolyKetide |
| <i>PL</i> | PhosphoLipid |
| <i>Pre</i> | Precursor-ion |
| <i>PS</i> | PhosphatidylSerine |
| <i>qTOF</i> | quadrupole-Time-Of-Flight |
| <i>RF</i> | Response Factor |
| <i>RP</i> | Reversed Phase |
| <i>SL</i> | SphingoLipid |
| <i>SM</i> | SphingoMyelin |
| <i>TAG</i> | TriAcylGlycerol |
| <i>UHPLC</i> | Ultra-High-Performance Liquid Chromatography |

9. Appendix

Table S1: Sample information table

| Mouse Nr. | Mouseline | Geno-type | Age (weeks) | Tissue | Body weight (g) | Tissue weight (mg) | Resolved in PMW | Dilution for MS |
|-----------|-----------------|-----------|-------------|---------------|-----------------|--------------------|-----------------|-----------------|
| 95982 | ATGL-ko/MHC-A35 | A0 | 8.43 | brain | 18.95 | 456 | 500µl | |
| 95982 | ATGL-ko/MHC-A35 | A0 | 8.43 | adrenal gland | 18.95 | 3 | 250µl | |
| 95982 | ATGL-ko/MHC-A35 | A0 | 8.43 | liver | 18.95 | 231 | 1000µl | 1:5 |
| 95982 | ATGL-ko/MHC-A35 | A0 | 8.43 | tongue | 18.95 | 42 | 250µl | |
| 95982 | ATGL-ko/MHC-A35 | A0 | 8.43 | heart | 18.95 | 133 | 1500µl | |
| 95982 | ATGL-ko/MHC-A35 | A0 | 8.43 | lung | 18.95 | 131 | 500µl | |
| 95982 | ATGL-ko/MHC-A35 | A0 | 8.43 | spleen | 18.95 | 36 | 250µl | |
| 95982 | ATGL-ko/MHC-A35 | A0 | 8.43 | pancreas | 18.95 | 67 | 250µl | |
| 95982 | ATGL-ko/MHC-A35 | A0 | 8.43 | kidney | 18.95 | 240 | 250µl | |
| 95982 | ATGL-ko/MHC-A35 | A0 | 8.43 | BAT | 18.95 | 488 | 1500µl | 1:5 |
| 95982 | ATGL-ko/MHC-A35 | A0 | 8.43 | quadriceps | 18.95 | 210 | 250µl | |
| 95982 | ATGL-ko/MHC-A35 | A0 | 8.43 | plasma | 18.95 | 89 | 200µl | |
| 95987 | ATGL-ko/MHC-A35 | A0 | 8.43 | brain | 18.21 | 421 | 500µl | |
| 95987 | ATGL-ko/MHC-A35 | A0 | 8.43 | adrenal gland | 18.21 | 6 | 250µl | |
| 95987 | ATGL-ko/MHC-A35 | A0 | 8.43 | liver | 18.21 | 140 | 1000µl | 1:5 |
| 95987 | ATGL-ko/MHC-A35 | A0 | 8.43 | tongue | 18.21 | 75 | 250µl | |
| 95987 | ATGL-ko/MHC-A35 | A0 | 8.43 | heart | 18.21 | 146 | 1500µl | |
| 95987 | ATGL-ko/MHC-A35 | A0 | 8.43 | lung | 18.21 | 116 | 500µl | |
| 95987 | ATGL-ko/MHC-A35 | A0 | 8.43 | spleen | 18.21 | 41 | 250µl | |
| 95987 | ATGL-ko/MHC-A35 | A0 | 8.43 | pancreas | 18.21 | 33 | 250µl | |
| 95987 | ATGL-ko/MHC-A35 | A0 | 8.43 | kidney | 18.21 | 241 | 250µl | |
| 95987 | ATGL-ko/MHC-A35 | A0 | 8.43 | BAT | 18.21 | 445 | 1500µl | 1:5 |
| 95987 | ATGL-ko/MHC-A35 | A0 | 8.43 | quadriceps | 18.21 | 217 | 250µl | |
| 95987 | ATGL-ko/MHC-A35 | A0 | 8.43 | plasma | 18.21 | 100 | 200µl | |
| 95988 | ATGL-ko/MHC-A35 | A0 | 8.43 | brain | 19.10 | 403 | 500µl | |
| 95988 | ATGL-ko/MHC-A35 | A0 | 8.43 | adrenal gland | 19.10 | 4 | 250µl | |
| 95988 | ATGL-ko/MHC-A35 | A0 | 8.43 | liver | 19.10 | 117 | 1000µl | 1:5 |
| 95988 | ATGL-ko/MHC-A35 | A0 | 8.43 | tongue | 19.10 | 47 | 250µl | |
| 95988 | ATGL-ko/MHC-A35 | A0 | 8.43 | heart | 19.10 | 131 | 1500µl | |
| 95988 | ATGL-ko/MHC-A35 | A0 | 8.43 | lung | 19.10 | 120 | 500µl | |
| 95988 | ATGL-ko/MHC-A35 | A0 | 8.43 | spleen | 19.10 | 39 | 250µl | |
| 95988 | ATGL-ko/MHC-A35 | A0 | 8.43 | pancreas | 19.10 | 87 | 250µl | |
| 95988 | ATGL-ko/MHC-A35 | A0 | 8.43 | kidney | 19.10 | 214 | 250µl | |
| 95988 | ATGL-ko/MHC-A35 | A0 | 8.43 | BAT | 19.10 | 403 | 1500µl | 1:5 |
| 95988 | ATGL-ko/MHC-A35 | A0 | 8.43 | quadriceps | 19.10 | 222 | 250µl | |
| 95988 | ATGL-ko/MHC-A35 | A0 | 8.43 | plasma | 19.10 | 97 | 200µl | |
| 95990 | ATGL-ko/MHC-A35 | A0 | 8.43 | brain | 16.80 | 434 | 500µl | |

| | | | | | | | | |
|-------|-----------------|----|------|---------------|-------|-----|--------|-----|
| 95990 | ATGL-ko/MHC-A35 | A0 | 8.43 | adrenal gland | 16.80 | 5 | 250µl | |
| 95990 | ATGL-ko/MHC-A35 | A0 | 8.43 | liver | 16.80 | 172 | 1000µl | 1:5 |
| 95990 | ATGL-ko/MHC-A35 | A0 | 8.43 | tongue | 16.80 | 46 | 250µl | |
| 95990 | ATGL-ko/MHC-A35 | A0 | 8.43 | heart | 16.80 | 120 | 1500µl | |
| 95990 | ATGL-ko/MHC-A35 | A0 | 8.43 | lung | 16.80 | 95 | 500µl | |
| 95990 | ATGL-ko/MHC-A35 | A0 | 8.43 | spleen | 16.80 | 30 | 250µl | |
| 95990 | ATGL-ko/MHC-A35 | A0 | 8.43 | pancreas | 16.80 | 58 | 250µl | |
| 95990 | ATGL-ko/MHC-A35 | A0 | 8.43 | kidney | 16.80 | 180 | 250µl | |
| 95990 | ATGL-ko/MHC-A35 | A0 | 8.43 | BAT | 16.80 | 345 | 1500µl | 1:5 |
| 95990 | ATGL-ko/MHC-A35 | A0 | 8.43 | quadriceps | 16.80 | 176 | 250µl | |
| 95990 | ATGL-ko/MHC-A35 | A0 | 8.43 | plasma | 16.80 | 102 | 200µl | |
| 95970 | ATGL-ko/MHC-A35 | A2 | 8.43 | brain | 14.51 | 414 | 500µl | |
| 95970 | ATGL-ko/MHC-A35 | A2 | 8.43 | adrenal gland | 14.51 | 4 | 250µl | |
| 95970 | ATGL-ko/MHC-A35 | A2 | 8.43 | liver | 14.51 | 262 | 1000µl | 1:5 |
| 95970 | ATGL-ko/MHC-A35 | A2 | 8.43 | tongue | 14.51 | 58 | 250µl | |
| 95970 | ATGL-ko/MHC-A35 | A2 | 8.43 | heart | 14.51 | 72 | 1500µl | |
| 95970 | ATGL-ko/MHC-A35 | A2 | 8.43 | lung | 14.51 | 98 | 500µl | |
| 95970 | ATGL-ko/MHC-A35 | A2 | 8.43 | spleen | 14.51 | 39 | 250µl | |
| 95970 | ATGL-ko/MHC-A35 | A2 | 8.43 | pancreas | 14.51 | 103 | 250µl | |
| 95970 | ATGL-ko/MHC-A35 | A2 | 8.43 | kidney | 14.51 | 208 | 250µl | |
| 95970 | ATGL-ko/MHC-A35 | A2 | 8.43 | BAT | 14.51 | 31 | 500µl | 1:5 |
| 95970 | ATGL-ko/MHC-A35 | A2 | 8.43 | quadriceps | 14.51 | 211 | 250µl | |
| 95970 | ATGL-ko/MHC-A35 | A2 | 8.43 | plasma | 14.51 | 100 | 200µl | |
| 95995 | ATGL-ko/MHC-A35 | A2 | 8.43 | brain | 13.63 | 423 | 500µl | |
| 95995 | ATGL-ko/MHC-A35 | A2 | 8.43 | adrenal gland | 13.63 | 5 | 250µl | |
| 95995 | ATGL-ko/MHC-A35 | A2 | 8.43 | liver | 13.63 | 219 | 1000µl | 1:5 |
| 95995 | ATGL-ko/MHC-A35 | A2 | 8.43 | tongue | 13.63 | 47 | 250µl | |
| 95995 | ATGL-ko/MHC-A35 | A2 | 8.43 | heart | 13.63 | 117 | 1500µl | |
| 95995 | ATGL-ko/MHC-A35 | A2 | 8.43 | lung | 13.63 | 105 | 500µl | |
| 95995 | ATGL-ko/MHC-A35 | A2 | 8.43 | spleen | 13.63 | 37 | 250µl | |
| 95995 | ATGL-ko/MHC-A35 | A2 | 8.43 | pancreas | 13.63 | 69 | 250µl | |
| 95995 | ATGL-ko/MHC-A35 | A2 | 8.43 | kidney | 13.63 | 181 | 250µl | |
| 95995 | ATGL-ko/MHC-A35 | A2 | 8.43 | BAT | 13.63 | 16 | 500µl | 1:5 |
| 95995 | ATGL-ko/MHC-A35 | A2 | 8.43 | quadriceps | 13.63 | 203 | 250µl | |
| 95995 | ATGL-ko/MHC-A35 | A2 | 8.43 | plasma | 13.63 | 94 | 200µl | |
| 95996 | ATGL-ko/MHC-A35 | A2 | 8.43 | brain | 16.40 | 426 | 500µl | |
| 95996 | ATGL-ko/MHC-A35 | A2 | 8.43 | adrenal gland | 16.40 | 6 | 250µl | |
| 95996 | ATGL-ko/MHC-A35 | A2 | 8.43 | liver | 16.40 | 230 | 1000µl | 1:5 |
| 95996 | ATGL-ko/MHC-A35 | A2 | 8.43 | tongue | 16.40 | 51 | 250µl | |
| 95996 | ATGL-ko/MHC-A35 | A2 | 8.43 | heart | 16.40 | 93 | 1500µl | |
| 95996 | ATGL-ko/MHC-A35 | A2 | 8.43 | lung | 16.40 | 120 | 500µl | |

| | | | | | | | | |
|-------|-----------------|----|------|---------------|-------|-----|--------|-----|
| 95996 | ATGL-ko/MHC-A35 | A2 | 8.43 | spleen | 16.40 | 53 | 250µl | |
| 95996 | ATGL-ko/MHC-A35 | A2 | 8.43 | pancreas | 16.40 | 88 | 250µl | |
| 95996 | ATGL-ko/MHC-A35 | A2 | 8.43 | kidney | 16.40 | 222 | 250µl | |
| 95996 | ATGL-ko/MHC-A35 | A2 | 8.43 | BAT | 16.40 | 38 | 500µl | 1:5 |
| 95996 | ATGL-ko/MHC-A35 | A2 | 8.43 | quadriceps | 16.40 | 215 | 250µl | |
| 95996 | ATGL-ko/MHC-A35 | A2 | 8.43 | plasma | 16.40 | 101 | 200µl | |
| 96034 | ATGL-ko/MHC-A35 | A2 | 8.14 | brain | 15.92 | 436 | 500µl | |
| 96034 | ATGL-ko/MHC-A35 | A2 | 8.14 | adrenal gland | 15.92 | 5 | 250µl | |
| 96034 | ATGL-ko/MHC-A35 | A2 | 8.14 | liver | 15.92 | 226 | 1000µl | 1:5 |
| 96034 | ATGL-ko/MHC-A35 | A2 | 8.14 | tongue | 15.92 | 42 | 250µl | |
| 96034 | ATGL-ko/MHC-A35 | A2 | 8.14 | heart | 15.92 | 93 | 1500µl | |
| 96034 | ATGL-ko/MHC-A35 | A2 | 8.14 | lung | 15.92 | 127 | 500µl | |
| 96034 | ATGL-ko/MHC-A35 | A2 | 8.14 | spleen | 15.92 | 44 | 250µl | |
| 96034 | ATGL-ko/MHC-A35 | A2 | 8.14 | pancreas | 15.92 | 93 | 250µl | |
| 96034 | ATGL-ko/MHC-A35 | A2 | 8.14 | kidney | 15.92 | 208 | 250µl | |
| 96034 | ATGL-ko/MHC-A35 | A2 | 8.14 | BAT | 15.92 | 36 | 500µl | 1:5 |
| 96034 | ATGL-ko/MHC-A35 | A2 | 8.14 | quadriceps | 15.92 | 177 | 250µl | |
| 96034 | ATGL-ko/MHC-A35 | A2 | 8.14 | plasma | 15.92 | 106 | 200µl | |

Table S2: LDA 2 masslist information table. *FA carbon atoms:double bonds, MF...molecular formula, MW...molecular weight, RT...retention time

| Class | Species* | MF* | MW* | Adduct Ion | m/z | RT* (min) |
|-------|----------|-----------|--------|------------|--------|-----------|
| TAG | 42:0 | C45H86O6 | 722.64 | (M+NH4)+ | 740.68 | 15.02 |
| TAG | 42:1 | C45H84O6 | 720.63 | (M+NH4)+ | 738.66 | 14.95 |
| TAG | 42:2 | C45H82O6 | 718.61 | (M+NH4)+ | 736.65 | 14.17 |
| TAG | 42:3 | C45H80O6 | 716.60 | (M+NH4)+ | 734.63 | 13.67 |
| TAG | 42:4 | C45H78O6 | 714.58 | (M+NH4)+ | 732.61 | 13.30 |
| TAG | 42:5 | C45H76O6 | 712.56 | (M+NH4)+ | 730.60 | 12.77 |
| TAG | 42:6 | C45H74O6 | 710.55 | (M+NH4)+ | 728.58 | 12.45 |
| TAG | 44:0 | C47H90O6 | 750.67 | (M+NH4)+ | 768.71 | 15.59 |
| TAG | 44:1 | C47H88O6 | 748.66 | (M+NH4)+ | 766.69 | 15.18 |
| TAG | 44:2 | C47H86O6 | 746.64 | (M+NH4)+ | 764.68 | 14.76 |
| TAG | 44:3 | C47H84O6 | 744.63 | (M+NH4)+ | 762.66 | 14.35 |
| TAG | 44:4 | C47H82O6 | 742.61 | (M+NH4)+ | 760.65 | 13.93 |
| TAG | 44:5 | C47H80O6 | 740.60 | (M+NH4)+ | 758.63 | 13.65 |
| TAG | 44:6 | C47H78O6 | 738.58 | (M+NH4)+ | 756.61 | 13.40 |
| TAG | 46:0 | C49H94O6 | 778.71 | (M+NH4)+ | 796.74 | 16.14 |
| TAG | 46:1 | C49H92O6 | 776.69 | (M+NH4)+ | 794.72 | 15.75 |
| TAG | 46:2 | C49H90O6 | 774.67 | (M+NH4)+ | 792.71 | 15.36 |
| TAG | 46:3 | C49H88O6 | 772.66 | (M+NH4)+ | 790.69 | 14.96 |
| TAG | 46:4 | C49H86O6 | 770.64 | (M+NH4)+ | 788.68 | 14.65 |
| TAG | 46:5 | C49H84O6 | 768.63 | (M+NH4)+ | 786.66 | 14.21 |
| TAG | 46:6 | C49H82O6 | 766.61 | (M+NH4)+ | 784.65 | 13.91 |
| TAG | 48:0 | C51H98O6 | 806.74 | (M+NH4)+ | 824.77 | 16.64 |
| TAG | 48:1 | C51H96O6 | 804.72 | (M+NH4)+ | 822.76 | 16.29 |
| TAG | 48:2 | C51H94O6 | 802.71 | (M+NH4)+ | 820.74 | 15.90 |
| TAG | 48:3 | C51H92O6 | 800.69 | (M+NH4)+ | 818.72 | 15.53 |
| TAG | 48:4 | C51H90O6 | 798.67 | (M+NH4)+ | 816.71 | 15.16 |
| TAG | 48:5 | C51H88O6 | 796.66 | (M+NH4)+ | 814.69 | 14.87 |
| TAG | 48:6 | C51H86O6 | 794.64 | (M+NH4)+ | 812.68 | 14.50 |
| TAG | 48:7 | C51H84O6 | 792.63 | (M+NH4)+ | 810.66 | 14.21 |
| TAG | 50:0 | C53H102O6 | 834.77 | (M+NH4)+ | 852.80 | 17.06 |
| TAG | 50:1 | C53H100O6 | 832.75 | (M+NH4)+ | 850.79 | 16.75 |
| TAG | 50:2 | C53H98O6 | 830.74 | (M+NH4)+ | 848.77 | 16.45 |
| TAG | 50:3 | C53H96O6 | 828.72 | (M+NH4)+ | 846.76 | 16.07 |
| TAG | 50:4 | C53H94O6 | 826.71 | (M+NH4)+ | 844.74 | 15.68 |
| TAG | 50:5 | C53H92O6 | 824.69 | (M+NH4)+ | 842.72 | 15.31 |
| TAG | 50:6 | C53H90O6 | 822.67 | (M+NH4)+ | 840.71 | 15.04 |
| TAG | 50:7 | C53H88O6 | 820.66 | (M+NH4)+ | 838.69 | 14.76 |
| TAG | 50:8 | C53H86O6 | 818.64 | (M+NH4)+ | 836.68 | 14.43 |
| TAG | 52:0 | C55H106O6 | 862.80 | (M+NH4)+ | 880.83 | 17.49 |

| | | | | | | |
|-----|-------|-----------|--------|----------|--------|-------|
| TAG | 52:1 | C55H104O6 | 860.78 | (M+NH4)+ | 878.82 | 17.19 |
| TAG | 52:2 | C55H102O6 | 858.77 | (M+NH4)+ | 876.80 | 16.86 |
| TAG | 52:3 | C55H100O6 | 856.75 | (M+NH4)+ | 874.79 | 16.58 |
| TAG | 52:4 | C55H98O6 | 854.74 | (M+NH4)+ | 872.77 | 16.23 |
| TAG | 52:5 | C55H96O6 | 852.72 | (M+NH4)+ | 870.76 | 15.85 |
| TAG | 52:6 | C55H94O6 | 850.71 | (M+NH4)+ | 868.74 | 15.57 |
| TAG | 52:7 | C55H92O6 | 848.69 | (M+NH4)+ | 866.72 | 15.20 |
| TAG | 52:8 | C55H90O6 | 846.67 | (M+NH4)+ | 864.71 | 15.00 |
| TAG | 52:9 | C55H88O6 | 844.66 | (M+NH4)+ | 862.69 | 14.67 |
| TAG | 54:0 | C57H110O6 | 890.83 | (M+NH4)+ | 908.86 | 17.82 |
| TAG | 54:1 | C57H108O6 | 888.81 | (M+NH4)+ | 906.85 | 17.58 |
| TAG | 54:2 | C57H106O6 | 886.80 | (M+NH4)+ | 904.83 | 17.28 |
| TAG | 54:3 | C57H104O6 | 884.78 | (M+NH4)+ | 902.82 | 16.94 |
| TAG | 54:4 | C57H102O6 | 882.77 | (M+NH4)+ | 900.80 | 16.68 |
| TAG | 54:5 | C57H100O6 | 880.75 | (M+NH4)+ | 898.79 | 16.36 |
| TAG | 54:6 | C57H98O6 | 878.74 | (M+NH4)+ | 896.77 | 16.01 |
| TAG | 54:7 | C57H96O6 | 876.72 | (M+NH4)+ | 894.76 | 15.75 |
| TAG | 54:8 | C57H94O6 | 874.71 | (M+NH4)+ | 892.74 | 15.40 |
| TAG | 54:9 | C57H92O6 | 872.69 | (M+NH4)+ | 890.72 | 15.04 |
| TAG | 56:0 | C59H114O6 | 918.86 | (M+NH4)+ | 936.90 | 18.04 |
| TAG | 56:1 | C59H112O6 | 916.85 | (M+NH4)+ | 934.88 | 17.89 |
| TAG | 56:2 | C59H110O6 | 914.83 | (M+NH4)+ | 932.86 | 17.65 |
| TAG | 56:3 | C59H108O6 | 912.81 | (M+NH4)+ | 930.85 | 17.36 |
| TAG | 56:4 | C59H106O6 | 910.80 | (M+NH4)+ | 928.83 | 17.08 |
| TAG | 56:5 | C59H104O6 | 908.78 | (M+NH4)+ | 926.82 | 16.80 |
| TAG | 56:6 | C59H102O6 | 906.77 | (M+NH4)+ | 924.80 | 16.60 |
| TAG | 56:7 | C59H100O6 | 904.75 | (M+NH4)+ | 922.79 | 16.33 |
| TAG | 56:8 | C59H98O6 | 902.74 | (M+NH4)+ | 920.77 | 16.10 |
| TAG | 56:9 | C59H96O6 | 900.72 | (M+NH4)+ | 918.76 | 15.73 |
| TAG | 56:10 | C59H94O6 | 898.71 | (M+NH4)+ | 916.74 | 15.40 |
| TAG | 56:11 | C59H92O6 | 896.69 | (M+NH4)+ | 914.72 | 15.20 |
| TAG | 58:1 | C61H116O6 | 944.88 | (M+NH4)+ | 962.91 | 18.09 |
| TAG | 58:2 | C61H114O6 | 942.86 | (M+NH4)+ | 960.90 | 17.95 |
| TAG | 58:3 | C61H112O6 | 940.85 | (M+NH4)+ | 958.88 | 17.73 |
| TAG | 58:4 | C61H110O6 | 938.83 | (M+NH4)+ | 956.86 | 17.47 |
| TAG | 58:5 | C61H108O6 | 936.81 | (M+NH4)+ | 954.85 | 17.21 |
| TAG | 58:6 | C61H106O6 | 934.80 | (M+NH4)+ | 952.83 | 17.02 |
| TAG | 58:7 | C61H104O6 | 932.78 | (M+NH4)+ | 950.82 | 16.73 |
| TAG | 58:8 | C61H102O6 | 930.77 | (M+NH4)+ | 948.80 | 16.45 |
| TAG | 58:9 | C61H100O6 | 928.75 | (M+NH4)+ | 946.79 | 16.29 |
| TAG | 58:10 | C61H98O6 | 926.74 | (M+NH4)+ | 944.77 | 15.92 |

| | | | | | | |
|-----|-------|-----------|---------|----------|---------|-------|
| TAG | 58:11 | C61H96O6 | 924.72 | (M+NH4)+ | 942.76 | 15.59 |
| TAG | 58:12 | C61H94O6 | 922.71 | (M+NH4)+ | 940.74 | 15.29 |
| TAG | 60:1 | C63H120O6 | 972.91 | (M+NH4)+ | 990.94 | 18.24 |
| TAG | 60:2 | C63H118O6 | 970.89 | (M+NH4)+ | 988.93 | 18.13 |
| TAG | 60:3 | C63H116O6 | 968.88 | (M+NH4)+ | 986.91 | 17.99 |
| TAG | 60:4 | C63H114O6 | 966.86 | (M+NH4)+ | 984.90 | 17.82 |
| TAG | 60:5 | C63H112O6 | 964.85 | (M+NH4)+ | 982.88 | 17.58 |
| TAG | 60:6 | C63H110O6 | 962.83 | (M+NH4)+ | 980.86 | 17.38 |
| TAG | 60:7 | C63H108O6 | 960.81 | (M+NH4)+ | 978.85 | 17.12 |
| TAG | 60:8 | C63H106O6 | 958.80 | (M+NH4)+ | 976.83 | 16.88 |
| TAG | 60:9 | C63H104O6 | 956.78 | (M+NH4)+ | 974.82 | 16.62 |
| TAG | 60:10 | C63H102O6 | 954.77 | (M+NH4)+ | 972.80 | 16.40 |
| TAG | 60:11 | C63H100O6 | 952.75 | (M+NH4)+ | 970.79 | 16.12 |
| TAG | 60:12 | C63H98O6 | 950.74 | (M+NH4)+ | 968.77 | 15.90 |
| TAG | 60:13 | C63H96O6 | 948.72 | (M+NH4)+ | 966.76 | 15.57 |
| TAG | 62:0 | C65H126O6 | 1002.96 | (M+NH4)+ | 1020.99 | 18.42 |
| TAG | 62:1 | C65H124O6 | 1000.94 | (M+NH4)+ | 1018.97 | 18.37 |
| TAG | 62:2 | C65H122O6 | 998.92 | (M+NH4)+ | 1016.96 | 18.26 |
| TAG | 62:3 | C65H120O6 | 996.91 | (M+NH4)+ | 1014.94 | 18.17 |
| TAG | 62:4 | C65H118O6 | 994.89 | (M+NH4)+ | 1012.93 | 18.02 |
| TAG | 62:5 | C65H116O6 | 992.88 | (M+NH4)+ | 1010.91 | 17.89 |
| TAG | 62:6 | C65H114O6 | 990.86 | (M+NH4)+ | 1008.90 | 17.71 |
| TAG | 62:7 | C65H112O6 | 988.85 | (M+NH4)+ | 1006.88 | 17.47 |
| TAG | 62:8 | C65H110O6 | 986.83 | (M+NH4)+ | 1004.86 | 17.38 |
| TAG | 62:9 | C65H108O6 | 984.81 | (M+NH4)+ | 1002.85 | 17.10 |
| TAG | 62:10 | C65H106O6 | 982.80 | (M+NH4)+ | 1000.83 | 16.92 |
| TAG | 62:11 | C65H104O6 | 980.78 | (M+NH4)+ | 998.82 | 16.73 |
| TAG | 62:12 | C65H102O6 | 978.77 | (M+NH4)+ | 996.80 | 16.45 |
| TAG | 62:13 | C65H100O6 | 976.75 | (M+NH4)+ | 994.79 | 16.12 |
| TAG | 62:14 | C65H98O6 | 974.74 | (M+NH4)+ | 992.77 | 15.79 |
| TAG | 64:1 | C67H128O6 | 1028.97 | (M+NH4)+ | 1047.01 | 18.46 |
| TAG | 64:2 | C67H126O6 | 1026.96 | (M+NH4)+ | 1044.99 | 18.37 |
| TAG | 64:3 | C67H124O6 | 1024.94 | (M+NH4)+ | 1042.97 | 18.30 |
| TAG | 64:4 | C67H122O6 | 1022.92 | (M+NH4)+ | 1040.96 | 18.21 |
| TAG | 64:5 | C67H120O6 | 1020.91 | (M+NH4)+ | 1038.94 | 18.13 |
| TAG | 64:6 | C67H118O6 | 1018.89 | (M+NH4)+ | 1036.93 | 18.00 |
| TAG | 64:7 | C67H116O6 | 1016.88 | (M+NH4)+ | 1034.91 | 17.83 |
| TAG | 64:8 | C67H114O6 | 1014.86 | (M+NH4)+ | 1032.90 | 17.63 |
| TAG | 64:9 | C67H112O6 | 1012.85 | (M+NH4)+ | 1030.88 | 17.39 |
| TAG | 64:10 | C67H110O6 | 1010.83 | (M+NH4)+ | 1028.86 | 17.12 |
| TAG | 66:1 | C69H132O6 | 1057.00 | (M+NH4)+ | 1075.04 | 18.52 |

| | | | | | | |
|-----|------|------------|---------|----------|---------|-------|
| TAG | 66:2 | C69H130O6 | 1054.99 | (M+NH4)+ | 1073.02 | 18.46 |
| TAG | 66:3 | C69H128O6 | 1052.97 | (M+NH4)+ | 1071.01 | 18.39 |
| TAG | 66:4 | C69H126O6 | 1050.96 | (M+NH4)+ | 1068.99 | 18.32 |
| TAG | 66:5 | C69H124O6 | 1048.94 | (M+NH4)+ | 1066.97 | 18.24 |
| TAG | 66:6 | C69H122O6 | 1046.92 | (M+NH4)+ | 1064.96 | 18.15 |
| TAG | 66:7 | C69H120O6 | 1044.91 | (M+NH4)+ | 1062.94 | 18.01 |
| TAG | 66:8 | C69H118O6 | 1042.89 | (M+NH4)+ | 1060.93 | 17.91 |
| TAG | 68:1 | C71H136O6 | 1085.03 | (M+NH4)+ | 1103.07 | 18.54 |
| TAG | 68:2 | C71H134O6 | 1083.02 | (M+NH4)+ | 1101.05 | 18.52 |
| TAG | 68:3 | C71H132O6 | 1081.00 | (M+NH4)+ | 1099.04 | 18.48 |
| TAG | 68:4 | C71H130O6 | 1078.99 | (M+NH4)+ | 1097.02 | 18.41 |
| TAG | 68:5 | C71H128O6 | 1076.97 | (M+NH4)+ | 1095.01 | 18.37 |
| TAG | 68:6 | C71H126O6 | 1074.96 | (M+NH4)+ | 1092.99 | 18.30 |
| TAG | 68:7 | C71H124O6 | 1072.94 | (M+NH4)+ | 1090.97 | 18.21 |
| TAG | 70:2 | C73H138O6 | 1111.05 | (M+NH4)+ | 1129.08 | 18.59 |
| TAG | 70:3 | C73H136O6 | 1109.03 | (M+NH4)+ | 1127.07 | 18.54 |
| TAG | 70:4 | C73H134O6 | 1107.02 | (M+NH4)+ | 1125.05 | 18.50 |
| TAG | 70:5 | C73H132O6 | 1105.00 | (M+NH4)+ | 1123.04 | 18.44 |
| TAG | 70:6 | C73H130O6 | 1102.99 | (M+NH4)+ | 1121.02 | 18.39 |
| TAG | 72:2 | C75H142O6 | 1139.08 | (M+NH4)+ | 1157.11 | 18.66 |
| TAG | 72:3 | C75H140O6 | 1137.06 | (M+NH4)+ | 1155.10 | 18.63 |
| TAG | 72:4 | C75H138O6 | 1135.05 | (M+NH4)+ | 1153.08 | 18.56 |
| PC | 26:3 | C34H62O8PN | 643.42 | (M+H)+ | 644.43 | 6.07 |
| PC | 28:0 | C36H72O8PN | 677.50 | (M+H)+ | 678.51 | 7.73 |
| PC | 30:0 | C38H76O8PN | 705.53 | (M+H)+ | 706.54 | 8.56 |
| PC | 30:1 | C38H74O8PN | 703.52 | (M+H)+ | 704.52 | 8.03 |
| PC | 30:2 | C38H72O8PN | 701.50 | (M+H)+ | 702.51 | 7.46 |
| PC | 32:0 | C40H80O8PN | 733.56 | (M+H)+ | 734.57 | 9.43 |
| PC | 32:1 | C40H78O8PN | 731.55 | (M+H)+ | 732.55 | 8.84 |
| PC | 32:2 | C40H76O8PN | 729.53 | (M+H)+ | 730.54 | 8.27 |
| PC | 32:3 | C40H74O8PN | 727.52 | (M+H)+ | 728.52 | 7.90 |
| PC | 34:1 | C42H82O8PN | 759.58 | (M+H)+ | 760.59 | 9.67 |
| PC | 34:2 | C42H80O8PN | 757.56 | (M+H)+ | 758.57 | 9.08 |
| PC | 34:3 | C42H78O8PN | 755.55 | (M+H)+ | 756.55 | 8.64 |
| PC | 34:4 | C42H76O8PN | 753.53 | (M+H)+ | 754.54 | 8.29 |
| PC | 34:5 | C42H74O8PN | 751.52 | (M+H)+ | 752.52 | 7.88 |
| PC | 36:0 | C44H88O8PN | 789.62 | (M+H)+ | 790.63 | 11.01 |
| PC | 36:1 | C44H86O8PN | 787.61 | (M+H)+ | 788.62 | 10.59 |
| PC | 36:2 | C44H84O8PN | 785.59 | (M+H)+ | 786.60 | 9.95 |
| PC | 36:3 | C44H82O8PN | 783.58 | (M+H)+ | 784.59 | 9.49 |
| PC | 36:4 | C44H80O8PN | 781.56 | (M+H)+ | 782.57 | 9.21 |

| | | | | | | |
|----|-------|-------------|--------|--------|--------|-------|
| PC | 36:5 | C44H78O8PN | 779.55 | (M+H)+ | 780.55 | 8.62 |
| PC | 36:6 | C44H76O8PN | 777.53 | (M+H)+ | 778.54 | 8.29 |
| PC | 36:7 | C44H74O8PN | 775.52 | (M+H)+ | 776.52 | 7.88 |
| PC | 38:0 | C46H92O8PN | 817.66 | (M+H)+ | 818.66 | 11.90 |
| PC | 38:1 | C46H90O8PN | 815.64 | (M+H)+ | 816.65 | 11.44 |
| PC | 38:2 | C46H88O8PN | 813.62 | (M+H)+ | 814.63 | 10.93 |
| PC | 38:3 | C46H86O8PN | 811.61 | (M+H)+ | 812.62 | 10.39 |
| PC | 38:4 | C46H84O8PN | 809.59 | (M+H)+ | 810.60 | 9.89 |
| PC | 38:5 | C46H82O8PN | 807.58 | (M+H)+ | 808.59 | 9.45 |
| PC | 38:6 | C46H80O8PN | 805.56 | (M+H)+ | 806.57 | 8.91 |
| PC | 38:7 | C46H78O8PN | 803.55 | (M+H)+ | 804.55 | 8.56 |
| PC | 38:8 | C46H76O8PN | 801.53 | (M+H)+ | 802.54 | 8.07 |
| PC | 40:0 | C48H96O8PN | 845.69 | (M+H)+ | 846.70 | 12.86 |
| PC | 40:1 | C48H94O8PN | 843.67 | (M+H)+ | 844.68 | 12.29 |
| PC | 40:2 | C48H92O8PN | 841.66 | (M+H)+ | 842.66 | 11.77 |
| PC | 40:3 | C48H90O8PN | 839.64 | (M+H)+ | 840.65 | 11.29 |
| PC | 40:4 | C48H88O8PN | 837.62 | (M+H)+ | 838.63 | 10.76 |
| PC | 40:5 | C48H86O8PN | 835.61 | (M+H)+ | 836.62 | 10.32 |
| PC | 40:6 | C48H84O8PN | 833.59 | (M+H)+ | 834.60 | 10.00 |
| PC | 40:7 | C48H82O8PN | 831.58 | (M+H)+ | 832.59 | 9.41 |
| PC | 40:8 | C48H80O8PN | 829.56 | (M+H)+ | 830.57 | 8.84 |
| PC | 40:9 | C48H78O8PN | 827.55 | (M+H)+ | 828.55 | 8.36 |
| PC | 42:1 | C50H98O8PN | 871.70 | (M+H)+ | 872.71 | 13.04 |
| PC | 42:2 | C50H96O8PN | 869.69 | (M+H)+ | 870.70 | 12.57 |
| PC | 42:3 | C50H94O8PN | 867.67 | (M+H)+ | 868.68 | 11.86 |
| PC | 42:4 | C50H92O8PN | 865.66 | (M+H)+ | 866.66 | 11.42 |
| PC | 42:5 | C50H90O8PN | 863.64 | (M+H)+ | 864.65 | 10.93 |
| PC | 42:6 | C50H88O8PN | 861.62 | (M+H)+ | 862.63 | 10.65 |
| PC | 42:7 | C50H86O8PN | 859.61 | (M+H)+ | 860.62 | 10.22 |
| PC | 42:8 | C50H84O8PN | 857.59 | (M+H)+ | 858.60 | 9.63 |
| PC | 42:9 | C50H82O8PN | 855.58 | (M+H)+ | 856.59 | 9.30 |
| PC | 42:10 | C50H80O8PN | 853.56 | (M+H)+ | 854.57 | 8.84 |
| PC | 42:11 | C50H78O8PN | 851.55 | (M+H)+ | 852.55 | 8.32 |
| PC | 44:1 | C52H102O8PN | 899.73 | (M+H)+ | 900.74 | 13.82 |
| PC | 44:2 | C52H100O8PN | 897.72 | (M+H)+ | 898.73 | 13.40 |
| PC | 44:3 | C52H98O8PN | 895.70 | (M+H)+ | 896.71 | 12.97 |
| PC | 44:4 | C52H96O8PN | 893.69 | (M+H)+ | 894.70 | 12.62 |
| PC | 44:5 | C52H94O8PN | 891.67 | (M+H)+ | 892.68 | 11.92 |
| PC | 44:6 | C52H92O8PN | 889.66 | (M+H)+ | 890.66 | 11.37 |
| PC | 46:4 | C54H100O8PN | 921.72 | (M+H)+ | 922.73 | 13.40 |
| PC | 46:5 | C54H98O8PN | 919.70 | (M+H)+ | 920.71 | 12.71 |

| | | | | | | |
|----|------|-------------|--------|--------|--------|-------|
| PE | 28:0 | C33H66O8PN | 635.45 | (M-H)- | 634.44 | 7.70 |
| PE | 30:0 | C35H70O8PN | 663.48 | (M-H)- | 662.48 | 8.55 |
| PE | 30:1 | C35H68O8PN | 661.47 | (M-H)- | 660.46 | 7.93 |
| PE | 32:0 | C37H74O8PN | 691.52 | (M-H)- | 690.51 | 9.44 |
| PE | 32:1 | C37H72O8PN | 689.50 | (M-H)- | 688.49 | 8.81 |
| PE | 32:2 | C37H70O8PN | 687.48 | (M-H)- | 686.48 | 8.24 |
| PE | 34:1 | C39H76O8PN | 717.53 | (M-H)- | 716.52 | 9.81 |
| PE | 34:2 | C39H74O8PN | 715.52 | (M-H)- | 714.51 | 9.27 |
| PE | 34:3 | C39H72O8PN | 713.50 | (M-H)- | 712.49 | 8.66 |
| PE | 34:4 | C39H70O8PN | 711.48 | (M-H)- | 710.48 | 8.24 |
| PE | 36:1 | C41H80O8PN | 745.56 | (M-H)- | 744.55 | 10.66 |
| PE | 36:2 | C41H78O8PN | 743.55 | (M-H)- | 742.54 | 10.17 |
| PE | 36:3 | C41H76O8PN | 741.53 | (M-H)- | 740.52 | 9.51 |
| PE | 36:4 | C41H74O8PN | 739.52 | (M-H)- | 738.51 | 8.98 |
| PE | 36:5 | C41H72O8PN | 737.50 | (M-H)- | 736.49 | 8.46 |
| PE | 38:1 | C43H84O8PN | 773.59 | (M-H)- | 772.59 | 11.43 |
| PE | 38:2 | C43H82O8PN | 771.58 | (M-H)- | 770.57 | 11.00 |
| PE | 38:3 | C43H80O8PN | 769.56 | (M-H)- | 768.55 | 10.49 |
| PE | 38:4 | C43H78O8PN | 767.55 | (M-H)- | 766.54 | 10.29 |
| PE | 40:4 | C45H82O8PN | 795.58 | (M-H)- | 794.57 | 10.48 |
| PE | 40:7 | C45H76O8PN | 789.53 | (M-H)- | 788.52 | 9.55 |
| PE | 40:8 | C45H74O8PN | 787.52 | (M-H)- | 786.51 | 9.00 |
| PE | 40:9 | C45H72O8PN | 785.50 | (M-H)- | 784.49 | 8.48 |
| PE | 42:5 | C47H84O8PN | 821.59 | (M-H)- | 820.59 | 10.47 |
| PE | 42:6 | C47H82O8PN | 819.58 | (M-H)- | 818.57 | 9.97 |
| PE | 42:7 | C47H80O8PN | 817.56 | (M-H)- | 816.55 | 9.34 |
| PE | 42:8 | C47H78O8PN | 815.55 | (M-H)- | 814.54 | 8.81 |
| PS | 32:0 | C38H74O10PN | 735.50 | (M-H)- | 734.50 | 8.44 |
| PS | 34:1 | C40H76O10PN | 761.52 | (M-H)- | 760.51 | 8.66 |
| PS | 34:2 | C40H74O10PN | 759.50 | (M-H)- | 758.50 | 8.24 |
| PS | 36:0 | C42H82O10PN | 791.57 | (M-H)- | 790.56 | 10.23 |
| PS | 36:1 | C42H80O10PN | 789.55 | (M-H)- | 788.54 | 9.53 |
| PS | 36:2 | C42H78O10PN | 787.54 | (M-H)- | 786.53 | 9.00 |
| PS | 36:3 | C42H76O10PN | 785.52 | (M-H)- | 784.51 | 8.21 |
| PS | 36:4 | C42H74O10PN | 783.50 | (M-H)- | 782.50 | 7.72 |
| PS | 38:1 | C44H84O10PN | 817.58 | (M-H)- | 816.58 | 10.36 |
| PS | 38:2 | C44H82O10PN | 815.57 | (M-H)- | 814.56 | 9.77 |
| PS | 38:3 | C44H80O10PN | 813.55 | (M-H)- | 812.54 | 9.22 |
| PS | 38:4 | C44H78O10PN | 811.54 | (M-H)- | 810.53 | 8.96 |
| PS | 40:4 | C46H82O10PN | 839.57 | (M-H)- | 838.56 | 9.66 |
| PS | 40:6 | C46H78O10PN | 835.54 | (M-H)- | 834.53 | 8.90 |

| | | | | | | |
|-----|------|-------------|--------|----------|--------|-------|
| PS | 40:7 | C46H76O10PN | 833.52 | (M-H)- | 832.51 | 8.27 |
| PS | 42:1 | C48H92O10PN | 873.65 | (M-H)- | 872.64 | 11.82 |
| PS | 42:2 | C48H90O10PN | 871.63 | (M-H)- | 870.62 | 11.34 |
| PI | 34:2 | C43H79O13P | 834.53 | (M-H)- | 833.52 | 7.87 |
| PI | 36:2 | C45H83O13P | 862.56 | (M-H)- | 861.55 | 8.68 |
| PI | 36:3 | C45H81O13P | 860.54 | (M-H)- | 859.53 | 8.24 |
| PI | 36:4 | C45H79O13P | 858.53 | (M-H)- | 857.52 | 7.93 |
| PI | 38:2 | C47H87O13P | 890.59 | (M-H)- | 889.58 | 9.42 |
| PI | 38:3 | C47H85O13P | 888.57 | (M-H)- | 887.56 | 9.02 |
| PI | 38:4 | C47H83O13P | 886.56 | (M-H)- | 885.55 | 8.74 |
| PI | 40:5 | C49H85O13P | 912.57 | (M-H)- | 911.56 | 9.24 |
| PI | 40:6 | C49H83O13P | 910.56 | (M-H)- | 909.55 | 8.70 |
| PI | 40:7 | C49H81O13P | 908.54 | (M-H)- | 907.53 | 8.19 |
| LPC | 14:0 | C22H46O7N | 467.30 | (M+H)+ | 468.31 | 3.94 |
| LPC | 16:0 | C24H50O7N | 495.33 | (M+H)+ | 496.34 | 4.53 |
| LPC | 16:1 | C24H48O7N | 493.32 | (M+H)+ | 494.32 | 4.16 |
| LPC | 18:0 | C26H54O7N | 523.36 | (M+H)+ | 524.37 | 5.06 |
| LPC | 18:1 | C26H52O7N | 521.35 | (M+H)+ | 522.36 | 4.71 |
| LPC | 18:2 | C26H50O7N | 519.33 | (M+H)+ | 520.34 | 4.38 |
| LPC | 18:3 | C26H48O7N | 517.32 | (M+H)+ | 518.32 | 4.05 |
| LPC | 20:0 | C28H58O7N | 551.40 | (M+H)+ | 552.40 | 5.75 |
| LPC | 20:1 | C28H56O7N | 549.38 | (M+H)+ | 550.39 | 5.21 |
| LPC | 20:2 | C28H54O7N | 547.36 | (M+H)+ | 548.37 | 4.73 |
| LPC | 20:3 | C28H52O7N | 545.35 | (M+H)+ | 546.36 | 4.27 |
| LPC | 22:0 | C30H62O7N | 579.43 | (M+H)+ | 580.43 | 6.61 |
| LPC | 22:1 | C30H60O7N | 577.41 | (M+H)+ | 578.42 | 5.89 |
| LPC | 22:5 | C30H52O7N | 569.35 | (M+H)+ | 570.36 | 4.55 |
| LPC | 22:6 | C30H50O7N | 567.33 | (M+H)+ | 568.34 | 4.27 |
| LPC | 24:0 | C32H66O7N | 607.46 | (M+H)+ | 608.47 | 7.46 |
| LPC | 24:1 | C32H64O7N | 605.44 | (M+H)+ | 606.45 | 6.66 |
| LPC | 24:2 | C32H62O7N | 603.43 | (M+H)+ | 604.43 | 6.15 |
| Cer | 16:0 | C34H67O3N | 537.51 | (M-H2O)+ | 520.51 | 9.69 |
| Cer | 16:1 | C34H65O3N | 535.50 | (M-H2O)+ | 518.49 | 9.19 |
| Cer | 18:0 | C36H71O3N | 565.54 | (M-H2O)+ | 548.54 | 10.61 |
| Cer | 18:1 | C36H69O3N | 563.53 | (M-H2O)+ | 546.52 | 9.95 |
| Cer | 20:0 | C38H75O3N | 593.57 | (M-H2O)+ | 576.57 | 11.48 |
| Cer | 20:1 | C38H73O3N | 591.56 | (M-H2O)+ | 574.56 | 10.91 |
| Cer | 22:0 | C40H79O3N | 621.61 | (M-H2O)+ | 604.60 | 12.31 |
| Cer | 22:1 | C40H77O3N | 619.59 | (M-H2O)+ | 602.59 | 11.77 |
| Cer | 22:2 | C40H75O3N | 617.57 | (M-H2O)+ | 600.57 | 11.07 |
| Cer | 24:0 | C42H83O3N | 649.64 | (M-H2O)+ | 632.63 | 13.08 |

| | | | | | | |
|------------|------|-------------|--------|----------|--------|-------|
| Cer | 24:1 | C42H81O3N | 647.62 | (M-H2O)+ | 630.62 | 12.42 |
| Cer | 24:2 | C42H79O3N | 645.61 | (M-H2O)+ | 628.60 | 11.90 |
| Cer | 24:3 | C42H77O3N | 643.59 | (M-H2O)+ | 626.59 | 11.31 |
| Cer | 24:4 | C42H75O3N | 641.57 | (M-H2O)+ | 624.57 | 10.79 |
| Cer | 26:0 | C44H87O3N | 677.67 | (M-H2O)+ | 660.67 | 13.80 |
| Cer | 26:1 | C44H85O3N | 675.65 | (M-H2O)+ | 658.65 | 13.17 |
| Cer | 28:0 | C46H91O3N | 705.70 | (M-H2O)+ | 688.70 | 14.41 |
| Cer | 28:1 | C46H89O3N | 703.68 | (M-H2O)+ | 686.68 | 13.82 |
| Cer | 30:0 | C48H95O3N | 733.73 | (M-H2O)+ | 716.73 | 15.02 |
| Cer | 32:0 | C50H99O3N | 761.76 | (M-H2O)+ | 744.76 | 15.53 |
| Cer | 32:1 | C50H97O3N | 759.75 | (M-H2O)+ | 742.74 | 15.14 |
| Cer | 34:1 | C52H101O3N | 787.78 | (M-H2O)+ | 770.78 | 15.64 |
| Cer | 34:2 | C52H99O3N | 785.76 | (M-H2O)+ | 768.76 | 15.29 |
| Cer-OH | 24:0 | C42H83O4N | 665.63 | (M-H2O)+ | 648.63 | 12.71 |
| Hex-Cer | 14:0 | C38H73O8N | 671.53 | (M-H2O)+ | 654.53 | 7.94 |
| Hex-Cer | 16:0 | C40H77O8N | 699.56 | (M-H2O)+ | 682.56 | 8.80 |
| Hex-Cer | 18:0 | C42H81O8N | 727.60 | (M-H2O)+ | 710.59 | 9.67 |
| Hex-Cer | 18:1 | C42H79O8N | 725.58 | (M-H2O)+ | 708.58 | 9.10 |
| Hex-Cer | 20:0 | C44H85O8N | 755.63 | (M-H2O)+ | 738.62 | 10.54 |
| Hex-Cer | 22:0 | C46H89O8N | 783.66 | (M-H2O)+ | 766.66 | 11.40 |
| Hex-Cer | 24:0 | C48H93O8N | 811.69 | (M-H2O)+ | 794.69 | 12.21 |
| Hex-Cer | 24:1 | C48H91O8N | 809.67 | (M-H2O)+ | 792.67 | 11.48 |
| Hex-Cer | 26:0 | C50H97O8N | 839.72 | (M-H2O)+ | 822.72 | 12.95 |
| Hex-Cer | 26:1 | C50H95O8N | 837.71 | (M-H2O)+ | 820.70 | 12.27 |
| Hex-Cer-OH | 16:0 | C40H77O9N | 715.56 | (M-H2O)+ | 698.56 | 8.49 |
| Hex-Cer-OH | 18:0 | C42H81O9N | 743.59 | (M-H2O)+ | 726.59 | 9.39 |
| Hex-Cer-OH | 18:1 | C42H79O9N | 741.58 | (M-H2O)+ | 724.57 | 8.80 |
| Hex-Cer-OH | 20:0 | C44H85O9N | 771.62 | (M-H2O)+ | 754.62 | 10.26 |
| Hex-Cer-OH | 20:1 | C44H83O9N | 769.61 | (M-H2O)+ | 752.60 | 9.67 |
| Hex-Cer-OH | 22:0 | C46H89O9N | 799.65 | (M-H2O)+ | 782.65 | 11.13 |
| Hex-Cer-OH | 22:1 | C46H87O9N | 797.64 | (M-H2O)+ | 780.64 | 10.57 |
| Hex-Cer-OH | 24:0 | C48H93O9N | 827.68 | (M-H2O)+ | 810.68 | 11.94 |
| Hex-Cer-OH | 24:1 | C48H91O9N | 825.67 | (M-H2O)+ | 808.67 | 11.22 |
| Hex-Cer-OH | 24:2 | C48H89O9N | 823.65 | (M-H2O)+ | 806.65 | 10.67 |
| Hex-Cer-OH | 26:0 | C50H97O9N | 855.72 | (M-H2O)+ | 838.71 | 12.69 |
| Hex-Cer-OH | 26:1 | C50H95O9N | 853.70 | (M-H2O)+ | 836.70 | 12.01 |
| SM | 14:0 | C37H75O6PN2 | 674.54 | (M+H)+ | 675.54 | 7.55 |
| SM | 16:0 | C39H79O6PN2 | 702.57 | (M+H)+ | 703.58 | 8.38 |
| SM | 16:1 | C39H77O6PN2 | 700.55 | (M+H)+ | 701.56 | 7.81 |
| SM | 18:0 | C41H83O6PN2 | 730.60 | (M+H)+ | 731.61 | 9.27 |
| SM | 18:1 | C41H81O6PN2 | 728.58 | (M+H)+ | 729.59 | 8.69 |

| | | | | | | |
|------------|------|-------------|--------|----------|--------|-------|
| SM | 20:0 | C43H87O6PN2 | 758.63 | (M+H)+ | 759.64 | 10.17 |
| SM | 20:1 | C43H85O6PN2 | 756.61 | (M+H)+ | 757.62 | 9.56 |
| SM | 22:0 | C45H91O6PN2 | 786.66 | (M+H)+ | 787.67 | 11.05 |
| SM | 22:1 | C45H89O6PN2 | 784.65 | (M+H)+ | 785.65 | 10.46 |
| SM | 24:0 | C47H95O6PN2 | 814.69 | (M+H)+ | 815.70 | 11.88 |
| SM | 24:1 | C47H93O6PN2 | 812.68 | (M+H)+ | 813.68 | 11.13 |
| SM | 24:2 | C47H91O6PN2 | 810.66 | (M+H)+ | 811.67 | 10.59 |
| SM | 24:3 | C47H89O6PN2 | 808.65 | (M+H)+ | 809.65 | 10.13 |
| SM | 26:0 | C49H99O6PN2 | 842.72 | (M+H)+ | 843.73 | 12.69 |
| SM | 26:1 | C49H97O6PN2 | 840.71 | (M+H)+ | 841.72 | 11.94 |
| SM | 26:2 | C49H95O6PN2 | 838.69 | (M+H)+ | 839.70 | 11.42 |
| Ubichinone | 9:0 | C54H82O4 | 794.62 | (M+H)+ | 795.63 | 14.61 |
| Ubichinone | 10:0 | C59H90O4 | 862.68 | (M+H)+ | 863.69 | 15.59 |
| TAG (ISTD) | 45:0 | C48H92O6 | 764.69 | (M+NH4)+ | 782.72 | 15.97 |
| TAG (ISTD) | 51:0 | C54H104O6 | 848.78 | (M+NH4)+ | 866.82 | 17.28 |
| TAG (ISTD) | 57:0 | C60H116O6 | 932.88 | (M+NH4)+ | 950.91 | 18.13 |
| PC (ISTD) | 24:0 | C32H64O8PN | 621.44 | (M+H)+ | 622.44 | 6.11 |
| PC (ISTD) | 34:0 | C42H84O8PN | 761.59 | (M+H)+ | 762.60 | 10.32 |
| PE (ISTD) | 24:0 | C29H58O8PN | 579.39 | (M-H)- | 578.38 | 6.17 |
| PE (ISTD) | 34:0 | C39H78O8PN | 719.55 | (M-H)- | 718.54 | 10.38 |
| PS (ISTD) | 34:0 | C40H78O10PN | 763.54 | (M-H)- | 762.53 | 9.34 |
| LPC (ISTD) | 17:0 | C25H52O7N | 509.35 | (M+H)+ | 510.36 | 4.80 |
| Cer (ISTD) | 17:0 | C35H69O3N | 551.53 | (M-H2O)+ | 534.52 | 10.13 |